A note on the steady–Hopf mode interaction in the presence of O(2) symmetry

Javier Sierra[1,2], David Fabre[1] and Edgar Knobloch[3]

[1] *UPS-IMFT, Allée du Professeur Camille Soula, 31000 Toulouse, France*
[2] *Università degli Studi di Salerno, 132 Via Giovanni Paolo II, 84084 Fisciano,Salerno, Italy. and*
[3] *Department of Physics, University of California at Berkeley, Berkeley, California 94720, USA*
(Dated: February 2, 2023)

The purpose of this note is to present in detail a mathematical study of a truncated normal form relevant to the bifurcations observed in axisymmetric wakes, in particular, a disk and a sphere. We employ abstract normal form analysis to identify possible bifurcations and the corresponding bifurcation diagrams in parameter space. The bifurcations and the bifurcation diagrams are interpreted in terms of symmetry considerations. Particular emphasis is placed on the presence of attracting robust homoclinic and heteroclinic cycles in certain parameter regimes. The normal form coefficients are computed for several examples of wake flows and the resulting predictions compared with the results of direct numerical flow simulations. In general, satisfactory agreement is obtained.

I. INTRODUCTION

We consider the interaction between a steady state bifurcation and Hopf bifurcation in a system with $O(2)$ symmetry when both modes have the same wavenumber. This situation arises naturally in some problems in fluid dynamics, for example, Taylor–Couette flow (TCF), wake flow of axisymmetric objects (WFA) and the wake of axisymmetric objects in mixed convection (WFA-MC). Golubitsky and collaborators [1, 2] investigated solutions of this problem (called here pure modes and mixed modes) and explored the possible secondary bifurcations. However, they do not provide a systematic study of the problem and many details are left to the reader. The purpose of this note is to reproduce these results and to explain how they can be applied to the TFC, WFA, and WFA-MC problems. Our method differs from that of Golubitsky *et al.* [1, 2] in several aspects:

- The study is restricted to a truncated problem where only third-order nonlinearities are considered.

- Two systems are introduced: a polar coordinate representation which eliminates the two continuous symmetries of the system and a second system written in its natural Hilbert basis which reduces the dynamics to its fundamental domain. These techniques, when systematically employed, reduce the six-dimensional system to a four-dimensional one and reduce the fixed-point solutions to a single representative of each group orbit.

- The amplification rates λ_s and λ_h of the two primary modes are included explicitly in the unfolding of the problem. Golubitsky *et al.* considered the amplification rates as unspecified functions of a single control parameter.

Our method is thus much more in line with that used by Hirschberg & Knobloch [3, 4] for the related problem of interaction of two steady-state modes with $O(2)$ symmetry. There are strong similarities between these two situations, as emphasized in what follows.

The paper is organized as follows. Section II presents the normal form and introduces a reduction to polar coordinates, which is used in what follows. Section III proposes a general nomenclature for the various solutions of the problem. Section IV reviews the fixed-point solutions of the normal form: pure modes, mixed modes, and possible bifurcations of higher order. Section V considers a degenerate case in which a number of details can be investigated analytically. Section VI presents a numerical exploration of various solutions of the truncated problem. Next, section VII explains how the various results can be used to construct consistent stability diagrams, while section VIII applies these results to flow past a fixed axisymmetric object, in particular, a disk and a sphere. The paper concludes with a brief discussion in Section IX. Some background to the techniques we use and their application to problems arising in fluid mechanics may be found in [5].

II. NORMAL FORM AND REDUCTION TO AMPLITUDE EQUATIONS

A. Problem parametrization

The flow state $\mathbf{q} = [\mathbf{u}, p]$ is specified by the velocity field $\mathbf{u}$ and the hydrodynamic pressure p (the WFA-MC also includes the temperature field T). Near the mode interaction (a codimension-two bifurcation) the flow state takes the form

$$\mathbf{q} = \mathbf{Q}_0 + \mathrm{Re}\big[a_0(t)e^{-i\theta}\hat{\mathbf{q}}_s\big] + \mathrm{Re}\big[a_1(t)e^{-i\theta}\hat{\mathbf{q}}_{h,-1} + a_2(t)e^{i\theta}\hat{\mathbf{q}}_{h,1}\big] + \text{h.o.t.} \tag{1}$$

Here $\mathbf{Q}_0$ is the steady-state flow state that is invariant under the action of the whole $O(2)$ group, $\hat{\mathbf{q}}_s$ is the steady mode and $\hat{\mathbf{q}}_h$ is the Hopf (unsteady) mode. The Ansatz in eq. (1) takes into account the continuous (translation or rotation) symmetry via the terms $e^{\pm i\theta}$, where $\theta \in S^1$ is an angle-like variable in the periodicity direction; for axisymmetric problems it corresponds to the azimuthal angle, while in the TCF it corresponds to the axial direction: $\theta \equiv -2\pi x/\Lambda$, where Λ is the mode wavelength.

Here without loss of generality the azimuthal wavenumber m is taken to be $m = 1$. Both the steady-state flow and the eigenmodes are functions of other spatial variables (radial distance and azimuthal angle for the TFC; radial and axial distances for axisymmetric wake problems), but this dependence is not of importance here.

In the following we shall be interested in the dynamics arising from the interaction between the amplitude a_0 of the steady mode and the amplitudes a_1, a_2 of the left and right-traveling waves associated with the Hopf mode. All three amplitudes are in general complex functions of the time t and their behavior near the mode interaction is described by normal form theory.

B. Universal normal form

The normal form is obtained in a standard way: provided the original system of equations is Γ-equivariant under the group $\Gamma \equiv O(2) \times S^1$, the normal form must also be Γ-equivariant. The Hilbert–Weyl and Poénaru theorems, stated in [1, Ch 1], ensure the existence of a finite set of Γ-equivariant polynomials generating the Γ-equivariant Taylor expansion (at the origin) of any smooth mapping. The group Γ acts on $\mathbb{C}^3$ which decomposes into irreducibles $\mathbb{C} \oplus \mathbb{C}^2$ corresponding to the steady and Hopf modes. The action of the group Γ is generated by rotations R_α, reflection κ, and the temporal phase shift Φ of the Hopf mode. The canonical representation of these actions is as follows:

$$
\begin{aligned}
R_\alpha &: (a_0, a_1, a_2) \to \left(a_0 e^{i\alpha}, a_1 e^{i\alpha}, a_2 e^{-i\alpha}\right) \\
\Phi &: (a_0, a_1, a_2) \to \left(a_0, a_1 e^{i\phi}, a_2 e^{i\phi}\right) \\
\kappa &: (a_0, a_1, a_2) \to \left(\bar{a}_0, a_2, a_1\right).
\end{aligned} \tag{2}
$$

Based on these considerations, Golubitsky $et\ al.$ [1, 2] show that the resulting normal form can be written as follows:

$$
\begin{aligned}
\begin{pmatrix} \dot{a}_0 \\ \dot{a}_1 \\ \dot{a}_2 \end{pmatrix} &= (c^1 + i\delta c^2) \begin{pmatrix} a_0 \\ 0 \\ 0 \end{pmatrix} + (c^3 + i\delta c^4) \begin{pmatrix} \bar{a}_0 a_1 \bar{a}_2 \\ 0 \\ 0 \end{pmatrix} \\
&+ (p^1 + iq^1) \begin{pmatrix} 0 \\ a_1 \\ a_2 \end{pmatrix} + (p^2 + iq^2)\delta \begin{pmatrix} 0 \\ a_1 \\ -a_2 \end{pmatrix} \\
&+ (p^3 + iq^3) \begin{pmatrix} 0 \\ a_0^2 a_2 \\ \bar{a}_0^2 a_1 \end{pmatrix} + (p^4 + iq^4)\delta \begin{pmatrix} 0 \\ a_0^2 a_2 \\ -\bar{a}_0^2 a_1 \end{pmatrix},
\end{aligned} \tag{3}
$$

where $\delta \equiv |a_2|^2 - |a_1|^2$, and the 12 real quantities c^i, p^i and q^i, $i = 1, 2, 3, 4$, are functions of the control parameters and of the five generators of the ring of invariant polynomials under the action of the group Γ:

$$
\rho \equiv |a_0|^2, \quad N \equiv |a_1|^2 + |a_2|^2, \quad \Delta \equiv \left(|a_2|^2 - |a_1|^2\right)^2,
$$
$$
\eta \equiv \mathrm{Re}\left(a_0^2 \bar{a}_1 a_2\right), \quad \xi \equiv \left(|a_2|^2 - |a_1|^2\right)\mathrm{Im}\left(a_0^2 \bar{a}_1 a_2\right). \tag{4}
$$

C. Normal form in polar coordinates

Using the polar representation of the complex amplitudes $a_j = r_j e^{i\phi_j}$ for $j = 0, 1, 2$, eq. (3) can be reduced to a system of four coupled equations governing the amplitudes r_0, r_1, r_2 and the phase $\Psi \equiv \phi_1 - \phi_2 - 2\phi_0$:

$$
\begin{aligned}
\dot{r}_0 &= \left[c^1 + c^3 r_1 r_2 \cos\Psi - c^4 \delta \sin\Psi\right] r_0 \\
\dot{r}_1 &= \left[p^1 + \delta p^2\right] r_1 \\
&+ \left[\left(p^3 + \delta p^4\right)\cos\Psi + \left(q^3 + \delta q^4\right)\sin\Psi\right] r_0^2 r_2 \\
\dot{r}_2 &= \left[p^1 - \delta p^2\right] r_2 \\
&+ \left[\left(p^3 - \delta p^4\right)\cos\Psi - \left(q^3 - \delta q^4\right)\sin\Psi\right] r_0^2 r_1 \\
\dot{\Psi} &= 2\left(q^2\delta - c^2\delta - c^3\sin\Psi - c^4\delta\cos\Psi\right) \\
&+ \frac{r_0^2}{r_1 r_2}\left[\left(q^3 + Nq^4\right)\cos\Psi - \left(Np^3 + \Delta p^4\right)\sin\Psi\right].
\end{aligned} \tag{5}
$$

Note that this system is four-dimensional due to the two continuous symmetries of the system (3). Invariance under the action of the phase shift Φ reduces the three angle-like variables (ϕ_0, ϕ_1, ϕ_2) to two $(\phi_0, \phi_1 - \phi_2)$; invariance under the rotations R_α then leads to the single phase Ψ.

The polar system is equivariant under the action of the group Γ_ρ which is isomorphic to the Pauli group $\Gamma_\rho \simeq D_4 \rtimes \mathbb{Z}_2$, where the symbol $\rtimes$ indicates the semi-direct product between groups. The generators of the group are the reflection κ and $R_{\pi/2}\Phi_{\pi/2}$, the discrete rotation through $\pi/2$ with an equal time shift. For the sake of conciseness, let us introduce the action of the following group elements on the polar vector field:

$$
\begin{aligned}
\kappa &: \left(r_0, r_1, r_2, \Psi\right) \to \left(r_0, r_2, r_1, -\Psi\right) \\
R_{\pi/2}\Phi_{\pi/2} &: \left(r_0, r_1, r_2, \Psi\right) \to \left(r_0, -r_1, r_2, \Psi + \pi\right) \\
R_\pi\Phi_\pi &: \left(r_0, r_1, r_2, \Psi\right) \to \left(-r_0, r_1, r_2, \Psi\right) \\
R_{\pi/2}\Phi_{-\pi/2} &\ \left(r_0, r_1, r_2, \Psi\right) \to \left(r_0, r_1, -r_2, \Psi + \pi\right),
\end{aligned} \tag{6}
$$

where $R_{\pi/2}\Phi_{-\pi/2} = \kappa \cdot \left(R_{\pi/2}\Phi_{\pi/2}\right)^3 \cdot \kappa$ and $R_\pi\Phi_\pi = \left(R_{\pi/2}\Phi_{\pi/2}\right)^2$. In the next section we present a classification of the various solutions based on the polar representation.

D. Group-theoretic considerations

Branching of solutions is determined by the structure of the isotropy lattice acting on fixed points of the normal form (3). The isotropy subgroups of solutions that arise at primary bifurcations correspond to maximal isotropy subgroups of Γ, that is, isotropy subgroups that are not included in any other isotropy subgroup other than Γ itself. In a similar manner, solutions arising at secondary bifurcations have isotropy subgroups that are maximal in a subgroup strictly smaller than Γ. This process continues until the trivial group is reached, corresponding
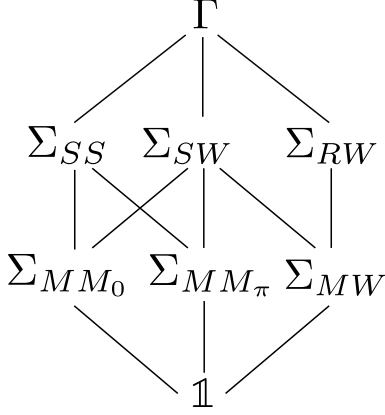
FIG. 1: Lattice of isotropy subgroups of the symmetry group Γ (resp. Γ_ρ).

to the most general fixed point subspace of the normal form.

Prior to the introduction of the isotropy lattice of the normal form (3), let us introduce the following notation to denote some of the isotropy subgroups of Γ: the group of rotations $\widetilde{SO(2)}$,

$$\widetilde{SO(2)} \equiv \{R_\phi \Phi_{-\phi} \mid \phi \in [0, 2\pi)\}, \qquad (7a)$$

and the group $\mathbb{Z}_n(g)$, a cyclic subgroup generated by the element g, satisfying $g^n = \text{Id}$. The isotropy lattice of the normal form (3) is represented in fig. 1. In section III we use the information extracted from this lattice to determine the types of invariant solutions admitted by the normal form. In addition to the isotropy subgroups of the complex normal form, table III lists the isotropy subgroups of the solutions of the polar system (5).

E. Third order normal form

Here we will not deal with the general case, instead we consider a truncated form retaining only nonlinearities of third order. Such a truncated system can be expressed in the following explicit form:

$$\dot{a}_0 = \lambda_s a_0 + l_0 a_0 |a_0|^2 + l_1 \big(|a_1|^2 + |a_2|^2\big) a_0 \\ + i l_2 \big(|a_2|^2 - |a_1|^2\big) a_0 + l_3 \bar{a}_0 \bar{a}_2 a_1 \qquad (8a)$$

$$\dot{a}_1 = \big(\lambda_h + i\omega_h\big) a_1 + \big(B|a_1|^2 + (A+B)|a_2|^2\big) a_1 \\ + C a_1 |a_0|^2 + D a_0^2 a_2 \qquad (8b)$$

$$\dot{a}_2 = \big(\lambda_h + i\omega_h\big) a_2 + \big(B|a_2|^2 + (A+B)|a_1|^2\big) a_2 \\ + C a_2 |a_0|^2 + D \bar{a}_0^2 a_1 , \qquad (8c)$$

where l_0, l_1, l_2, l_3 are real coefficients and A, B, C, D are complex coefficients. The correspondence with the notation of Golubitsky et al. [1, 2] is reported in tables I and II.

The system (8) then corresponds to the polar equations

$$\dot{r}_0 = \big[\ \lambda_s + l_0 r_0^2 + l_1\big(r_1^2 + r_2^2\big)\big] r_0 \\ + l_3 r_0 r_1 r_2 \cos \Psi \qquad (9a)$$

$$\dot{r}_1 = \big[\ \lambda_h + B_r r_1^2 + (A_r + B_r) r_2^2 + C_r r_0^2\big] r_1 \\ + r_0^2 r_2 \big(D_r \cos \Psi + D_i \sin \Psi\big) \qquad (9b)$$

$$\dot{r}_2 = \big[\ \lambda_h + B_r r_2^2 + (A_r + B_r) r_1^2 + C_r r_0^2\big] r_2 \\ + r_0^2 r_1 \big(D_r \cos \Psi - D_i \sin \Psi\big) \qquad (9c)$$

$$\dot{\Psi} = (A_i - 2l_2)(r_2^2 - r_1^2) - 2l_3 r_1 r_2 \sin \Psi \\ + r_0^2 D_i \cos \Psi \Big[\frac{r_2}{r_1} - \frac{r_1}{r_2}\Big] - r_0^2 D_r \sin \Psi \Big[\frac{r_2}{r_1} + \frac{r_1}{r_2}\Big], \qquad (9d)$$

Interestingly, the polar system only involves 9 of the 13 original coefficients, namely: l_0, l_1, l_3, A_r, B_r, C_r, D_r, D_i and $A_i - 2l_2$. The system (9) is decoupled from the evolution of the phase ϕ_0 and the "mean phase" of the Hopf component $\phi_m = (\phi_1 + \phi_2)/2$, which evolve according to

$$\dot{\phi}_0 = l_2(r_2^2 - r_1^2) + l_3 r_1 r_2 \sin \Psi, \qquad (10a)$$

$$\dot{\phi}_m = \omega_h + \big(B_i + \tfrac{1}{2} A_i\big)(r_1^2 + r_2^2) + C_i r_0^2 \\ + \frac{1}{2} r_0^2 D_i \cos \Psi \Big[\frac{r_2}{r_1} + \frac{r_1}{r_2}\Big] \\ + \frac{1}{2} r_0^2 D_i \sin \Psi \Big[\frac{r_1}{r_2} - \frac{r_2}{r_1}\Big]. \qquad (10b)$$

In addition we introduce a system whose coordinates are invariant under the group action, except for the reflection symmetry in Ψ. We do this primarily because we would like to use the resulting system to study a particular degenerate case in section V. The advantage of such a system is that dynamics occur in the "fundamental domain", that is, there is only one representative of each group orbit. The system is defined in terms of the invariants

$$R = r_0^2, \ S = r_1^2 + r_2^2, \ P = r_1 r_2, \ Q = \cos \Psi. \qquad (11)$$

In term of these coordinates the evolution equations become

$$\dot{R} = 2\big[\lambda_s + l_0 R + l_1 S + l_3 P\big] R \qquad (12a)$$

TABLE I: Correspondence of the real coefficients of the normal form (8) with the literature.

	λ_s	λ_h	ω_h	l_0	l_1	l_2	l_3
[1, 2]	$c_\mu^1 \cdot \mu$	$p_\mu^1 \cdot \mu$	q_0^1	c_ρ^1	c_N^1	c_0^2	c_0^3
[6]	$\alpha_0 \mu + \beta_0 \nu$	$\alpha_1 \mu + \beta_1 \nu$	ω_0	c_0	$\text{Re}(d_0)$	$-\text{Im}(d_0)$	f_0

$$\dot{S} = \; 2\big[\lambda_h + B_r S + C_r R\big] S \\ \qquad + 4\big[A_r P + D_r Q R\big] P \qquad (12b)$$

$$\dot{P} = \; \big[\lambda_h + B_r S + C_r R\big] P \\ \qquad + 4\big[A_r P + D_r Q R\big] S - D_i R \sqrt{(1 - Q^2)(S^2 - 4P^2)} \\ \qquad\qquad (12c)$$

$$\dot{Q} = \; \big[2l_3 + \tfrac{D_r R S}{P}\big](1 - Q^2) \\ \qquad + \big[(A_i - 2l_2) - \tfrac{D_i R Q}{P}\big]\sqrt{(1 - Q^2)(S^2 - 4P^2)}. \\ \qquad\qquad (12d)$$

In the study that follows, we take the nonlinear coefficients l_j for $j = 1, 2, 3, 4$, A, B, C, D as well as the frequency ω_h of the Hopf mode as constant. The amplification rates λ_s and λ_h will be used as unfolding parameters. Our study provides predictions for the existence and stability of the possible solutions in the (λ_s, λ_h) plane. To apply these results to the flows we are interested in, we have to specify the dependence of the amplification rates on the control parameters of the problem. The WFA problem employs a single control parameter R while the WFA-MC problem is specified by two control parameters R_1 and R_2 related to the magnitude of the incoming velocity and the temperature difference between the object and the background, respectively. In this case the amplification rates can be assumed to have the following dependence:

$$\lambda_s = \alpha_s(R_1 - R_1^*) + \beta_s(R_2 - R_2^*), \\ \lambda_h = \alpha_h(R_1 - R_1^*) + \beta_h(R_2 - R_2^*), \qquad (13)$$

where R_1^* and R_2^* are the threshold values given by the linear stability analysis of the axisymmetric steady state; for the WFA problem $\beta_s = \beta_h = 0$.

In the TCF problem R_1, R_2 are related to the angular velocities of the inner and outer cylinders; in the vicinity of the bicritical (codimension-two) point (R_1^*, R_2^*) the amplification rates can be assumed to depend linearly on the distance to this point:

$$\lambda_s = c_{R_1}^1(R_1 - R_1^*) + c_{R_2}^1(R_2 - R_2^*), \\ \lambda_h = p_{R_1}^1(R_1 - R_1^*) + p_{R_2}^1(R_2 - R_2^*). \qquad (14)$$

Numerical values for (R_1^*, R_2^*) and for the parameters $c_{R_1}^1, c_{R_2}^1, p_{R_1}^1, p_{R_2}^1$ are tabulated in [2] for several values of the radius ratio $\eta < 1$ (i.e. the ratio of the radii of the inner and outer cylinders).

TABLE II: Correspondence of the complex coefficients of the normal form (8) with the literature.

	A	B	C	D
[1, 2]	$2(p_0^2 + iq_0^2)$	$(p_N^1 - p_0^2) + i(q_N^1 - q_0^2)$	$p_\rho^1 + iq_\rho^1$	$p_0^3 + iq_0^3$
[6]	$e_1 - d_1$	d_1	c_1	f_1

III. CLASSIFICATION OF THE SOLUTIONS

The nomenclature used to classify the various solutions is given in tables III and IV. We describe every possible solution, although the emphasis will be put on the solutions that arise generically in the third-order problem and in the degenerate case considered in section V.

To illustrate the various solutions graphically, we project the four-dimensional phase space into a plane spanned either by the complex amplitude $A(t)$ or by $A'_j(t)$ for $j = 0, 1$, where

$$A(t) \equiv a_0(t) + a_1(t) + \bar{a}_2(t), \\ A'_j(t) \equiv A(t)e^{-i\phi_j(t)}, \text{ for } j = 0, 1, \qquad (15)$$

hereafter referred to as the A-projection and the A'-projection, respectively.

The function A provides a global measure of the dynamics of the system and combines contributions from both the steady and unsteady components. In the wake problem, the real and imaginary parts of A can be identified with the leading order contribution to the lift forces in the y and z directions, respectively. In the TCF problem they represent, for example, the vorticity levels at two points located a quarter of a wavelength apart in the periodicity direction.

The solutions that are stationary in the polar representation are summarized in the table III. The simplest solution is the trivial solution (TS) $(a_0, a_1, a_2) = (0, 0, 0)$. This solution corresponds to Couette flow in the TCF problem, and to the axisymmetric solution in the WFA and WFA-MC problems. In the A-projection this solution corresponds to the origin (Figure 2a). There are three primary solutions: steady-state modes (SS), rotating waves (RW) and standing waves (SW). The steady state mode (SS) takes the form $(a_0, 0, 0)$, $a_0 \neq 0$. This state corresponds to the Taylor Vortex state in the TCF problem and the Steady Shedding mode in the wake problems. In the A-projection this state is represented by an off-center point (Figure 2b). As shown in table V and in fig. 2b using a thin dashed-dotted line there is a circle of such states related by rotations R_{ϕ_0}; each state is in addition reflection-symmetric.

The RW and SW solutions arise in a primary Hopf bifurcation of the trivial state. Because of $O(2)$ symmetry, the eigenvalues at the Hopf bifurcation are doubled, and the Hopf bifurcation produces simultaneously a branch of rotating waves (RW, $(a_0, a_1, a_2) = (0, a_1, 0)$) and standing waves (SW, $(a_0, a_1, a_2) = (0, a_1, a_1)$). The RW break reflection symmetry; consequently, there are two RW, rotating in opposite directions and related by reflection. In contrast, the SW are reflection-symmetric oscillations with zero mean. In the TCF problem the RW correspond to the Spiral Vortex state, while in the wake problem they correspond to the Spiral Shedding state, observed, for example, in the wake of a rising bubble [7]. In the A-projection the RW state corresponds to a limit cycle centered at the origin (Figure 2c), while the SW

TABLE III: Nomenclature and symmetry groups of the steady-state solutions of the system (5).

Name	Representative	Isotropy group (complex)	Isotropy group (polar)	Frequencies
Pure modes:				
TS	$(0,0,0,nd)$	$O(2) \times S^1$	$D_4 \rtimes \mathbb{Z}_2(\kappa)$	0
SS	$(r_a,0,0,nd)$	$\mathbb{Z}_2(\kappa) \times S^1$	$\mathbb{Z}_2(\kappa) \times \mathbb{Z}_2(\Phi_\pi)$	0
RW	$(0,r_a,0,nd)$	$SO(2)$	$\mathbb{Z}_4(R_{\pi/2}\Phi_{\pi/2})$	1
SW	$(0,r_a,r_a,nd)$	$\mathbb{Z}_2(\kappa) \times \mathbb{Z}_2(R_\pi\Phi_\pi)$	$\mathbb{Z}_2(\kappa) \times \mathbb{Z}_2(R_\pi\Phi_\pi)$	1
Mixed modes:				
MM$_0$	$(r_a,r_b,r_b,0)$	$\mathbb{Z}_2(\kappa)$	$\mathbb{Z}_2(\kappa)$	1
MM$_\pi$	(r_a,r_b,r_b,π)	$\mathbb{Z}_2(\kappa \cdot R_\pi\Phi_\pi)$	$\mathbb{Z}_2(\kappa \cdot R_\pi\Phi_\pi)$	1
MW	$(0,r_a,r_b,\Psi)$	$\mathbb{Z}_2(R_\pi\Phi_\pi)$	$\mathbb{Z}_2(R_\pi\Phi_\pi)$	1
Precessing waves:				
General	(r_a,r_b,r_c,Ψ)	$\mathbb{1}$	$\mathbb{1}$	2
Type A	(r_a,r_b,r_b,Ψ)	$\mathbb{1}$	$\mathbb{1}$	2
Type B	$(r_a,r_b,r_c,0 \text{ or } \pi)$	$\mathbb{1}$	$\mathbb{1}$	2
Type C	$(r_a,r_b,0,\Psi)$	$\mathbb{1}$	$\mathbb{1}$	2

(a) TS (b) SS (c) RW (d) SW
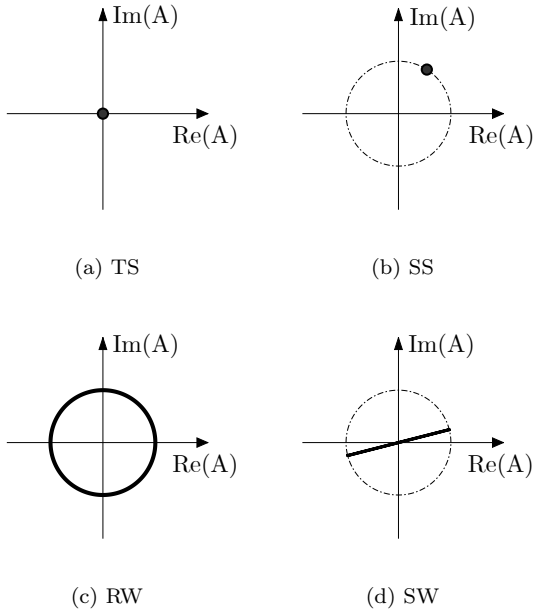
FIG. 2: The trivial state (TS) and the primary branching solutions SS, RW and SW in the complex A plane.

state is represented by a radial oscillation through the origin (Figure 2d). In the TCF problem, the SW state corresponds, respectively, to the Ribbon state and the Symmetric Periodic Shedding state observed, for example, in the wake of a disk when $R \approx 150$. As for SS, there is a circle of SW states related by rotations, see fig. 2d. Each of these solutions corresponds to a one-dimensional fixed point subspace spanned either by a_0 or a_1, and their presence is therefore guaranteed by the equivariant branching lemma.

Secondary bifurcations may lead to states with a higher-dimensional fixed point subspace. These states correspond to the next rung of the lattice of isotropy subgroups. An example is provided by mixed mode states that correspond to a (nonlinear) superposition of the SS and SW modes. There are two possible states of this type. The first is denoted by MM$_0$, and corresponds, respectively, to a pattern called Twisted Vortices in the TCF problem and to the reflection symmetry-preserving mode (RSP) in the wake problem. In the A-projection the solution oscillates back and forth in the radial direction but now with non-zero mean (Figure 3a). The second mixed mode, MM$_\pi$, corresponds, respectively, to Wavy Vortices in the TCF problem and to the reflection symmetry-breaking mode (RSB) in the wake problem. In the A-projection this solution corresponds to a back-and-forth along a line segment perpendicular to the radial direction (Figure 3b). The phase ϕ_0 of both these states is arbitrary. In other words, there is a circle of solutions of each type, as indicated in fig. 3a) and fig. 3b). Finally, one can also find a mixed mode state involving the Hopf modes, referred to as a modulated wave state (MW), consisting of a (nonlinear) superposition of two rotating wave modes. This state is referred to as the Modulated Spiral mode (MSP) in the TCF problem and the Modulated Wave mode (MW) in the wake problem. It is a mode with two temporal frequencies, which are in general incommensurate, and so corresponds to a 2-torus as sketched in fig. 3c. This type of solution does not occur generically in the third-order system, although it arises in higher order normal forms or in the degenerate case corresponding to $A_r = 0$ [8].

The last solution type, that is, a state arising in a tertiary bifurcation, corresponds to a fixed point in the (r_0, r_1, r_2, Ψ) coordinates with no further symmetry. According to eq. (10), in such states the phase ϕ_0 of the steady mode generically precesses at a constant rate given by $\dot\phi_0$. Consequently, states of this type display two frequencies, one of which is close to the critical Hopf frequency while the other is a low frequency given by eq. (10a). Such modes have been called "modulated ro-
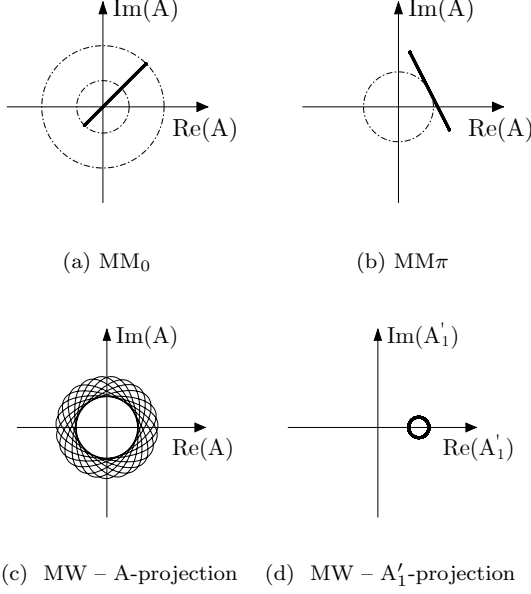
(a) MM$_0$

(b) MMπ

(c) MW – A-projection   (d) MW – A$'_1$-projection

FIG. 3: The secondary states (a) MM$_0$, (b) MM$_\pi$ and (c) MW in the complex A plane. (d) The A$'$-projection of the MW state.

(a) A-projection of PrW   (b) A$'_0$-projection of PrW

FIG. 4: The tertiary state PrW.

(a) A-projection of $\widetilde{\mathrm{MM}}_\pi$ (b) A$'_0$-projection of $\widetilde{\mathrm{MM}}_\pi$

FIG. 5: The Modulated Mixed Mode $\widetilde{\mathrm{MM}}_\pi$ in the complex A plane.

tating waves" in [2], but here we prefer to avoid the ambiguous word "modulated" which has been used to describe a large variety of very different states in the past. Instead, these solutions will be referred to as Precessing Waves (PrW) or "drifting waves".

The precession of these states is best appreciated in the A'-projection, showing the state in a frame of reference precessing with the steady-state component a_0. In this frame of reference, the PrW is periodic and takes the form of an ellipse (Figure 4b. Note that in this representation the polar coordinates (r_0, r_1, r_2, Ψ) can be interpreted graphically: r_0 is the distance of the center of the ellipse to the origin, $(r_1 + r_2)/2$ and $(r_1 - r_2)/2$ are the major and minor axes, and Ψ is twice the angle between the major axis of the ellipse and the direction of the steady-state component.

There are in fact four types of PrW as explained in Table III. The general solution, PrW General, occurs generically in the third order normal form and corresponds to the most general fixed-point solution of eq. (9). In addition, there are special PrW states. The first two, called PrW Type A and Type B, do not occur generically in the third order problem, but they are found in normal forms of higher order or in the degenerate case considered in section V. The third solution, PrW Type C is another degenerate solution that arises in the third order normal form but only when the three conditions $A_i - 2l_2 = D_r = D_i = 0$ are satisfied.

The solutions that are periodic in the polar representation are summarized in table IV. We distinguish three types of solutions. The first type is referred to as a Modu-
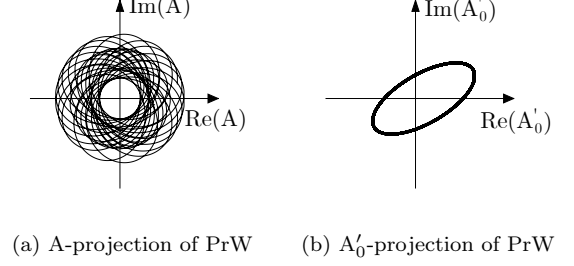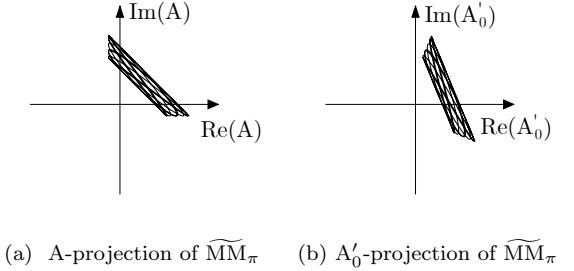
lated Mixed Mode since it displays the same spatial symmetries as the mixed modes already described. For example, in the A-projection the Modulated Mixed Mode state $\widetilde{\mathrm{MM}}_\pi$ evolves on a 2-torus, whose shape resembles that of MM$_\pi$ (Figure 5a). The A'_0-projection (Figure 5b) yields an identical but rotated picture, indicating that the phase of the steady-state component remains constant. The related state $\widetilde{\mathrm{MM}}_0$ is not displayed, since its A-projection is identical to that of the MM$_0$ state. Its modulus $|A|$, however, pulsates with two independent frequencies.

We also find periodic states we call Pulsating Waves (PuW). In such states, the polar coordinates (r_0, r_1, r_2, Ψ) all oscillate periodically in time, but the pulsation retains a certain symmetry. Specifically, $\overline{r}_1 = \overline{r}_2$ and $\overline{\sin \Psi} = 0$, where the overbar indicates an average over the pulsation period. According to eq. (10) the phase ϕ_0 of the steady-state component also pulsates periodically, but the average value of its derivative over one pulsation period vanishes. Consequently, the pattern does not precess. In the A-projection the solution evolves on a 2-torus that remains confined within a given angular sector (Figure 6a), indicating the absence of net precession. The A'_0-projection (Figure 6b) also reveals a 2-torus, albeit of different form.

The last type of periodic solution corresponds to the case where the (r_0, r_1, r_2, Ψ) coordinates are once again all periodic, but the conditions $\overline{r}_1 = \overline{r}_2$ and $\overline{\sin \Psi} = 0$ are violated. In the A-projection, this state appears ir-

TABLE IV: Nomenclature and symmetry group of limit cycle solutions of the system (5).

Name of solution	Representative in polar coordinates	Isotropy group	Frequencies in primitive coordinates
$\widetilde{\mathrm{MM}}_{0,\pi}$	$(r_a(t), r_b(t), r_b(t), 0 \text{ or } \pi)$	$\mathbb{1}$	2
$\widetilde{\mathrm{IMM}}$	$(0, r_b, r_c, \Psi(t))$	$\mathbb{1}$	2
PuW	$(r_a(t), r_b(t), r_c(t), \Psi(t))$ with $\overline{r}_b = \overline{r}_c$ and $\overline{\sin \Psi} = 0$	$\mathbb{1}$	2
3-frequency waves: (3FW)			
General	$(r_a(t), r_b(t), r_c(t), \Psi(t))$	$\mathbb{1}$	3
Type A	$(r_a(t), r_b(t), r_b(t), \Psi(t))$ with $\overline{\sin \Psi} \neq 0$	$\mathbb{1}$	3
Type B	$(r_a(t), r_b(t), r_c(t), 0 \text{ or } \pi)$ with $\overline{r}_b \neq \overline{r}_c$	$\mathbb{1}$	3
Type C	$(0, r_b(t), r_c(t), \text{nd})$ with $\overline{r}_b \neq \overline{r}_c$	$\mathbb{1}$	3
Type D	$(r_a(t), r_b(t), 0, \Psi(t))$ with $\overline{\sin \Psi} \neq 0$	$\mathbb{1}$	3
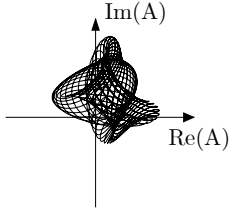
(a) A-projection of PuW   (b) A_0'-projection of PuW
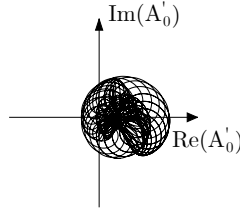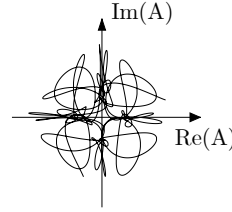
FIG. 6: The Pulsating Wave PuW in the complex A plane.
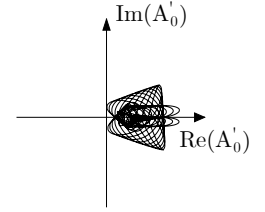

(a) A-projection of 3FW   (b) A_0'-projection of 3FW

FIG. 7: The Three-Frequency Wave 3FW in the complex A plane.

regular (Figure 7a), while the A_0'-projection (Figure 7b) revels a 2-torus. In fact, this solution actually evolves on a 3-torus, owing to net drift in the phase ϕ_0. We call these states Three-Frequency Waves (3FW), since they are characterized by a frequency near the critical Hopf frequency, the pulsation frequency, and finally the precession frequency.

The classification of the solutions of the generic steady-Hopf interaction with $O(2)$ symmetry presented by Golubitsky *et al.* [1, 2] and covered in section II D is based on maximal isotropy subgroups of the symmetry group $O(2) \times S^1$ of the normal form. This technique predicts the existence up to tertiary bifurcations of fixed points of the complex normal form 3. These isotropy subgroups correspond to the symmetries of the solutions within the fixed point subspace of each isotropy group (cf. table III). However, several of the states identified here have trivial symmetry (denoted by $\mathbb{1}$), and their existence cannot be established by group-theoretic arguments alone. Thus, the polar representation introduced here is helpful for the explicit computations required to establish the presence of these more complex states.

IV.   TYPES OF SOLUTIONS

In this section, we describe the various solutions of the truncated third-order system (8). We summarize not only the solutions but also their stability properties, assuming that all necessary non-degeneracy conditions hold.

A.   Pure modes

Table V contains the definition and eigenvalues of the trivial state and of the pure modes. Since the polar angle Ψ is undefined for these states, the results are obtained from the primitive amplitude equations (8). Therefore, six eigenvalues are listed for each branch. The condition for supercriticality of the primary branch is also given. This can be deduced from elementary considerations. For example, the SS branch is supercritical if $l_0 < 0$, as can be seen in both the equation for the branch (which is then defined for $\lambda_s > 0$) and the first non-zero eigenvalue (which is then negative, implying that stability has been transferred to the SS branch). The conditions for su-

TABLE V: Defining equations and eigenvalues of primary branches in the third order normal form (8).

Name of solutions (condition for supercriticality)	Definition	Eigenvalues	Notes
Pure modes:			
TS	$r_0 = r_1 = r_2 = 0$	λ_s (twice)	Bif. to SS
		$\lambda_h \pm i\omega_h$ (twice each)	Bif. to SW and RW
SS	$r_0 = \sqrt{-\frac{\lambda_s}{l_0}} \equiv r_P$	0	Inv. under rotation
$l_0 < 0$	ϕ_0 arbitrary	$2l_0 r_P^2$	Bif. from TS
	$r_1 = r_2 = 0$	$\lambda_h + i\omega_h + (C+D)r_P^2$ and c.c.	Bif. to MM_0
		$\lambda_h + i\omega_h + (C-D)r_P^2$ and c.c.	Bif. to MM_π
SW	$r_1 = r_2 = \sqrt{-\frac{\lambda_h}{(2B_r+A_r)}} \equiv r_S$	0	Inv. under time shift
$2B_r + A_r < 0$	$r_0 = 0$	0	Inv. under rotation
	$\phi_1 - \phi_2$ arbitrary	$(4B_r + 2A_r)r_S^2$	Bif. from TS
	$\dot\phi_1 = \dot\phi_2 = \omega_h + (2B_i + A_i)r_S^2$	$-2A_r r_S^2$	Bif. to RW
		$\lambda_s + (2l_1 + l_3)r_S^2$	Bif. to MM_0
		$\lambda_s + (2l_1 - l_3)r_S^2$	Bif. to MM_π
RW	$r_1 = \sqrt{-\frac{\lambda_h}{B_r}} \equiv r_R$	0	Inv. under time shift + rotation
$B_r < 0$	$r_0 = r_2 = 0$	$2B_r r_R^2$	Bif. from TS
	$\dot\phi_1 = \omega_h + B_i r_R^2$	Ar_R^2 and c.c.	Bif. to SW
		$\lambda_s + (l_1 + il_2)r_R^2$ and c.c.	Bif. to PrW

percriticality also provide the conditions for the subcriticality (if the corresponding parameter has the opposite sign) and non-degeneracy (if the corresponding quantity is non-zero).

The bifurcation at $\lambda_h = 0$ is the standard Hopf bifurcation with $O(2)$ symmetry, and so gives rise simultaneously to branches of RW and SW. The RW rotate counterclockwise (clockwise) when $\omega_h > 0$ ($\omega_h < 0$). Reflection symmetry implies that for each RW $(r_1, r_2) = (r_1, 0)$ there is also a RW $(r_1, r_2) = (0, r_1)$ rotating in the opposite direction. The condition $A_r = 0$ represents a degeneracy that is analysed theoretically in [5, 8–10]. In the vicinity of this degeneracy two-frequency states are present, and these are analyzed in section IV C 2.

B. Mixed modes

The defining equations for the mixed modes are given in table VI. We differentiate between nondegenerate solutions of the third-order truncated normal form, which are the Mixed Modes of type $MM_{0,\pi}$, and degenerate solutions, which are the Modulated Wave modes MW. The nondegeneracy conditions for the existence of MM branches are $\Delta_\pm = (2B_r + A_r)l_0 - (2l_1 \pm l_3)(C_r \pm D_r) \neq 0$, with the positive sign for MM_0 and the negative sign for MM_π. Inspection shows that these states bifurcate supercritically from the SS branch if $\Delta_\pm l_0 < 0$ and from the SW branch if $\Delta_\pm(2B_r + A_r) < 0$. Modulated Wave modes MW are degenerate solutions of the third order normal form (9) and exist when $A_r = 0$ and $\Delta_b = l_3 \sin\Psi \neq 0$.

At this point, it is interesting to point out the similarities between the present problem and the related problem of the interaction between two steady-state modes with opposite parity analysed by Hirschberg & Knobloch [3, 4]. The latter problem has two pure modes and two mixed modes, which are defined by equations similar to those defining our SS and SW pure modes and mixed modes. So, if we restrict to the subspace generated by the SS and SW pure modes, all the results of Hirschberg & Knobloch [3, 4] can be directly applied to the present case. This is not so, however, within the system (8), which reveals the presence of additional secondary bifurcations (see below).

C. Stability of mixed modes and tertiary bifurcations

Higher order bifurcations can be detected by linearizing the normal form (8) around the mixed modes in table VI. Working with the primitive equations, as done in Golubitsky et al. [1], leads to the same results, but the procedure is more involved. Within the polar representation four eigenvalues need to be computed; the remaining eigenvalues are both zero owing to the two continuous symmetries, the invariance of the mixed modes under rotation and time translation.

1. Mixed modes

To obtain the results listed in table VI, consider the following expansion: $r_0 = r_a + x_0$, $r_1 = r_b + x_1$, $r_2 = r_b + x_2$ and $\Psi = \Psi_0 + \psi$, with either $\Psi_0 = 0$ for MM_0 or $\Psi = \pi$ for MM_π; in either case we suppose the perturbation is infinitesimal, $|x_0|, |x_1|, |x_2|, |\psi| \ll 1$. In terms of the quantities $\rho = x_1 - x_2$ and $x_M = (x_1 + x_2)/2$ the resulting liner stability problem is block-diagonal:

9

TABLE VI: Defining equations and eigenvalues of mixed modes in the third order normal form (8).

Name of solutions (condition for supercriticality)	Definition	Eigenvalues	Notes
MM_0	$r_a^2 = \frac{(2l_1+l_3)\lambda_h - (2B_r+A_r)\lambda_s}{\Delta_+}$	eigs of M_a^+	Bif. to $\widetilde{MM}_0$
$\Delta_+ \neq 0$	$r_b^2 = \frac{(C_r+D_r)\lambda_s - l_0\lambda_h}{\Delta_+}$	eigs of M_b^+	Bif. to PrW and/or PuW
	$\Delta_+ = (2B_r+A_r)l_0 - (2l_1+l_3)(C_r+D_r)$		
MM_π	$r_a^2 = \frac{(2l_1-l_3)\lambda_h - (2B_r+A_r)\lambda_s}{\Delta_-}$	eigs of M_a^-	Bif. to $\widetilde{MM}_\pi$
$\Delta_- \neq 0$	$r_b^2 = \frac{(C_r-D_r)\lambda_s - l_0\lambda_h}{\Delta_-}$	eigs of M_b^-	Bif. to PrW and/or PuW
	$\Delta_- = (2B_r+A_r)l_0 - (2l_1-l_3)(C_r-D_r)$		
$MW_{\Psi_0^\pm}$	$r_a^2 = \frac{1}{2}\left[-\frac{A_r}{2E_r} - \sqrt{\frac{\chi}{4F_rE_r}}\right]$	$\lambda_s - l_1\frac{A_r}{E_r} + l_3 r_a r_b \cos\Psi_0^\pm$	Bif. to PrW or 3FW
$2B_r + A_r < 0,\ A_r > 0$	$r_b^2 = \frac{1}{2}\left[-\frac{A_r}{2E_r} + \sqrt{\frac{\chi}{4F_rE_r}}\right]$	$-2l_3 r_a r_b \cos(\Psi_0^\pm)$	Stability of $MW_{\Psi^\pm}$
$E_r < 0,\ F_r < 0$	$\sin\Psi_0^\pm = \frac{A_i-2l_2}{l_3}\frac{\left(\chi/(F_rE_r)\right)^{1/2}}{\left((A_r/E_r)^2 - \chi/(F_rE_r)\right)^{1/2}}$	$\sin\Psi_0^\pm > 1$	Bif. to $\widetilde{IMM}$
Existence I: $A_r/E_r < 0$			
Existence II: $0 < \frac{\chi}{F_rE_r} < \frac{A_r^2}{E_r^2}$	$\chi = A_r(A_r + 2B_r) - 4E_r\lambda_h$		

$$\begin{pmatrix}\dot{x}_0\\ \dot{x}_M\end{pmatrix} = M_a^\pm \begin{pmatrix}x_0\\ x_M\end{pmatrix} \text{ with}$$

$$M_a^\pm = 2\begin{pmatrix} l_0 r_a^2 & (2l_1 \pm l_3)r_a r_b\\ (C_r \pm D_r)r_a r_b & (2B_r + A_r)r_b^2\end{pmatrix},$$

$$\begin{pmatrix}\dot{\rho}\\ \dot{\psi}\end{pmatrix} = M_b^\pm \begin{pmatrix}\rho\\ \psi\end{pmatrix} \text{ with}$$

$$M_b^\pm = 2\begin{pmatrix} -A_r r_b^2 \mp D_r r_a^2 & \pm D_i r_a^2 r_b\\ (2l_2 - A_i)r_b \mp D_i r_a^2/r_b & \mp(D_r r_a^2 + l_3 r_b^2)\end{pmatrix},$$
(16)

with the upper sign applying to MM_0 and the lower one to MM_π. The matrices M_a^+, M_b^+, M_a^-, M_b^- correspond, respectively, to the matrices denoted M_0, M_1, N_0 and N_1 in Golubitsky et al. [1], but are obtained here in a much more straightforward way. The expressions are identical, except for the prefactor 2 which is missing in Golubitsky et al. and an overall change of sign in their matrix M_1.

Let us first discuss the situation in the subspace (x_0, x_M), which is governed by the system (16a). This system is completely analogous to that studied by Hirschberg & Knobloch [3], since it involves perturbations within the SS/SW invariant subspace of the problem. In particular, the determinant of the matrix $M_a^\pm$ (i.e. the product of the eigenvalues) is $4r_a r_b \Delta_\pm$. It follows that a steady state bifurcation cannot occur along either mixed mode within the SS/SW subspace. This fact could have been anticipated by noting that this subspace does not admit symmetry-breaking bifurcations of these states. As a result only Hopf bifurcations are possible. It follows that the eigenvalues of the matrix $M_a^\pm$ are either real with constant sign, or complex conjugate with a possible Hopf bifurcation. Inspection shows that the situation depends upon the signs of the quantities l_0, $2B_r + A_r$, and $\Delta_\pm$. If $\Delta_\pm < 0$, both eigenvalues

are real and their product is negative. Therefore, one of the eigenvalues is stable and the other unstable. This means that the corresponding branch $MM_{0,\pi}$ is always less stable than the primary SS and SW branches. In the case $\Delta_\pm > 0$, the product of the eigenvalues is positive, and their sum is given by the trace of the matrix, i.e. $2\left(l_0 r_a^2 + (2B_r + A_r)r_b^2\right)$. When $l_0 < 0$ and $2B_r + A_r < 0$, i.e., when both primary bifurcations are supercritical, the trace remains negative, indicating that both eigenvalues are stable along the whole mixed mode branch. Similarly, when $l_0 > 0$, and $2B_r + A_r > 0$, i.e. when both primary bifurcations are subcritical, the trace remains positive, indicating that both eigenvalues are unstable along the whole branch. The last possibility, $l_0(2B_r + A_r) < 0$, arises when one of the primary bifurcations is subcritical while the other is supercritical. In this case, the real part of the eigenvalues changes sign somewhere along the branch, signaling the occurrence of a Hopf bifurcation. The solution born at such a Hopf bifurcation is referred to here as a Modulated Mixed Kode ($\widetilde{MM}_{\Psi_0}$, see table IV). The frequency of oscillation of the Modulated Mixed Mode at the Hopf bifurcation is given by the determinant of the matrix $M_a^\pm$ and may be expressed in terms of r_a^2 as follows:

$$\omega_a^2 = -\frac{l_0 \Delta_\pm}{2B_r + A_r}r_a^4. \tag{17}$$

According to Hirschberg & Knobloch [3], the corresponding bifurcation is degenerate within the third order truncation, and higher order terms are required to determine whether it is subcritical or supercritical.

Consider now the situation in the (ρ, ψ) subspace, governed by the system (16b). Inspection shows that the matrix $M_b^\pm$ may have complex or real eigenvalues. So, in this subspace, each of the mixed modes can experience steady bifurcations (associated with the vanishing of a single eigenvalue of $M_b^\pm$) and/or Hopf bifurcations

(associated with the vanishing of the real part of a pair of complex eigenvalues of $M_b^{\pm}$). To discuss the nature of the solutions born at these tertiary bifurcations it is useful to note that the phase drift $\dot{\phi}_0$ of the steady mode component is related to these quantities by the equation

$$\dot{\phi}_0 = -2l_2 r_b \rho \pm l_3 r_b^2 \psi + \mathcal{O}(\rho^3, \rho^2\psi, \psi^2\rho, \psi^3)\,, \quad (18)$$

obtained from eq. (10a).

A steady state bifurcation will generically give rise to a branch with constant, nonzero (ρ, ψ), and according to eq. (18) such a state will therefore precess at a constant angular velocity. The corresponding bifurcation will be referred to as a parity-breaking bifurcation, and the states produced as Precessing Waves (PrW, see table III). On the other hand, a Hopf bifurcation will generically give rise to a limit cycle in the (ρ, ψ) plane. Since this cycle is symmetric about $(\rho, \psi) = (0, 0)$, eq. (18) implies that the resulting state will drift back and forth with zero net drift. The result is a direction-reversing wave [11] and we refer here to states of this type as Pulsating Waves (PuW, see table IV).

These predictions are in agreement with those of Golubitsky et al. except for their expectation that the symmetry-breaking Hopf bifurcation (i.e. the Hopf bifurcation in the (ρ, ψ) subspace) gives rise to a 3-frequency state. We see that while the bifurcation is indeed associated with translations of the pattern and hence motion along a three-torus, this motion is in fact a two-frequency motion (in the original variables).

The eigenvalues of the matrix $M_b^{\pm}$ solve a quadratic equation which cannot be simplified easily, and generally has to be investigated on a case-by-case basis. However, it is instructive to consider the situation in the vicinity of the bifurcation points of the mixed modes from the pure modes. In the vicinity of the bifurcation from the SS mode one has $r_b \ll r_a$, and the eigenvalues of $M_b^{\pm}$ are, at leading order, $(\mp 2Dr_a^2, \mp \overline{D}r_a^2)$. Thus, if $D_r > 0$ (resp. $D_r < 0$), the MM_0 is more (resp. less) stable than the MM_π mode in the vicinity of the bifurcation from the SS mode. Similarly, near the bifurcation from the SW mode, the requirement $r_a \ll r_b$ shows that the eigenvalues of $M_b^{\pm}$ are, at leading order, $(-2A_r r_b^2, \mp 2l_3 r_b^2)$. The first eigenvalue indicates stability for both MM_0 and MM_π modes provided $A_r > 0$. Recall that the parameter A_r also determines if the SW branch is more or less stable than the RW branch. Thus, the mixed modes inherit this property from the SW branch in the vicinity of the bifurcation point. The second eigenvalue likewise implies that if $l_3 > 0$ (resp. $l_3 < 0$), the MM_0 is more (resp. less) stable than the MM_π in the vicinity of the bifurcation from the SW mode.

2. Modulated wave mode

The modulated wave mode is a degenerate solution of the normal form (8) truncated at third order. This type of pattern requires the degeneracy condition $A_r = 0$ in order to exist, although it exists under weaker assumptions in the general normal form (5).

To resolve this indeterminacy, we return to the general polar normal form (5). The existence of the MW solution is subject to the following conditions

$$\begin{aligned} p^1(0, r_1^2 + r_2^2, (r_2^2 - r_1^2)^2, 0, 0, \lambda) &\equiv 0 \\ p^2(0, r_1^2 + r_2^2, (r_2^2 - r_1^2)^2, 0, 0, \lambda) &\equiv 0\,. \end{aligned} \quad (19)$$

Hill and Stewart [12] observed that the condition $p^2 \equiv 0$ is a degeneracy condition if one evaluates the polynomial p^2 at the origin, i.e. $p^2(0, 0, 0, 0, 0, 0) \equiv A_r$. Since, to fifth order,

$$\begin{aligned} &p^1(0, r_1^2 + r_2^2, (r_2^2 - r_1^2)^2, 0, 0, \lambda) \equiv \\ &\lambda_h + (\tfrac{1}{2}A_r + B_r)(r_1^2 + r_2^2) \\ &+p_\Delta^1(r_2^2 - r_1^2)^2 + p_N^1(r_1^2 + r_2^2)^2\,, \\ &p^2(0, r_1^2 + r_2^2, (r_2^2 - r_1^2)^2, 0, 0, \lambda) \equiv \\ &\tfrac{1}{2}A_r + p_N^2(r_1^2 + r_2^2) + p_\Delta^2(r_2^2 - r_1^2)^2\,, \end{aligned} \quad (20)$$

the $\{r_1, r_2\}$ evolution is given by

$$\begin{aligned} \dot{r}_1 =\ & r_1\Big[\lambda_h + B_r r_1^2 + (A_r + B_r)r_2^2 \\ &+(p_\Delta^1 + p_{N^2}^1 - p_N^2)r_1^4 + (p_\Delta^1 + p_{N^2}^1 + p_N^2)r_2^4 \\ &+2(p_{N^2}^1 - p_\Delta^1)r_2^2 r_1^2 + p_\Delta^2(r_2^2 - r_1^2)^3\Big], \\ \dot{r}_2 =\ & \kappa \cdot \dot{r}_1, \end{aligned} \quad (21)$$

where $\kappa \cdot \dot{r}_1$ stands for the action of the reflection symmetry, defined in eq. (6). First, let us consider the fixed points of eq. (21) with $p_N^1 = p_\Delta^2 = 0$ and a slight change in the notation: $p_N^2 = E_r$ and $p_\Delta^1 \equiv F_r$. Inspection of eq. (21) shows that the fixed points r_a, r_b satisfy

$$\begin{aligned} r_a^2 &= \frac{1}{2}\Big[-\frac{A_r}{2E_r} - \sqrt{\frac{\chi}{4E_r F_r}}\Big] \\ r_b^2 &= \frac{1}{2}\Big[-\frac{A_r}{2E_r} + \sqrt{\frac{\chi}{4E_r F_r}}\Big], \end{aligned} \quad (22)$$

where the symbol χ, which is a function of the parameter λ_h, is defined in table VI. Evidently, the MW states exist when $A_r/E_r < 0$ and $0 < \chi/E_r F_r < A_r^2/E_r^2$.

The stability within the MW subspace, i.e. with respect to perturbations in $\{r_1, r_2\}$ only, can be analysed in terms of the determinant and trace of the Jacobian stability matrix restricted to this subspace:

$$\begin{aligned} \det(M^{MW}) =\ & 16 r_a^2 r_b^2 (r_b^2 - r_a^2) E_r F_r \\ &-16 r_a^2 r_b^2 (r_b^2 - r_a^2)^2 p_\Delta^2, \end{aligned} \quad (23a)$$

$$\begin{aligned} \text{tr}(M^{MW}) =\ & -\frac{A_r}{E_r}(2B_r + A_r) + p_{N^2}^1 \frac{A_r^2}{E_r^2} \\ &+4F_r(r_b^2 - r_a^2)^2 + 4E_r r_b^2 r_a^2, \end{aligned} \quad (23b)$$

In view of the MW existence conditions, inspection of eq. (23) shows that the resulting MW solutions are stable when $2B_r + A_r < 0$ and $E_r F_r > 0$, i.e. a necessary condition for a positive determinant and negative trace.

In addition, inspection of eq. (22) requires the condition $F_r < 0$ (resp. $F_r > 0$) for supercriticality (resp. subcriticality). The conditions for the existence and supercriticality are summarized in table VI.

Prior to a discussion regarding the possible bifurcations of the MW branch, let us consider the effect of higher order jets, i.e. coefficients $p_N^1 \neq 0$ and $p_\Delta^2 \neq 0$. Inspection of eq. (22) shows that the total amplitude $r_a^2 + r_b^2 = -\frac{A_r}{2E_r}$ remains constant regardless the value of the parameter λ_h. Such a property is a consequence of the hypothesis $p_\Delta^2 = 0$, i.e. the truncation of the normal form up to fifth order terms. A coefficient $p_\Delta^2 \neq 0$ will introduce a small modification of the total amplitude with respect to a variation in the parameter λ_h, which in this case is equal to $r_a^2 + r_b^2 = -\frac{A_r}{2E_r} - \frac{p_\Delta^2}{E_r}(r_b^2 - r_a^2)^2$. A simple perturbation analysis, with

$$r_i^2 = \varepsilon r_{i,1}^2 + \varepsilon^2 r_{i,2}^2 + \text{h.o.t.}$$

and $\varepsilon \ll 1$ for $i = 1, 2$, allows one to determine the effect of including higher order terms. The first order fixed point is as expected given by eq. (22) while the second order solution is given by

$$
\begin{aligned}
r_{a,2}^2 &= \frac{p_\Delta^2}{8E_r}\frac{\chi}{F_r E_r} \\
&\quad -p_{N^2}^1\left(\frac{A_r}{2E_r}\right)^2 \frac{E_r}{2\sqrt{F_r E_r \chi} - E_r(A_r + 2B_r)}, \\
r_{b,2}^2 &= \frac{p_\Delta^2}{8E_r}\frac{\chi}{F_r E_r} \\
&\quad +p_{N^2}^1\left((\frac{A_r}{2E_r}\right)^2 \frac{E_r}{2\sqrt{F_r E_r \chi} - E_r(A_r + 2B_r)}.
\end{aligned}
\tag{24}
$$

As expected, the correction (24) is indeed of second order, i.e. a function of $(A_r/2E_r)^2$ and $\chi/(4E_r F_r)$ which are second order corrections to $(r_{a,1}^2 + r_{b,1}^2)^2$ and $(r_{b,1}^2 - r_{a,1}^2)^2$, respectively. Similarly, one may observe that p_Δ^2 and p_N^1 are second order corrections as long as the system is nondegenerate, i.e. $F_r \neq 0$, $E_r \neq 0$, $A_r \neq 0$ and $2B_r + A_r \neq 0$. Assuming that these nondegeneracy conditions hold, we conclude that the hypothesis of $p_\Delta^2 = p_{N^2}^1 = 0$ does not induce any qualitative change in the dynamics near the MW branch.

Let us now focus on the stability of the MW branch with respect to perturbations in the variables r_0 and Ψ. In this form the MW solutions arise as a pair of solutions $\text{MW}_{\Psi_0^\pm}$. The $\text{MW}_{\Psi_0^+}$ (resp. $\text{MW}_{\Psi_0^-}$) solution is characterized by $\cos\Psi^+ > 0$ (resp. $\cos\Psi^- < 0$). The pair of solutions $\text{MW}_{\Psi_0^\pm}$ can bifurcate into Precessing Waves or a modulated interacting mixed mode $\widetilde{\text{IMM}}$ solution. One of the branches is always unstable with respect to perturbations in the phase Ψ whereas the other is always stable, depending on the sign of l_3. In the case that $l_3 < 0$ (resp. $l_3 > 0$) the branch $\text{MW}_{\Psi_0^-}$ (resp. $\text{MW}_{\Psi_0^+}$) is stable (resp. unstable) with respect to perturbations in Ψ. The $\text{MW}_{\Psi_0^-}$ solution is stable if the eigenvalue $\lambda_s - l_1\frac{A_r}{E_r} - l_3 r_a r_b|\cos\Psi_0^-| < 0$ and it loses stability to a

Precessing Wave whenever this eigenvalue changes sign. The branch $\text{MW}_{\Psi_0^+}$ bifurcates to a $\widetilde{\text{IMM}}$ solution, which is a 2-torus in the original coordinates, whenever

$$\frac{A_i - 2l_2}{l_3}\frac{\left(\chi/E_r F_r\right)^{1/2}}{\left((A_r/E_r)^2 - \chi/(E_r F_r)\right)^{1/2}} > 1,$$

implying no fixed point Ψ_0 is present. In this case the phase Ψ is associated with a constant drift. The modulated interacting mixed mode branch is thus stable whenever both

$$\lambda_s - l_1\frac{A_r}{E_r} \pm \frac{l_3}{4}\left[\frac{A_r^2}{E_r^2} - \frac{\chi}{F_r E_r}\right] < 0,$$

while a bifurcation to a Precessing Wave occurs whenever

$$\lambda_s - l_1\frac{A_r}{E_r} + |\frac{l_3}{4}\left[\frac{A_r^2}{E_r^2} - \frac{\chi}{F_r E_r}\right]\cos\Psi^\pm| \geq 0.$$

In the supercritical case the PrW connects in parameter space a Mixed Mode with a Modulated Wave Mode. Finally, a possible scenario for a bifurcation from a PrW towards a three frequency wave arises whenever eq. (9d) does not possess a fixed point.

D. Bifurcation from Rotating Waves to Precessing Waves

As indicated in table III, the RW branch has a couple of complex eigenvalues which may lead to a bifurcation to a Precessing Wave (PrW). This situation was investigated by Crawford et al. [13] using the primitive sixth-order system. The derivation was lengthy and required the demonstration of an extension of the Hopf theorem to complex equations. The use of the polar representation introduced here leads to substantial simplifications because, within this representation, this bifurcation is in fact a steady-state one, and the resulting Precessing Wave is a stationary solution of the polar equations.

We consider here the clockwise ($\omega_h > 0$) RW with $(r_1, r_2) \equiv (r_R, 0)$, where r_R is given in table III. According to the table, a bifurcation occurs along this branch when the bifurcation parameter, defined by

$$\sigma_R \equiv \lambda_s + l_1 r_R^2, \tag{25}$$

vanishes. Inspection shows that the corresponding eigenvector breaks the symmetry of the mixed mode (i.e., it points in the a_0 direction). We expect, therefore, that the branch originating in this bifurcation will be characterized by $r_0 = \mathcal{O}(\sigma_R^{1/2})$. We further anticipate that $r_2 = \mathcal{O}(\sigma_R)$ and $r_1 = r_R + x_1$ with $x_1 = \mathcal{O}(\sigma_R)$. We also assume that Ψ has a finite limit in the vicinity of the bifurcation point. With these assumptions, the stationary solutions of the polar system (12) obey the following equations at leading order:

$$\sigma_R + l_0 r_0^2 + 2l_1 r_R x_1 + l_3 r_R r_2 \cos\Psi = 0 \qquad (26a)$$

$$2B_r r_R x_1 + C_r r_0^2 = 0 \qquad (26b)$$

$$A_r r_R r_2 = -r_0^2\big(D_r \cos\Psi - D_i \sin\Psi\big) \qquad (26c)$$

$$(A_i - 2l_2)r_R r_2 = -r_0^2\big(D_i \cos\Psi + D_r \sin\Psi\big). \qquad (26d)$$

To solve these equations, we add the squares of equations eqs. (26c) and (26d) to obtain

$$\Big[A_r^2 + (A_i - 2l_2)^2 r_R^2 r_2^2\Big] = |D|^2 r_0^4. \qquad (27)$$

This equation allows us to express r_2 in terms of r_0. Eliminating $\sin\Psi$ from eqs. (26c) and (26d) leads to

$$\cos\Psi = -\frac{D_r A_r + D_i\big(A_i - 2l_2\big)}{|D|\sqrt{A_r^2 + (A_i - 2l_2)^2}}. \qquad (28)$$

Finally, x_1 is easily expressed as a function of r_0 from eq. (26b). Introducing these expressions into eq. (26a) yields a classical branching equation which can be cast in the form

$$\sigma_R + H^r r_0^2 = 0,$$
$$\text{with } H^r = l_0 - l_1 \frac{C_r}{B_r} - l_3 \frac{D_r A_r + D_i(A_i - 2l_2)}{A_r^2 + (A_i - 2l_2)^2}. \qquad (29)$$

It follows that in the vicinity of the bifurcation point, the Precessing Waves are given by the branching equation $r_0 \approx (-\sigma_R/H^r)^{1/2}$, and the bifurcation is then supercritical if $H_r < 0$.

The precession rate corresponding to this solution is given by eq. (10a) and reads

$$\dot\phi_0 = -l_2 r_R^2 + H^i r_0^2$$
$$\text{with } H^i = l_2 \frac{C_r}{B_r} + l_3 \frac{D_i A_r - D_r(A_i - 2l_2)}{A_r^2 + (A_i - 2l_2)^2}. \qquad (30)$$

Note that the branching parameter H^r and the term H^i correspond, respectively, to the real and imaginary parts of the complex Hopf coefficient H computed in [13], at the end of a much lengthier analysis.

E. Robust heteroclinic cycles

As already mentioned one may expect the presence of structurally stable or robust heteroclinic cycles in our system in view of its similarity to the mode interaction problem studied in [3, 4] when written in polar coordinates. More generally, a heteroclinic cycle is a set of trajectories $\{\big(\bar{r}_0^{(j)}(t), \bar{r}_1^{(j)}(t), \bar{r}_2^{(j)}(t), \overline{\Psi}^{(j)}(t)\big)\}_{j=1,2,\ldots,m}$ that connect equilibrium solutions $\{\big(r_0^{(j)}, r_1^{(j)}, r_2^{(j)}, \Psi^{(j)}\big)\}_{j=1,2,\ldots,m}$ with the property that $\big(\bar{r}_0^{(j)}(t), \bar{r}_1^{(j)}(t), \bar{r}_2^{(j)}(t), \overline{\Psi}^{(j)}(t)\big)$ is backward asymptotic to $\big(r_0^{(j)}, r_1^{(j)}, r_2^{(j)}, \Psi^{(j)}\big)$ and forward asymptotic to $\big(r_0^{(j+1)}, r_1^{(j+1)}, r_2^{(j+1)}, \Psi^{(j+1)}\big)$
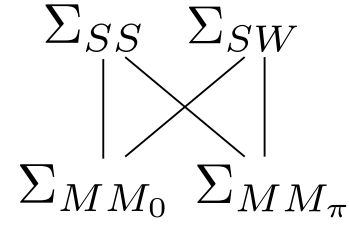

FIG. 8: Structure within in the isotropy lattice suggesting that there may exist of a robust heteroclinic cycle.

with the convention $\big(r_0^{(m+1)}, r_1^{(m+1)}, r_2^{(m+1)}, \Psi^{(m+1)}\big) = \big(r_0^{(1)}, r_1^{(1)}, r_2^{(1)}, \Psi^{(1)}\big)$. Such cycles are *robust* if each connection is robust, i.e. cannot be destroyed by changing parameters. Robust heteroclinic cycles typically do not exist in general nonsymmetric vector fields. However, they may exist in symmetric systems such as ours. First examples of robust heteroclinic cycles connecting saddle points were found in [14, 15]. Afterwards, Melbourne, Krupa and collaborators [16, 17] established a general approach to the existence and stability of structurally stable heteroclinic cycles in Γ-equivariant systems. The existence of a robust heteroclinic cycle requires the following conditions:

- Each saddle solution sits on a flow-invariant line l_j, say, and each such line is the fixed-point subspace for the isotropy subgroup of the saddle solution, i.e. $l_j = \text{Fix}(\Sigma_{j-1}) \cap \text{Fix}(\Sigma_j)$.

- The isotropy subgroups of the invariant lines are maximal isotropy subgroups.

- The invariant plane containing the invariant line is the fixed point subspace of a maximal isotropy subgroup.

The proof of this result is based on the existence of cycles in the isotropy lattice, such as fig. 8 for the present case, and suggests that the present system may possess robust heteroclinic cycles.

Indeed, the isotropy lattice in fig. 8 suggests the existence of a robust heteroclinic cycle between the steady-state mode SS and the standing wave mode SW. Such a heteroclinic cycle possesses two connections that lie within the $\text{Fix}\big(\mathbb{Z}(\kappa)\big)$ and $\text{Fix}\big(\mathbb{Z}(\kappa\cdot(\pi,\pi))$ subspaces. In our notation the heteroclinic connections lie in the invariant subspaces of the two MM solutions. Melbourne et al. [18] found that in the supercritical case such a cycle exists whenever the steady-state mode SS is a saddle (resp. sink) in the fixed-point subspace $\text{Fix}\big(\mathbb{Z}(\kappa)\big)$ of the isotropy subgroup of the MM_0 mode and a sink (resp. saddle) in the fixed-point subspace $\text{Fix}\big(\mathbb{Z}(\kappa\cdot(\pi,\pi))\big)$ of the isotropy subgroup of the MM_π mode. Similarly, the SW mode must be a sink (resp. saddle) in $\text{Fix}\big(\mathbb{Z}(\kappa)\big)$ and a saddle (resp. sink) in $\text{Fix}(\mathbb{Z}\big(\kappa\cdot(\pi,\pi)\big)$. These conditions are satisfied if the first three existence conditions in

TABLE VII: Defining conditions for structurally and asymptotically stable heteroclinic cycles connecting SS and SW. Here $\nu_{SS}^{\pm} \equiv \lambda_h + (C_r \pm D_r)r_P^2$ and $\nu_{SW}^{\pm} \equiv \lambda_s + (2l_1 \pm l_3)r_S^2$.

Name of solution (condition for supercriticality)	Existence	Asymptotic stability (Asymp. stable if ii) and either i-a) or i-b))
Het_{SS-SW}	$\nu_{SS}^+ \nu_{SS}^- < 0$	i-a) $\nu_{SS}^+ \nu_{SW}^- < -\nu_{SS}^- \min(-\nu_{SW}^+, \nu_{SW}^- + 2A_r r_s^2)$
$l_0 > 0$	$\nu_{SW}^+ \nu_{SW}^- < 0$	i-b) $\nu_{SS}^- \nu_{SW}^+ < -\nu_{SS}^+ \min(-\nu_{SW}^+, \nu_{SW}^- + 2A_r r_s^2)$
$A_r + 2B_r > 0$	$\nu_{SS}^+ \nu_{SW}^- > 0$	ii) $A_r > 0$
	$\frac{\lambda_s}{\lambda_h}\frac{(C_r+D_r)}{l_0} + \frac{\lambda_h}{\lambda_s}\frac{(2l_1+l_0)}{(2B_r+A_r)} > -2$	
	$\frac{\lambda_s}{\lambda_h}\frac{(C_r-D_r)}{l_0} + \frac{\lambda_h}{\lambda_s}\frac{(2l_1-l_0)}{(2B_r+A_r)} > -2$	

table VII are satisfied. In addition, no other fixed point solutions can be present in either of the fixed point subspaces and solutions starting in the neighborhood of the trivial mode are required to remain bounded, a condition that is satisfied if the last two existence conditions in table VII hold.

The necessary and sufficient conditions for the asymptotic stability of a particular type of robust heteroclinic cycle referred to as *Type A* are derived in [17]. This type of heteroclinic cycle is constructed in such a way that each trajectory connecting two fixed-point solutions lies within the fixed point subspace of an isotropy group isomorphic to $\mathbb{Z}_2$. Because of this the necessary and sufficient condition for asymptotic stability is

$$\prod_{j=1}^{m} \min\left(-\nu_j^c, \nu_j^e - \nu_j^t\right) > \prod_{j=1}^{m} \nu_j^e, \qquad (31)$$

where ν_j^c, ν_j^e, ν_j^t, ν_j^r denote the contracting, expanding, transversal and radial eigenvalues of the solution j. The *contracting* eigenvalue of the solution j corresponds to the minimum eigenvalue (maximum $-\nu_j$) in the fixed point subspace of solution j; the *expanding* eigenvalue corresponds to the eigenvalue with the largest real part among the eigenvalues restricted to the fixed point subspace of the backward asymptotic heteroclinic connection; the *radial* eigenvalue is the eigenvalue with the smallest real part (largest $-\nu_j^r$) within the intersection between the two previous fixed point subspaces and the *transverse* eigenvalue correspond to the eigenvalue with the largest real part among the eigenvalues restricted to the orthogonal complement. The proof of the identity eq. (31) is based on the use of a set of Poincaré return maps to obtain global estimates of stability from local ones. For more details the reader is referred to [16, 17]. The application of eq. (31) shows that in our case the heteroclinic cycle Het_{SS-SW} is asymptotically stable provided condition ii) and either condition i-a) or i-b) in table VII hold. This possibility was not considered in [1].

V. THE DEGENERATE CASE $D_i = 0$, $A_i - 2l_2 = 0$

In this section we consider a codimension-two degenerate case where the parameters D_i and $A_i - 2l_2$ both

vanish. This situation arises when all the nonlinear coefficients in eq. (8) are real. This case is of basic theoretical interest since it actually corresponds to the case where an additional $\mathbb{Z}_2$ symmetry is present in the primitive amplitude equations. In this case eq. (8) also reduces to a special case of the equations studied in generality by Silber & Knobloch [19] provided we also take $l_0 = A_r + 2B_r$, $\lambda_s = \lambda_h$.

In this case the equations in polar coordinates take the following form:

$$\dot{r}_0 = \left[\lambda_s + l_0 r_0^2 + l_1\left(r_1^2 + r_2^2\right) + l_3 r_1 r_2 \cos\Psi\right] r_0 \quad (32a)$$

$$\dot{r}_2 + \dot{r}_1 = \left[\begin{array}{l}\lambda_h + B_r(r_1^2 + r_2^2) + A_r r_1 r_2 \\ +r_0^2(C_r + D_r \cos\Psi)\end{array}\right](r_1 + r_2) \quad (32b)$$

$$\dot{r}_2 - \dot{r}_1 = \left[\begin{array}{l}\lambda_h + B_r(r_1^2 + r_2^2) - A_r r_1 r_2 \\ +r_0^2(C_r - D_r \cos\Psi)\end{array}\right](r_2 - r_1) \quad (32c)$$

$$\dot{\Psi} = -\left[2l_3 r_1 r_2 + D_r r_0^2 \frac{r_1^2 + r_2^2}{r_1 r_2}\right]\sin\Psi. \quad (32d)$$

In this case the $PQRS$ coordinates are particularly useful. The equations in these coordinates take the following form:

$$\dot{R} = 2\left[\lambda_s + l_0 R + l_1 S + l_3 PQ\right]R, \quad (33a)$$

$$\dot{S} = \begin{array}{l}2\left[\lambda_h + B_r S + C_r R\right]S \\ +4\left[A_r P + D_r RQ\right]P,\end{array} \quad (33b)$$

$$\dot{P} = \begin{array}{l}2\left[\lambda_h + B_r S + C_r R\right]P \\ +\left[A_r P + D_r RQ\right]S,\end{array} \quad (33c)$$

$$\dot{Q} = \left[2l_3 P^2 + D_r RS\right]\frac{1-Q^2}{P}. \quad (33d)$$

TABLE VIII: Nomenclature and isotropy group of steady-state solutions of the system (32).

| Name	Representative	Isotropy group (polar)	Frequencies
Primary bifurcations:			
SS	$(r_a, 0, 0, nd)$	$\mathbb{Z}_2(\kappa_r) \times \mathbb{Z}_2(\kappa) \times \mathbb{Z}_2(\Phi_\pi)$	0
RW_0	$(0, r_a, 0, nd)$	$D_4(R_{\pi/2}\Phi_{\pi/2}, \kappa \cdot \kappa_r)$	1
RW_π	$(0, r_a, 0, nd)$	$D_4(R_{\pi/2}\Phi_{\pi/2}, \kappa \cdot \kappa_r \cdot \Phi_\pi)$	1
SW_0	$(0, r_a, r_a, nd)$	$\mathbb{Z}_2(\kappa_r) \times \mathbb{Z}_2(\kappa) \times \mathbb{Z}_2(R_\pi\Phi_\pi)$	1
SW_π	$(0, r_a, r_a, nd)$	$\mathbb{Z}_2(\kappa_r\Phi_\pi) \times \mathbb{Z}_2(\kappa) \times \mathbb{Z}_2(R_\pi\Phi_\pi)$	1
Secondary bifurcations:			
MM_0	$(r_a, r_b, r_b, 0)$	$\mathbb{Z}_2(\kappa_r) \times \mathbb{Z}_2(\kappa)$	1
MM_π	(r_a, r_b, r_b, π)	$\mathbb{Z}_2(\kappa_r\Phi_\pi) \times \mathbb{Z}_2(\kappa \cdot R_\pi\Phi_\pi)$	1
IMM_0	$(0, r_a, r_b, 0)$	$\mathbb{Z}_2(\kappa_r \cdot \kappa) \times \mathbb{Z}_2(R_\pi\Phi_\pi)$	1
IMM_π	$(0, r_a, r_b, \pi)$	$\mathbb{Z}_2(\kappa_r \cdot \kappa \cdot \Phi_\pi) \times \mathbb{Z}_2(R_\pi\Phi_\pi)$	1
Tertiary bifurcations:			
PrW_A	(r_a, r_b, r_b, Ψ)	$\mathbb{Z}_2(\kappa_r)$	2
PrW_B	$(r_a, r_b, r_c, 0 \text{ or } \pi)$	$\mathbb{Z}_2(\kappa_r \cdot \kappa)$	2
$\widetilde{IMM}$	$(0, r_a, r_b, \Psi(t)), \ \Psi(t) = \phi_1(t) - \phi_2(t)$	$\mathbb{Z}_2(R_\pi\Phi_\pi)$	2
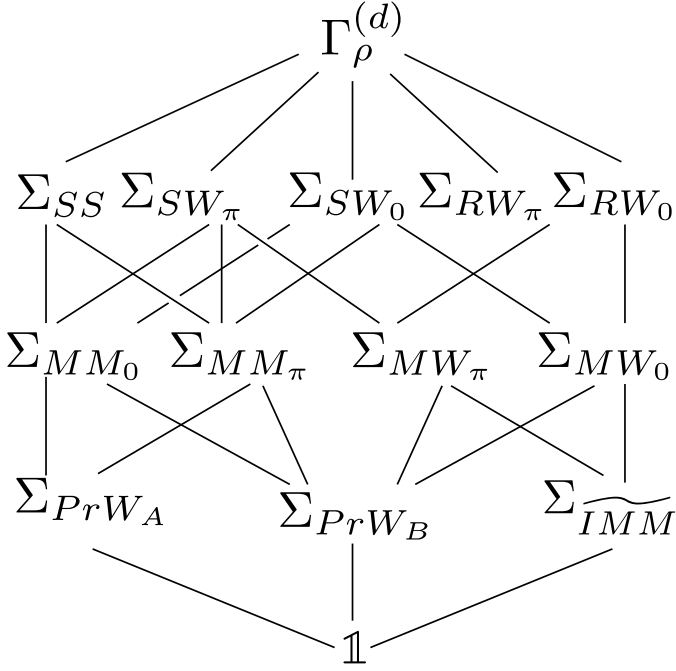
FIG. 9: Lattice of isotropy groups of the degenerate normal form.

These equations possess an additional reflection symmetry

$$\kappa_r : (r_0, r_1, r_2, \Psi) \to (r_0, r_2, r_1, \Psi) \qquad (34)$$

responsible for a reflection symmetry in Ψ:

$$(\kappa_r \cdot \kappa) \cdot (r_0, r_1, r_2, \Psi) = (r_0, r_1, r_2, -\Psi).$$

This symmetry has several consequences. First, the isotropy group of the polar normal form is now $\Gamma_\rho^{(d)} \simeq \mathbb{Z}_2^2 \rtimes D_4 \simeq \mathbb{Z}_2^4 \rtimes \mathbb{Z}_2$. Its isotropy lattice, depicted in fig. 9, displays new isotropy groups whose fixed point subspaces

are of dimension three, viz. Σ_{PrW_A}, Σ_{PrW_B}, $\Sigma_{\widetilde{IMM}}$. The fixed point subspaces $\text{Fix}(\Sigma_{PrW_A})$ and $\text{Fix}(\Sigma_{PrW_B})$ are characterized by $r_1 = r_2$ and $\sin \Psi = 0$, respectively, and are of dimension four in the space of complex amplitudes, i.e. they display two-frequency behavior, see table VIII. In contrast, the fixed point subspace $\text{Fix}(\Sigma_{\widetilde{IMM}})$ is characterized by $r_0 = 0$. Strictly speaking this is not an invariant subspace of the cubic truncation (since $A_r \neq 0$) but it does become so when the truncation is extended to fifth order, cf. section IV C 2. This subspace is also of dimension four, and is spanned by solutions of the form $(0, a_1, a_2)$, i.e., by $r_1 \neq r_2$ and the corresponding phases (ϕ_1, ϕ_2).

In addition, it turns out that the isotropy subgroups associated to the Interacting Mixed Modes Σ_{IMM_0} and Σ_{IMM_π} are not conjugates of each other, i.e. these solutions are distinct as in the case of the Mixed modes MM_0 and MM_π. The reason behind the distinction between the subgroups Σ_{SW_0}, Σ_{SW_π} (resp. Σ_{RW_0}, Σ_{RW_π}) is algebraic: these isotropy groups are not conjugate of each other, although their fixed point representative are of the same type. This is because the phase Ψ is undefined for either rotating waves and standing waves - a consequence of the fact that for these states $a_0 = 0$. However, we find it convenient to distinguish between SW_0 and SW_π (resp. RW_0 and RW_π) based on the limiting behavior of the Mixed Modes (resp. Mixed Waves) as $r_0 \to 0$, as indicated in the isotropy lattice fig. 9.

In this degenerate case the conditions for higher order bifurcations, as well as the complete definition of all possible branches of precessing waves, can be obtained explicitly. The corresponding results are tabulated in table IX. It will be found that there are at most three branches of precessing waves. The first two are denoted PrW_A and PrW_B, while the third kind is generic with no additional symmetry and hence trivial isotropy, and is denoted PrW_G.

A. Bifurcations from Mixed Modes and Rotating Waves

Bifurcations from Mixed Modes are governed by the eigenvalues of the matrices $M_b^\pm$ defined in section IV C (apart from the possible bifurcation to a modulated mixed mode if $l_0(2B_r + A_r) < 0$). In the present case, the matrix is diagonal with real eigenvalues. Therefore symmetry-breaking bifurcations from MM can only lead to PrW (Precessing Waves), excluding the possibility of PuW (Pulsating Waves). The number of such bifurcations follows from the eigenvalues of $M_b^\pm$. The first of these is $2(-A_r r_b^2 \mp D_r r_a^2)$, and this quantity changes sign along the MM_0 (MM_π) branch. The second eigenvalue of $M_b^\pm$ is $\mp 2(l_3 r_b^2 + D_r r_a^2)$. Thus if $l_3 D_r > 0$, this eigenvalue remains of one sign for both mixed modes. On the other hand, if $l_3 D_r < 0$, it changes sign somewhere along both branches. So, the number of branching points to Precessing Waves along the MM branches is either one (if $l_3 D_r > 0$) or three (if $l_3 D_r < 0$). These results are restated in the top part of table IX, where the conditions for a zero eigenvalue are stated in terms of λ_s and λ_h instead of r_a and r_b using table VI.

We also report in the table the branching point from the RW branch, investigated in section IV D. This point exists generically and the corresponding branch has $\Psi = 0$ (resp. $\Psi = \pi$) if $A_r D_r < 0$ (resp. $A_r D_r > 0$). We end up with a total number of either 2 or 4 bifurcation points to Precessing Waves.

The $\widetilde{\text{IMM}}$ solution is degenerate as was the case already for the generic third order normal form. The addition of higher order terms, as done in section IV C 2, leads to the existence of the solution $\widetilde{\text{IMM}}$, which in this degenerate case is a heteroclinic connection between the Interacting Modes IMM_0 and IMM_π. This last statement follows from the integration of eq. (32d) with $r_0 = 0$, which leads to $\Psi \to 0$ as $t \to \infty$ and $\Psi \to \pi$ as $t \to -\infty$ if $l_3 r_a r_b > 0$ and to $\Psi \to \pi$ as $t \to \infty$ and $\Psi \to 0$ as $t \to -\infty$ if $l_3 r_a r_b < 0$.

B. The subspace $r_1 = r_2$

The dynamics within the invariant subspace $\text{Fix}(\Sigma_{PrW_A})$, defined in polar coordinates as

$$\text{Fix}(\Sigma_{PrW_A}) = \{(r_0, r_1, r_2, \Psi) : r_1 = r_2\}, \quad (35)$$

take the form

$$\dot{r}_0 = \left[\lambda_s + l_0 r_0^2 + 2l_1 r_1^2 + l_3 r_1^2 \cos\Psi \right] r_0 \quad (36a)$$

$$\dot{r}_1 = \left[\lambda_h + (A_r + 2B_r)r_1^2 + (C_r + D_r \cos\Psi)r_0^2 \right] r_1 \quad (36b)$$

$$\dot{\Psi} = -2\left[l_3 r_1^2 + D_r r_0^2 \right] \sin\Psi. \quad (36c)$$

The PRQ coordinates can also be used in this subspace (which corresponds to $S = 2P$):

$$\dot{R} = 2\left[\lambda_s + l_0 R + (2l_1 + l_3 Q)P\right]R, \quad (37a)$$

$$\dot{P} = 2\left[\lambda_h + (2B_r + A_r)P + (C_r + D_r Q)R\right]P, \quad (37b)$$

$$\dot{Q} = 2\left[l_3 P + D_r R\right](1 - Q^2). \quad (37c)$$

The resulting systems are formally identical to those governing the interaction of two steady-state modes with opposite parity studied by Hirschberg & Knobloch, eq. (10) of [3], given by the correspondence

$$r_0 \equiv r, r_1 \equiv \rho, \Psi \equiv 2\Psi, \lambda_s \equiv \lambda, \lambda_h \equiv \mu, l_0 \equiv a,$$
$$2l_1 \equiv b, l_3 \equiv e, 2B_r + A_r \equiv d, C_r \equiv c, D_r \equiv f. \quad (38)$$

The results of [3, 4] can therefore be applied to the system eq. (36). We use these results to conclude that when $D_r l_3 < 0$ the two branches of mixed modes are connected by a tertiary branch of the form $r_0 \neq 0$, $r_1 = r_2 \neq 0$, $\sin\Psi \neq 0$. In the nomenclature of the present manuscript this branch corresponds to a Precessing Wave of type A (see table III). The defining equations for this solution are

$$R = r_0^2 = \frac{\sigma_{0A} - \sigma_{\pi A}}{2D_r \Sigma_A}, \quad (39a)$$

$$P = r_1^2 = r_2^2 = -\frac{\sigma_{0A} - \sigma_{\pi A}}{2l_3 \Sigma_A}, \quad (39b)$$

$$Q = \cos\Psi = \frac{\sigma_{\pi A} + \sigma_{0A}}{\sigma_{\pi A} - \sigma_{0A}}, \quad (39c)$$

where

$$\begin{aligned}
\Sigma_A &\equiv (2B_r + A_r + 2l_1)D_r - l_3(C_r + l_0) \neq 0, \\
\Sigma_A^a &\equiv D_r(A_r + 2B_r) - l_0 l_3, \\
H_A^{0,\pi} &\equiv (\Delta_+ + \Delta_-) - 4D_r l_3(1 - \Sigma_A/\Sigma_A^a) \\
\tfrac{1}{2}(\sigma_{0A} + \sigma_{\pi A}) &\equiv ((2B_r + A_r)D_r - C_r l_3)\lambda_s \\
&\quad + (2D_r l_1 - l_0 l_3)\lambda_h, \\
\tfrac{1}{2}(\sigma_{0A} - \sigma_{\pi A}) &\equiv D_r l_3(\lambda_s + \lambda_h),
\end{aligned} \quad (39d)$$

as in eq. (17) of [3]. The range of existence of this connecting branch in the (λ_s, λ_h) plane is obtained by imposing the condition $\cos\Psi \in [-1, 1]$ on eq. (39c); the conditions obtained from $\cos\Psi = \pm 1$ are identical to the conditions obtained from the vanishing of the second eigenvalue of $M_b^\pm$ and displayed in table IX, confirming that the PrW_A branch connects the two Mixed Mode branches.

The stability of all the solutions within the invariant subspace $\text{Fix}(\Sigma_{PrW_A})$ is determined as in Ref. [3]. The linearized dynamics within this subspace are governed by

TABLE IX: Higher order bifurcations in the degenerate case $D_i = 0$, $A_i - 2l_2 = 0$. Note: [1]Results for bifurcations to modulated mixed modes hold in the generic case. [2]Results relevant to the PrW of type A also hold in the less degenerate case to $D_i = 0$, $A_i - 2l_2 \neq 0$. [3]The bifurcation from rotating waves leads to a PrW_B in the present case, and to a general PrW in the generic case. [4]The conditions listed for the existence of Hopf bifurcations ensure an odd number of Hopf lines (1 or 3). The condition for an odd number of Hopf lines in the case of a termination at the MM_π fixed point is $\Delta_+ \Lambda_B^+ > 0$.

Branch	New solution	Bifurcation point		Condition for existence
MM_0	$PrW_A^{(2)}$	$\sigma_{0A} \equiv \left[l_3(C_r + D_r) - D_r(2B_r + A_r)\right]\lambda_s + \left[(2l_1 + l_3)D_r - l_0 l_3\right]\lambda_h = 0$		$l_3 D_r < 0$
	PrW_B	$\sigma_{0B} \equiv -\left[A_r C_r - 2B_r D_r\right]\lambda_s + \left[A_r l_0 - D_r(2l_1 + l_3)\right]\lambda_h = 0$		$A_r D_r < 0$
	$\widetilde{MM}_0^{(1)}$	$2(B_r + A_r)(C_r + D_r - l_0)\lambda_s + l_0(2l_1 + l_3 - 2B_r - A_r)\lambda_h = 0$		$(2B_r + A_r)l_0 < 0$
MM_π	$PrW_A^{(2)}$	$\sigma_{\pi A} \equiv \left[l_3(C_r - D_r) - D_r(2B_r + A_r)\right]\lambda_s + \left[(2l_1 - l_3)D_r - l_0 l_3\right]\lambda_h$		$l_3 D_r < 0$
	PrW_B	$\sigma_{\pi B} \equiv -[A_r C_r + 2B_r D_r]\lambda_s + [A_r l_0 + D_r(2l_1 - l_3)]\lambda_h = 0$		$A_r D_r > 0$
	$\widetilde{MM}_\pi^{(1)}$	$(2B_r + A_r)(C_r + D_r - l_0)\lambda_s + l_0(2l_1 + l_3 - 2B_r - A_r)\lambda_h = 0$		$(2B_r + A_r)l_0 < 0$
RW	$PrW_B^{(1,3)}$	$\sigma_R \equiv \lambda_s - l_1 \lambda_h / B_r = 0$		Generic
PrW_A	PrW_G	$\equiv \left(l_3(\sigma_{0A} + \sigma_{\pi A}) - A_r(\sigma_{\pi A} - \sigma_{0A})\right)/\left(\Sigma_A l_3\right) = 0$		$l_3 D_r < 0$, $A_r^2 < l_3^2$
	3FW(A)	$H_A = 0$		eq. (44).
PrW_B	PrW_G	$\sigma_{BG} \equiv [2l_3 B_r D_r - A_r^2 C_r]\lambda_s + [A_r^2 l_0 - 2l_1 l_3 D_r - l_3 A_r D_r]\lambda_h = 0$		If $A_r D_r < 0$, $A_r^2 - A_r l_3 < 0$,
				If $A_r D_r > 0$, $A_r^2 + A_r l_3 < 0$
	3FW(B)[4]	$H_B = 0$		eq. (55)
PrW_G	3FW	$\Omega^4 - II_G \Omega^2 + D_G = 0$, $\quad T_G \Omega^2 - I_G = 0$		$-$

a 3×3 matrix with determinant D_A, trace T_A and second invariant I_A given below:

$$D_A = -\frac{4}{D_r \Sigma_A^2 l_3} \sigma_{\pi A} \sigma_{0A} (\sigma_{\pi A} - \sigma_{0A}), \qquad (40a)$$

$$T_A = \frac{\Sigma_A^a (\sigma_{\pi A} - \sigma_{0A})}{D_r l_3 \Sigma_A}, \qquad (40b)$$

$$I_A = -\frac{\Delta_+ \sigma_{\pi A}^2 + \Delta_- \sigma_{0A}^2}{D_r l_3 \Sigma_A^2} + \frac{(-4D_r l_3 + \Delta_+ + \Delta_-)}{D_r l_3 \Sigma_A^2} \sigma_{\pi A} \sigma_{0A}. \qquad (40c)$$

Since $-1 < Q < 1$ along the PrW_A branch the quantity $\sigma_{\pi A} - \sigma_{0A} \equiv -2D_r l_3(\lambda_s + \lambda_h)$ cannot vanish along it. As a consequence, D_A only vanishes at the bifurcations to Mixed Modes (defined by $Q = \pm 1$), and no steady state bifurcations occurs within the invariant subspace Σ_{PrW_A} along the branch. The necessary and sufficient conditions for the stability of the branch within its fixed point subspace are $D_A < 0$, $T_A < 0$, $I_A > 0$ and $H_A \equiv I_A - D_A/T_A > 0$. Inspection of eq. (40a) shows that the determinant is negative (resp. positive) whenever $\sigma_{\pi A} - \sigma_{0A} > 0$, which occurs when $l_3 > 0$, $D_r < 0$ (resp. $l_3 < 0$, $D_r > 0$) corresponding to the bifurcation of PrW_A from the MM_π mode (resp. MM_0). Provided that the determinant is negative, then the trace is negative if and only if $\frac{\Sigma_A}{\Sigma_A^a} > 0$. If these two conditions are satisfied, the necessary and sufficient condition of the positivity of the second invariant I_A all along the branch is that $\Delta_+ \geq 0$ and $\Delta_- \geq 0$ (defined in table VI), since $\sigma_{0A}\sigma_{\pi A} \leq 0$

all along the branch. The fourth condition is as follows,

$$0 < H_A \equiv \frac{1}{D_r l_3 \Sigma_A^2}\Big[-\Delta_+ \sigma_{\pi A}^2 - \Delta_- \sigma_{0A}^2 + \sigma_{\pi A}\sigma_{0A}(\Delta_+ + \Delta_- - 4D_r l_3(1 - \Sigma_A/\Sigma_A^a))\Big]. \qquad (41)$$

Thus, if the previous three conditions are satisfied, the necessary and sufficient condition for $H_A > 0$ all along the branch is

$$\left|\left(1 - \frac{\Sigma_A}{\Sigma_A^a}\right) - \frac{\Delta_+ + \Delta_-}{4D_r l_3}\right| \geq -\frac{\sqrt{\Delta_+ \Delta_-}}{2D_r l_3}, \qquad (42)$$

which is immediately satisfied if $0 < \Sigma_A/\Sigma_A^a < 1$. Summarizing, the necessary and sufficient condition for the stability of the branch within the invariant subspace Σ_{PrW_A} all along its existence is

$$\Delta_+ > 0, \quad \Delta_- > 0, \quad 0 < \frac{\Sigma_A^a}{\Sigma_A} < 1, \quad l_3 > 0. \qquad (43)$$

The condition $\frac{\Sigma_A}{\Sigma_A^a} < 1$ can be replaced by eq. (42).

The quantity $H_A(\sigma_{0,A}, \sigma_{\pi,A})$ can be interpreted as the distance to a Hopf bifurcation of the PrW_A branch, which is located at $H_A(\sigma_{0,A}, \sigma_{\pi,A}) = 0$. In particular, because the trace T_A divides D_A, we have at most two Hopf bifurcations. There is a supercritical Hopf from the PrW_A branch leading to a stable 3FW if the following conditions are satisfied:

$$\Delta_+ > 0, \quad \Delta_- > 0, \quad l_3 D_r < 0,$$
$$\frac{\sqrt{\Delta_+ \Delta_-}}{2D_r l_3} \leq \left(1 - \frac{\Sigma_A}{\Sigma_A^a}\right) - \frac{\Delta_+ + \Delta_-}{4D_r l_3} \leq -\frac{\sqrt{\Delta_+ \Delta_-}}{2D_r l_3}. \qquad (44)$$

The case of a single Hopf bifurcation arises when the following two degeneracy conditions hold, $\Delta_-\Delta_+ = 0$ and $\Sigma_A = \Sigma_A^a$. Therefore, whenever eq. (44) is satisfied and $\Delta_+\Delta_- \neq 0$ we have two Hopf bifurcations in the $(\sigma_{0,A}, \sigma_{\pi,A})$ plane, located at

$$
\begin{aligned}
\sigma_{\pi A} &= K_{A,H}^\pm \sigma_{0A}, \\
K^\pm &\equiv \frac{H_A^{0,\pi}}{2\Delta_+} \pm \frac{1}{\Delta_+}\left((H_A^{0,\pi})^2 - 4\Delta_+\Delta_-\right)^{\frac{1}{2}},
\end{aligned}
\tag{45}
$$

with $H_A^{0,\pi}$ defined in eq. (39d).

In the present situation we also need to determine one additional eigenvalue that describes the stability in the $r_2 - r_1$ direction. This eigenvalue, hereafter σ_{AG}, is given by

$$
\begin{aligned}
\sigma_{AG} &\equiv 2P\left(l_3 Q - A_r\right) \\
&= \frac{l_3(\sigma_{0A} + \sigma_{\pi A}) - A_r(\sigma_{\pi A} - \sigma_{0A})}{\Sigma_A l_3}.
\end{aligned}
\tag{46}
$$

A necessary and sufficient condition ensuring the existence of a steady state bifurcation associated with the vanishing of σ_{AG} is that the signs of σ_{AG} at either end of the branch are opposite. This leads to the condition reported in the last column of table IX.

C.   The subspace $\sin\Psi = 0$

The second fixed point subspace corresponds to $\sin\Psi = 0$. At first glance, this subspace corresponds to two distinct cases, $\Psi = 0$ and $\Psi = \pi$. However, because of the symmetry of the polar equations, a jump in Ψ by π is equivalent to a change of sign of either r_1 or r_2. As a consequence, to investigate this subspace, we may set $\Psi = 0$ but allow arbitrary signs r_1 and r_2. Both Mixed Mode solutions belong to this subspace (MM_π corresponds to $\Psi = 0$, $r_2 = -r_1$). The pure modes can also be considered as part of this subspace, even though Ψ is not defined for these branches. Within this subspace, the equations take the form:

$$
\dot{r}_0 = \left[\lambda_s + l_0 r_0^2 + l_1\left(r_1^2 + r_2^2\right) + l_3 r_1 r_2\right]r_0
\tag{47a}
$$

$$
\dot{r}_1 = \left[\ \lambda_h + B_r r_1^2 + (A_r + B_r)r_2^2 + C_r r_0^2\ \right]r_1 \\
+ D_r r_0^2 r_2
\tag{47b}
$$

$$
\dot{r}_2 = \left[\ \lambda_h + B_r r_2^2 + (A_r + B_r)r_1^2 + C_r r_0^2\ \right]r_2 \\
+ D_r r_0^2 r_1
\tag{47c}
$$

$$
\dot{R} = 2\left[\lambda_s + l_0 R + l_1 S + l_3 P\right]R
\tag{48a}
$$

$$
\dot{S} = 2\left[\lambda_h + B_r S + C_r R\right]S \\
+ 4\left[A_r P + D_r R\right]P
\tag{48b}
$$

$$
\dot{P} = 2\left[\lambda_h + B_r S + C_r R\right]P \\
+ \left[A_r P + D_r R\right]S.
\tag{48c}
$$

To detect the existence of Precessing Waves in the present subspace, we look for steady solutions of the above equations. From eqs. (48b) and (48c) we obtain the conditions

$$
\lambda_h + B_r S + C_r R = 0, \qquad A_r P + D_r R = 0.
\tag{49}
$$

The Precessing Waves in question belong to this subspace, leading to

$$
R = r_0^2 = -\frac{A_r}{D_r}\frac{\sigma_{0B} - \sigma_{\pi B}}{4\Sigma_B},
\tag{50a}
$$

$$
P = r_1 r_2 = \frac{\sigma_{0B} - \sigma_{\pi B}}{4\Sigma_B},
\tag{50b}
$$

$$
S = r_1^2 + r_2^2 = -\frac{\sigma_{0B} + \sigma_{\pi B}}{2\Sigma_B},
\tag{50c}
$$

$$
\begin{aligned}
\text{where}\quad & \Sigma_B \equiv B_r(A_r l_0 - D_r l_3) - l_1(A_r C_r) \neq 0, \\
& \sigma_R \equiv \lambda_s - \frac{l_1}{B_r}\lambda_h, \\
& \sigma_{0B} + \sigma_{\pi B} \equiv 2\left[(A_r C_r)\lambda_s + (l_3 D_r - A_r l_0)\lambda_h\right], \\
& \sigma_{0B} - \sigma_{\pi B} \equiv 4B_r D_r \sigma_R.
\end{aligned}
\tag{50d}
$$

These expressions define a single branch of Precessing Waves referred to as the PrW_B branch. One may check that the conditions obtained on imposing $P = 0$ and $S = 2|P|$ yield, respectively, the conditions listed in table IX for the bifurcation from Rotating Waves and the relevant Mixed Mode, confirming that the PrW_B branch connects these two branches. Note that the sign of P is given by $A_r D_r$. So, had we adopted the convention that both r_1 and r_2 are positive and Ψ is either 0 or π we would have arrived at the conclusion that PrW_B is associated with $\Psi = 0$ if $A_r D_r < 0$ and $\Psi = \pi$ if $A_r D_r > 0$. Note that the precession frequency given by eq. (10a) vanishes when $l_2 = 0$. In this case, the resulting mode will actually be singly periodic in the primitive variables, instead of a two-frequency wave. However, this property is not visible when working with the polar variables.

The stability of the PrW_B branch within its invariant subspace $\text{Fix}(\Sigma_{PrW_B})$ can be determined by studying its characteristic polynomial in a similar manner as done for PrW_A in section V B. The invariants of the 3×3 stability matrix are the determinant D_B, trace T_B and I_B given below:

$$
\begin{aligned}
D_B &= -4\Sigma_B R(2P - S)(2P + S) \\
&= \frac{A_r}{D_r \Sigma_B^2}\sigma_{\pi B}\sigma_{0B}\left(\sigma_{\pi B} - \sigma_{0B}\right)
\end{aligned}
\tag{51a}
$$

$$T_B = 2l_0 R + (A_r + 2B_r)\,S$$
$$= \frac{A_r l_0 \big(\sigma_{\pi B} - \sigma_{0B}\big) - D_r(A_r + 2B_r)\big(\sigma_{0B} + \sigma_{\pi B}\big)}{2D_r \Sigma_B}$$
$$\tag{51b}$$

$$I_B = R\big(\Delta_+ (2P + S) + \Delta_- (-2P + S)\big)$$
$$+ 2A_r B_r \big(S^2 - 4P^2\big)$$
$$= \frac{A_r}{4D_r \Sigma_B^2}\big(\Delta_- \sigma_{\pi B}^2 - \Delta_+ \sigma_{0B}^2\big) \tag{51c}$$
$$+ \frac{A_r}{4D_r \Sigma_B^2}\big(8B_r D_r + \Delta_+ - \Delta_-\big)\sigma_{0B}\sigma_{\pi B}\,.$$

The vanishing of σ_R coincides with the origin of the PrW_B branch along the RW branch. Note that the vanishing of σ_R implies $\sigma_{0B} = \sigma_{\pi B}$. Similarly, one of the quantities σ_{0B} or $\sigma_{\pi B}$ vanishes on the termination of the PrW_B branch on one of the mixed modes. One may verify that the third point where D_B vanishes is located outside the existence interval of the branch, confirming that no parity-breaking bifurcation occurs along the branch. In addition, one may confirm that $\sigma_{0B}\sigma_{\pi B} > 0$, except at the termination point.

The necessary conditions for stability within the $\mathrm{Fix}(PrW_B)$ subspace are $D_B < 0$, $T_B < 0$, $I_B > 0$ and $H_B \equiv I_B - D_B/T_B > 0$. From eq. (51a) one may easily verify that the determinant is negative if and only if $\Sigma_B < 0$. Similarly, the trace has constant negative sign if $A_r + 2B_r < 0$ and $l_0 < 0$, which are the conditions for the supercriticality of Standing Waves and the Steady-State mode, respectively. If instead $l_0(A_r + 2B_r) < 0$, then the trace changes sign within the region of existence of the PrW_B solution. Analogously, the necessary conditions for a constant positive sign of the second invariant I_B everywhere along the branch are

$$A_r B_r > 0 \quad \text{and } \Delta_+ > 0 \text{ if } A_r D_r < 0$$
$$\text{or } \Delta_- > 0 \text{ if } A_r D_r > 0\,. \tag{52}$$

The first condition ensures that the second invariant is positive at its birth from the RW branch, while the second condition ensures that I_B is positive at its termination on the corresponding MM branch. To ensure that $I_B > 0$ along the whole PrW_B branch it suffices to have $\Delta_- > -C_+$ if $A_r D_r < 0$, a condition that depends only on Δ_+ and $B_r D_r$, or $\Delta_+ > -C_-$ if $A_r D_r > 0$ for $C_- > 0$, a condition that depends only on Δ_- and $B_r D_r$.

The PrW_B branch is stable when $H_B > 0$. If H_B changes sign along the PrW_B branch a Hopf bifurcation with frequency Ω takes place ($H_B = 0$), characterized by the following set of conditions

$$T_B \Omega^2 - D_B = 0, \qquad \Omega^2 - I_B = 0\,. \tag{53}$$

These equations yield the conditions for the presence of a Hopf bifurcation along the PrW_B branch stated above. In terms of the eigenvalues $\sigma_{0B}(\lambda_s, \lambda_h)$ and $\sigma_{\pi B}(\lambda_s, \lambda_h)$

of the Mixed Modes the Hopf distance H_B is given by

$$H_B \equiv -\frac{A_r}{8D_r^2 \Sigma_B^3}\Big(\Delta_- \Lambda_B^- \sigma_{\pi B}^3 - \Delta_+ \Lambda_B^+ \sigma_{0B}^3$$
$$+ \Big[\Lambda_B^+\big(8B_r D_r - \Delta_-\big) + 2A_r l_0 \Delta_+ - 8D_r \Sigma_B\Big]\sigma_{\pi B}\sigma_{0B}^2$$
$$+ \Big[\Lambda_B^-\big(8B_r D_r + \Delta_+\big) + 2A_r l_0 \Delta_- + 8D_r \Sigma_B\Big]\sigma_{\pi B}^2 \sigma_{0B}\Big)$$
$$\Lambda_B^\pm \equiv D_r(A_r + 2B_r) \pm A_r l_0\,. \tag{54}$$

The condition $H_B = 0$ describes a planar cubic algebraic curve in $(\sigma_{0B}, \sigma_{\pi B})$. A possible procedure is to determine the type of the planar curve isomorphic to one of the five canonical forms [20], and then determine the number of solutions from it. Instead of following this procedure we prefer to provide a sufficient condition for the appearance of a Hopf bifurcation along this branch. Provided eq. (52) holds, the frequency Ω is real, and there exists an odd number (one or three) of Hopf bifurcations whenever H_B has opposite signs at the two endpoints of the branch. This occurs when

$$\Delta_- \Lambda_B^- < 0 \quad (\mathrm{MM}_0), \quad \Delta_+ \Lambda_B^+ > 0 \quad (\mathrm{MM}_\pi)\,. \tag{55}$$

When eq. (55) does not hold the number of Hopf bifurcations is even (none or two). In such a case one can distinguish between the different scenarios using, for instance, the Descartes sign rule for positive roots.

In addition to the three eigenvalues governing the stability of the PrW_B branch within the $\sin\Psi = 0$ subspace discussed above, there is a fourth eigenvalue governing the stability in the orthogonal direction given by

$$\sigma_{BG} = -(2l_3 P - A_r S)\,. \tag{56}$$

The vanishing of this eigenvalue leads to the birth of a branch of General Precessing Waves. The resulting condition in terms of λ_s and λ_h is listed in table IX. A condition ensuring that such a bifurcation occurs somewhere along the branch is that σ_{BG} has opposite signs at its termination points on RW and the relevant MM. This leads to the condition reported in the last column of table IX. This condition is the same as for the bifurcation from PrW_A.

D. The third branch of precessing waves

As demonstrated in the previous sections, two bifurcations can occur along the precessing waves of type A and B giving rise to a precessing wave with no symmetry called PrW_G. Here we investigate this branch as well as its stability. We look for a steady solution of the polar equations with $r_0 \neq 0$, $r_1 \neq r_2$ and $\sin\Psi \neq 0$, cf. Table VIII. The same manipulations as before lead to the following conditions:

$$0 = PQl_3 + Rl_0 + Sl_1 + \lambda_s,$$
$$0 = B_r S + C_r R + \lambda_h,$$
$$0 = A_r P + D_r QR, \tag{57}$$
$$0 = D_r RS + 2P^2 l_3\,.$$

The solution of this system yields the conditions for the presence of the PrW_G branch:

$$
\begin{aligned}
R &= \frac{2B_r\lambda_s - (2l_1 + A_r)\lambda_h}{\Sigma_G}, \\
S &= 2\frac{C_r\lambda_s - l_0\lambda_h}{\Sigma_G}, \\
P &= \frac{-1}{l_3\Sigma_G}\Big(D_r l_3\big(B_r\lambda_s - (2l_1 + A_r)\lambda_h\big)\big(C_r\lambda_s - l_0\lambda_h\big)\Big)^{\frac{1}{2}}, \\
Q &= A_r\Big(\frac{C_r\lambda_s - l_0\lambda_h}{D_r l_3[2B_r\lambda_s - (2l_1 + A_r)\lambda_h]}\Big)^{\frac{1}{2}}, \\
&\text{where } \Sigma_G = C_r(A_r + 2l_1) - 2B_r l_0 \neq 0.
\end{aligned}
\tag{58}
$$

These expressions define a single solution branch. One may check that imposing $Q^2 = 1$ and $S = 2|P|$ yields, respectively, the same conditions as found for the steady bifurcations from the PrW_A and PrW_B branches listed in table IX, confirming that the PrW_G solution indeed links these two branches.

The invariants of the stability matrix are

$$
\begin{aligned}
T_G &= 2Rl_0 + S(A_r + 2B_r) \\
&= \frac{2(\sigma_S(A_r + 2B_r) + l_0\sigma_R)}{\Sigma_G}, \\
D_G &= 8\Sigma_G D_r l_3 R^2(4P^2 - S^2)(Q^2 - 1), \\
&= \frac{32}{\Sigma_G^3 l_3}\sigma_S\sigma_R\left(A_r^2\sigma_S + D_r l_3\sigma_R\right)(D_r\sigma_R + \sigma_S l_3), \\
I_G &= \frac{4A_r}{\Sigma_G^2}\Big(2(B_r - A_r)\sigma_S^2 - D_r^2\sigma_R^2\Big) \\
&\quad + \frac{\sigma_S\sigma_R}{\Sigma_G^2 l_3}\big(4D_r(2A_r B_r - 3l_3^2) + 4l_0 l_3(A_r + 2B_r)\big) \\
&\quad - 4\frac{\sigma_S\sigma_R}{\Sigma_G^2 l_3}\big((A_r + 2l_1)(A_r D_r + C_r l_3)\big) \\
II_G &= -\frac{8}{\Sigma_G^3}\big(D_r^2 l_0\sigma_R^3 + 4A_r^2 B_r\sigma_S^3\big) \\
&\quad + \frac{8D_r\sigma_S\sigma_R^2}{\Sigma_G^3 l_3}\big(2\Sigma_B + l_3(\Sigma_A - 4B_r D_r) - l_0(A_r^2 + l_3^2)\big) \\
&\quad + \frac{8\sigma_S^2\sigma_R}{\Sigma_G^3 l_3}\Big(A_r l_3\Sigma_G - 6B_r D_r l_3^2\Big) \\
&\quad + \frac{8\sigma_S^2\sigma_R}{\Sigma_G^3 l_3}A_r^2\Big(D_r A_r + 2D_r(l_1 - B_r) - 2l_3 l_0\Big).
\end{aligned}
\tag{59}
$$

The determinant D_G only vanishes at the termination points, that is, whenever $Q^2 = 1$ or $S = 2|P|$, which rules out the possibility of a steady state bifurcation. Thus there can only be Hopf bifurcations along the PrW_G branch. The frequency Ω solves the following equations obtained from the characteristic polynomial

$$
\Omega^4 - II_G\Omega^2 + D_G = 0, \qquad T_G\Omega^2 - I_G = 0,
\tag{60}
$$

leading to the following sixth order equation in terms of λ_s and λ_h:

$$
II_G^2 - II_G I_G T_G + T_G^2 D_G = 0.
\tag{61}
$$

E. A robust heteroclinic cycle

The isotropy lattice (see fig. 9) of the degenerate case under discussion suggests the possibility that new heteroclinic cycles may exit. One of the most intriguing possibilities is a connection between the isotropy subspace of Mixed Modes and the subspaces of Precessing Waves A and B, corresponding to a cycle of type C in the classification of Krupa and Melbourne [17]. The conditions for the existence of a robust heteroclinic cycle connecting Mixed Modes consists in demanding that MM_0 is a saddle whose unstable manifold is of dimension one (resp. sink) within Σ_{PrW_B} and a sink (resp. saddle) within Σ_{PrW_A}. Then MM_π would need to be a sink (resp. saddle) within Σ_{PrW_B} and a saddle (resp. sink) within Σ_{PrW_A}. However, for the mixed mode MM_π to be a saddle within Σ_{PrW_A} and the mixed mode MM_0 to be a sink it is necessary that $\sigma_{\pi_A} - \sigma_{0_A} < 0$ with $D_r l_3 < 0$, conditions that indicate that there is a fixed point within the invariant subspace Σ_{PrW_A}, i.e. PrW_A (resp. PrW_B). Despite the existence of a fixed point within the invariant subspace Σ_{PrW_A} (resp. Σ_{PrW_B}), a robust heteroclinic cycle may still exist, cf. [21] In the case of an invariant fixed point subspace of dimension two the existence of heteroclinic cycles relies on the use of the Poincaré-Bendixson theorem, see for instance [18]. In this case the fixed-point subspace is required to be free of any other fixed point other than those connected by the heteroclinic cycle. Instead when the dimension is three, one may use the invariant sphere theorem, or more generally a Lyapunov functional to establish attraction. In our case the presence of a robust heteroclinic cycle requires that the coefficients $C_r \pm D_r$ and $2l_1 \pm l_3$ should both be positive, since otherwise the Precessing Waves A and B are globally attractive except possibly within a ball of size $\mathcal{O}(\lambda_s, \lambda_h)$ in the subspace R, S, P. These conditions are listed in table X. Note that our reasoning does not exclude the existence of a small heteroclinic cycle within the $\mathcal{O}(\lambda_s, \lambda_h)$ ball near PrW, although such a state (if it exists) would require a larger set of defining conditions and would be restricted to a small region of phase space.

If the conditions listed in table X are satisfied then there exists a robust heteroclinic cycle between mixed modes, which bifurcates to a 3FW in the case $A_i - 2l_2 \neq 0$ and $D_i = 0$, and to a PuW or 3FW in the case with $A_i - 2l_2 \neq 0$ and $D_i \neq 0$, see fig. 10. Finally, the application of the theory of Krupa and Melbourne [17] also allows one to establish the existence of heteroclinic cycles between standing waves and mixed modes, whose existence and stability conditions are listed in table X. As for the heteroclinic cycles between mixed modes, these heteroclinic cycles persist in the form of limit cycles of the polar normal form when the degeneracy conditions are not satisfied, see fig. 11.

TABLE X: Defining conditions for structurally and asymptotically stable heteroclinic cycles connecting mixed modes or standing waves and a mixed mode.

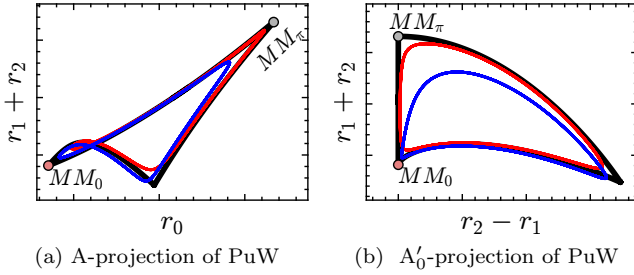| Name of solutions (comments)	Cond. of existence	Asymptotic stability (Asymp. stable if either i-a) or i-b))
$\text{Het}_{MM_0-MM_\pi}$ Stable radial dir. Sink-saddle conditions Non-attractivity of PrW	$\Delta_+ > 0, \quad \Delta_- > 0, l_0 < 0, \quad A_r + 2B_r < 0$ $\sigma_{0A}\sigma_{0B} > 0, \quad \sigma_{\pi A}\sigma_{\pi B} < 0, l_3 D_r < 0, \quad A_r D_r > 0,$ $2l_1 \pm l_3 > 0, \quad C_r \pm D_r > 0$	i-a) $\sigma_{\pi A} + \sigma_{\pi B} < 0,$ i-b) $\sigma_{0A} - \sigma_{0B} > 0$
Het_{SW-MM_π} Stable radial dir. SW saddle in $\text{Fix}(\Sigma_{MM_\pi})$ MM_π saddle in $\text{Fix}(\Sigma_{PrW_B})$	$\Delta_- > 0, l_0 < 0, A_r + 2B_r < 0, A_r > 0$ $\sigma_{SW}^- > 0, \sigma_{SW}^+ < 0$ $\sigma_{\pi A}\sigma_{\pi B} < 0, A_r D_r > 0$	i-a) $2(2B_r + A_r)\lambda_s - (2l_1 - A_r)\lambda_h > 0$ i-b) $\sigma_{\pi A} + \sigma_{\pi B} < 0$
Het_{SW-MM_0} Stable radial dir. SW saddle in $\text{Fix}(\Sigma_{MM_0})$ MM_0 saddle in $\text{Fix}(\Sigma_{PrW_B})$	$\Delta_+ > 0, l_0 < 0, A_r + 2B_r < 0, A_r > 0$ $\sigma_{SW}^- < 0, \sigma_{SW}^+ > 0$ $\sigma_{0A}\sigma_{0B} > 0, A_r D_r < 0$	i-a) $2(2B_r + A_r)\lambda_s - (2l_1 - A_r)\lambda_h > 0$ i-b) $\sigma_{\pi A} - \sigma_{\pi B} > 0$

(a) A-projection of PuW

(b) A_0'-projection of PuW

FIG. 10: Heteroclinic cycle between MM_π and MM_0 in the polar normal form (9) with $A_i - 2l_2 = D_i = \sin\Psi = 0$ (black line) and corresponding results when $A_i - 2l_2 \neq 0$ and $D_i = 0$ (red line) or $D_i \neq 0$ and $A_i - 2l_2 = 0$ (blue line).
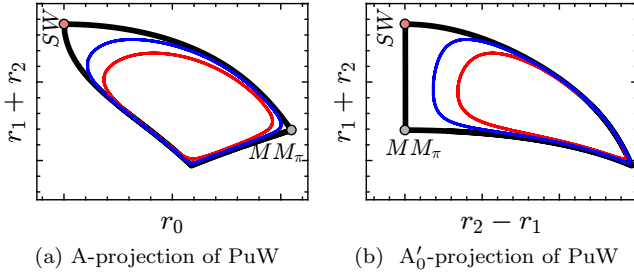

(a) A-projection of PuW

(b) A_0'-projection of PuW

FIG. 11: Heteroclinic cycle (black) between MM_π and SW in the polar normal form (9) with $A_i - 2l_2 = D_i = \sin\Psi = 0$ (black line) and corresponding results with $A_i - 2l_2 \neq 0$ (red line) or $D_i \neq 0$ (blue line).

VI. NUMERICAL EXPLORATION OF THE THIRD-ORDER NORMAL FORM (9)

The section V has shown the existence of multiple fixed points with additional symmetries, e.g. PrW_A and PrW_B, in the degenerate case (equivariant under the group $O(2) \times \mathbb{Z}_2 \times S^1$). The additional $\mathbb{Z}_2$ symmetry is characteristic of mode interactions in $O(2)$ symmetric systems with strong resonance conditions (1:2 [21], 1:3 [22]). Departure from the degeneracy condition $(A_i - 2l_2 = D_i = 0)$ breaks this additional $\mathbb{Z}_2$ symmetry and may be responsible for destroying the Het_{SS-SW} heteroclinic cycle, leading to more complex dynamics. This section is devoted to the numerical exploration of the degenerate case $A_i - 2l_2 = D_i = 0$ and the implications of the departure from this condition ($A_i - 2l_2 \neq 0$ and/or $D_i \neq 0$). For this purpose, we choose generic values for the normal form coefficients, listed in table XI. These coefficients are chosen in such a way that primary bifurcations, i.e., bifurcations leading to SS, SW and RW are supercritical, and the flow is globally stable, that is, there is no finite-time blow-up.

As the bifurcation parameter, we have selected the polar angle θ such that the unfolding parameters are $\lambda_S = \rho\cos\theta$ and $\lambda_H = \rho\sin\theta$, with $\rho = (0, \infty)$ and $\theta \in [0, 2\pi)$. In contrast to [21] the bifurcation diagram barely depends on ρ, and we have fixed the value of ρ at $\rho = 0.5$. The numerical continuation of the polar normal form is carried out with the numerical continuation software MATCONT [23]. In the following, we will show the bifurcation diagrams associated to the degenerate and non-degenerate cases. There are two major differences. First, the two connected branches of symmetric Precessing Waves (PrW_A and PrW_B) are a characteristic feature of the degenerate case (symmetry $O(2) \times \mathbb{Z}_2 \times S^1$). In the non-degenerate case, these two branches split into two disconnected branches of general Precessing Waves PrW_G. Secondly, in the degenerate

TABLE XI: Cubic coefficients of the normal form.

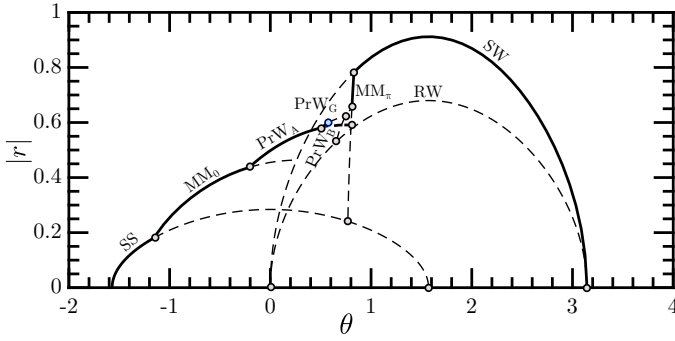| l_0	l_1	l_3	A_r	B_r	C_r	D_r
-6.19	-1.4	-1.7	0.96	-1.08	4	10

FIG. 12: Bifurcation diagram in the degenerate case when $\rho = 0.5$, showing $|r| = \sqrt{r_0^2 + r_1^2 + r_2^2}$ as a function of the angle θ.

case we observe Het_{SS-SW} cycles, which break apart as the orbit intersects the invariant subspace $r_1 = r_2$. Instead, in the non-degenerate case we have identified complex heteroclinic cycles around Het_{PrW_A}. Such a feature was also observed by Porter and Knobloch [21], who concluded that the transition from Het_{SS-SW} cycles to this second set is a characteristic of systems with $O(2) \times \mathbb{Z}_2$ symmetry where the $\mathbb{Z}_2$ symmetry is weakly broken.

A. The degenerate case $A_i - 2l_2 = D_i = 0$

Figure 12 shows the bifurcations of the fixed point branches of the polar normal form with the parameters listed in table XI and the degeneracy conditions $A_i - 2l_2 = D_i = 0$. Along this particular path, the trivial state first loses stability at $\theta = -\pi/2$ in a primary pitchfork bifurcation to the SS mode, which terminates at $\theta = \pi/2$. The SS mode gives birth to the MM_0 branch when $\theta = \arctan(C_r + D_r)/l_0 \approx -1.15$ and to the MM_π branch when $\theta = \arctan(C_r - D_r)/l_0 \approx 0.77$ (table V). The mixed mode MM_0 subsequently produces the PrW_A branch in a symmetry-breaking bifurcation when $\sigma_{0A} = 0$ (table IX) and then terminates on the SW branch. A magnified visualization is displayed in fig. 13(a), where we can observe the PrW_A which terminates on the MM_π branch and eventually gives birth to a general precessing wave PrW_G via a symmetry-breaking bifurcation when $\sigma_{AG} = 0$. The PrW_G mode experiences a Hopf bifurcation that leads to a 3FW (blue point in fig. 12). fig. 14 illustrates a stable periodic orbit (3FW) with a thick black line and the stable manifold of PrW_A with a thin gray line. The existence of a global attractor (PrW_A) in the invariant subspace $r_1 = r_2$ prevents the existence of a true heteroclinic cycle Het_{SS-SW}, but allows the existence of shadowing stable periodic orbits that approximate it, see fig. 14. These orbits exist in $0.52 < \theta < 0.592$ and collapse in a global bifurcation when the limit cycle intersects the invariant subspace $r_1 = r_2$ at $\theta \approx 0.592$. Once a trajectory intersects the $r_1 = r_2$ subspace, it is trapped within it and so is attracted to the only attrac-

tor in this subspace, i.e., the PrW_A state. The same phenomenon occurs in the small region of coexistence of MM_π and the heteroclinic cycle, $0.78 < \theta < 0.82$. The PrW_G branch terminates on the PrW_B branch, which connects RW and MM_π. Finally, the MM_π branch is stable between its endpoint on the SW branch and its symmetry-breaking bifurcation that leads to the PrW_B branch. For $0.82 < \theta \leq \pi$ the only stable state is the SW branch.

B. Non-degenerate case $A_i - 2l_2 = -1$, $D_i = 0.35$

The general picture of the bifurcation scenario, depicted in fig. 12, remains qualitatively unchanged. However, the Precessing Wave branches are modified. We first examine the case when one of the two degeneracy conditions is still satisfied. The case $A_i - 2l_2 = 0$ but $D_i \neq 0$ is illustrated in fig. 13(b) and reveals the existence of two distinct PrW_G branches. This case corresponds to an imperfect bifurcation, where the two symmetry-breaking pitchfork bifurcations leading to the PrW_G branch in the degenerate case are replaced by a saddle-node bifurcation on each branch. The second case, $D_i = 0$ but $A_i - 2l_2 \neq 0$, illustrated in fig. 13(c), shows the presence of PrW_A and PrW_G branches, the latter replacing the symmetric PrW_B branch. These branches connect via a transcritical bifurcation, which is responsible, in this case, for the stability of the whole upper section of the PrW_G branch since no Hopf bifurcation takes place.

We next turn our attention to the non-degenerate case $A_i - 2l_2 \neq 0$, $D_i \neq 0$. The bifurcation diagram of the fixed points of the polar normal form is depicted in fig. 15. The figure displays two disconnected branches of general Precessing Waves PrW_G. The first of these, referred to as $\text{PrW}_{G,1}$ in the figure, becomes unstable through a Hopf bifurcation, leading to a 3FW branch (not shown). The second PrW_G branch, labeled $\text{PrW}_{G,2}$, bifurcates from and terminates on the MM_π branch with a saddle-node bifurcation in between: the upper section is stable, whereas the lower is unstable. Because of the symmetry under reflection κ, there is in fact a pair of such saddle-node bifurcations, $\text{PrW}_{G,2}^{\pm}$, both occurring at $\theta = \theta_{SN} \approx 0.663445$. Moreover, each is of Saddle-Node-in-a-Periodic-Orbit (SNIPER) type but with complex leading eigenvalues at the fold points $\text{PrW}_{G,2}^{\pm}$: $(0, -0.6795, -0.0182 \pm 0.4418i)$. For a study of this situation in the absence of κ symmetry, see [24]. In the presence of this symmetry, this case can either lead to a pair of symmetry-related homoclinics to $\text{PrW}_{G,2}^{\pm}$ or, as in this case, to a heteroclinic cycle connecting $\text{PrW}_{G,2}^{+}$ to $\text{PrW}_{G,2}^{-}$ and vice versa, a consequence of intertwined nature of the stable and unstable manifolds of $\text{PrW}_{G,2}^{\pm}$. In the former case the near-homoclinic orbit to the left of $\text{PrW}_{G,2}^{\pm}$ contains a certain number of decreasing oscillations as it approaches and leaves $\text{PrW}_{G,2}^{\pm}$, the number of

(a) A_i-$2l_2 = 0$, $D_i = 0$ (b) A_i-$2l_2 = 0$, $D_i = 0.35$ (c) A_i-$2l_2 = -1$, $D_i = 0$

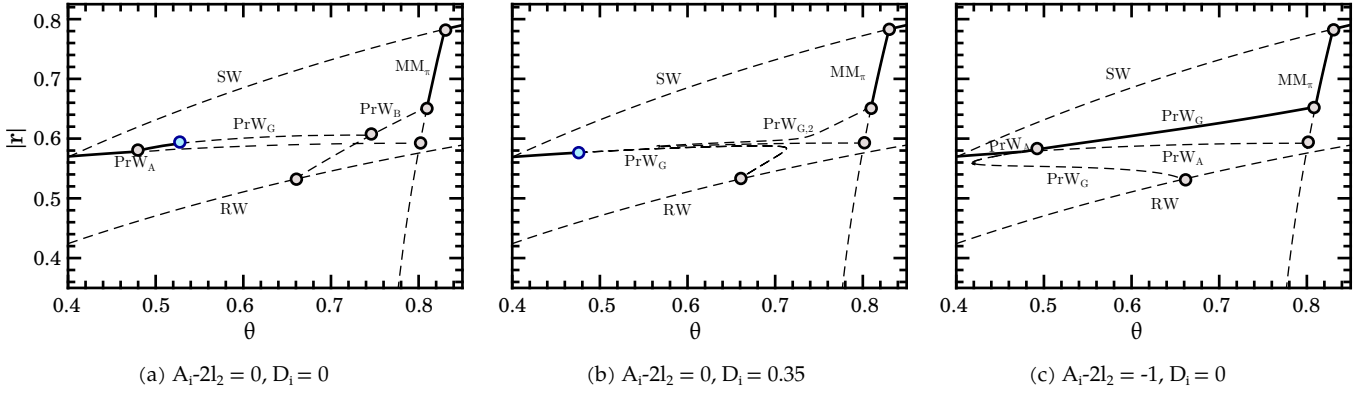FIG. 13: Bifurcation diagram in the degenerate case when $\rho = 0.5$, showing $|r| = \sqrt{r_0^2 + r_1^2 + r_2^2}$ as a function of the angle θ. Legend: Solid (dashed) lines are stable (unstable) fixed points. Symmetry-breaking bifurcations are illustrated with gray points and Hopf bifurcations with blue points. Note: in (a) as well as in fig. 12 the PrW_G branch has been artificially displaced upwards to visually differentiate it from the PrW_A branch.
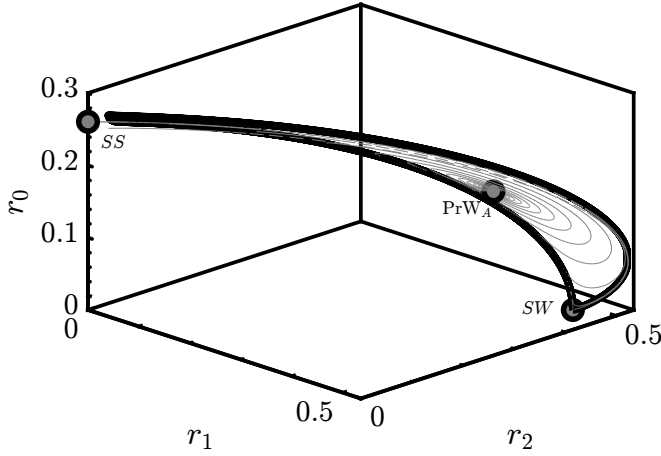
FIG. 14: Example of a heteroclinic cycle SS-SW (thick line). The gray line corresponds to the stable manifold of PrW_A.
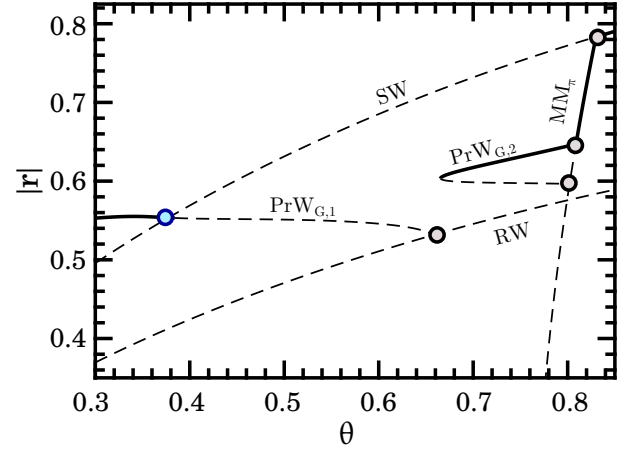

FIG. 15: Bifurcation scenario in the non-degenerate case showing $|r| = \sqrt{r_0^2 + r_1^2 + r_2^2}$ as a function of the angle θ with the same legend as in fig. 13. The end point of $PrW_{G,1}$ is located at $\theta \approx 0.6581$, i.e., below θ_{SN} but above the global bifurcation at $\theta \approx 0.6454$.

these oscillations depending on the speed with which the trajectory passes through the $\mathrm{PrW}_{G,2}^{\pm}$ neighborhood, and hence on the distance of θ from θ_{SN}. In the latter case the unstable manifold associated with the degenerate eigenvalue injects the trajectory into the image fold point and the same local behavior there leads to reinjection back into the original fold, generating a κ-symmetric heteroclinic cycle, cf. [25]. Figure 16 shows such an orbit in two projections, computed for θ just below $\theta_{SN} \approx 0.663445$. At this θ the $\mathrm{PrW}_{G,2}^{\pm}$ points are absent and the orbit shown is actually a long period periodic orbit. Figure 17a shows the period of such orbits as a function of $\theta_{SN} - \theta$, confirming the expected relation $T \sim (\theta_{SN} - \theta)^{-1/2}$. This divergence is a consequence of a slowdown of the trajectory in the vicinity of the phase space location where the $\mathrm{PrW}_{G,2}$ appear when θ increases through θ_{SN}, resulting

in increased accumulation of turns as this point is approached. Note that these orbits inherit the stability of the (upper) $\mathrm{PrW}_{G,2}$ branch (cf. fig. 15) and hence represent attractors of the system.

Figure 18 shows sample attractors found on decreasing θ further. Figure 18a shows a stable symmetric orbit at $\theta = 0.663$, followed by asymmetric chaotic attractors (with a positive Lyapunov exponent) generated with increasing distance from θ_{SN}. The absence of chaotic states near θ_{SN} is a consequence of the fact the flow in this region is locally contracting.

To understand the origin of these states, we examine the behavior of a typical periodic orbit associated with the SNIPER bifurcation. As already explained this orbit depends sensitively on the value of $\theta < \theta_{SN}$. In fig. 19a we show the period T of this orbit as a function of θ
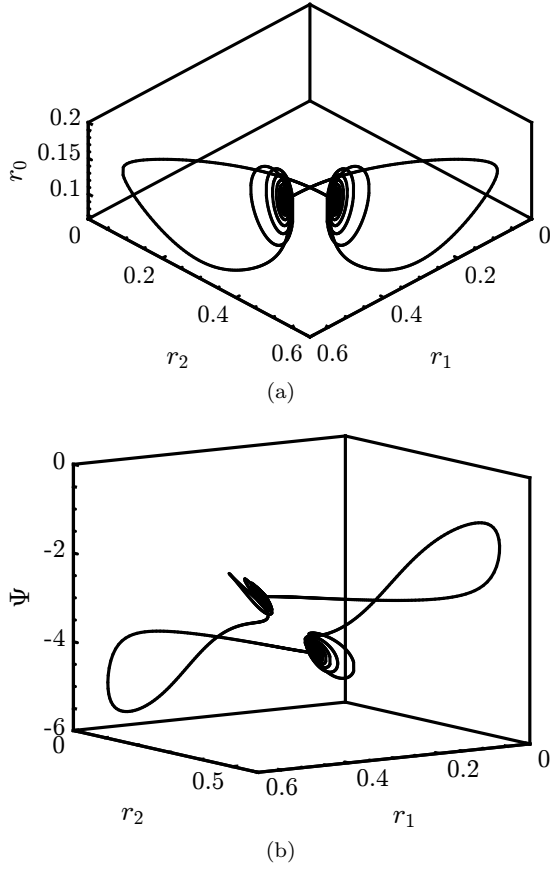
(a)

(b)

FIG. 16: Heteroclinic cycle at $\theta_{SN} \approx 0.663445$.
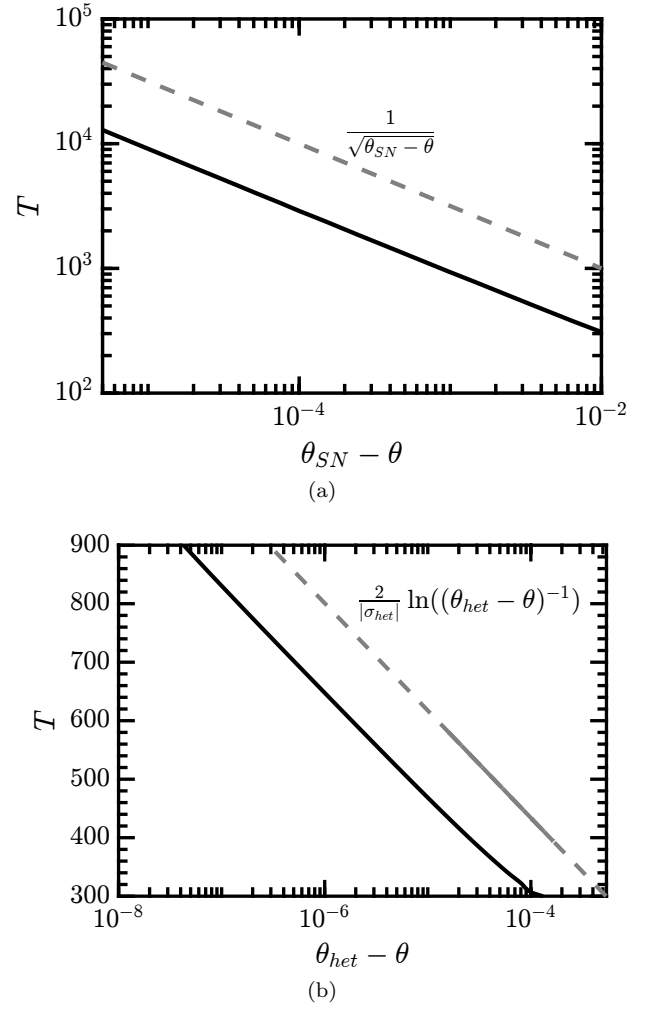

(a)

(b)

FIG. 17: (a) Evolution of the period of the stable limit cycles shadowing the heteroclinic cycle as a function of the distance $\theta_{SN} - \theta$ to the saddle-node bifurcation. (b) Evolution of the period near the heteroclinic bifurcation at θ_{het}, where $\sigma_{het} = -0.0251$ is the leading stable eigenvalue of the $\mathrm{PrW}_{G,1}$ fixed point.

obtained using numerical continuation. This period diverges as $\theta \to \theta_{SN}$ from below and the orbit approaches the heteroclinic cycle shown in fig. 16. As θ deceases the period T decreases, although this decrease is interrupted by a series of back-to-back folds. Each such pair is responsible for the elimination of one small amplitude turn of the trajectory (not shown), resulting in a gradual unwinding of the trajectory. As θ decreases towards the leftmost fold and beyond, the trajectory develops small loops in the vicinity of $\mathrm{PrW}_{G,1}$ (fig. 20) and its period begins to diverge again, this time logarithmically (fig. 17b), indicating approach to a heteroclinic connection involving $\mathrm{PrW}_{G,1}$ and located at $\theta = \theta_{het} \approx 0.6454$. Since the leading unstable eigenvalues of $\mathrm{PrW}_{G,1}$ at this parameter values are complex, $0.2446 \pm 0.3661i$, while the leading stable eigenvalue is real, -0.0251, these points are both saddle-foci. The complex unstable eigenvalues account for the oscillatory approach to the global bifurcation at $\theta \approx 0.6454$ while the fact that the flow near $\mathrm{PrW}_{G,1}$ is locally expanding implies that we should expect stable chaotic dynamics near this parameter value, as in the classical example of Shil'nikov where the signs of the eigenvalues are reversed [26–28].

In fig. 19a the solid line tracks the period of the κ-symmetric orbit. As $\theta \to 0.6454$ from above, this orbit collides with $\mathrm{PrW}_{G,1}$, forming a heteroclinic con-

nection from $\mathrm{PrW}_{G,1}$ to its image under κ and back again. Near θ_{het} this orbit is accompanied by back-to-back symmetry-breaking bifurcations, generating asymmetric periodic orbits (fig. 19b). These asymmetric orbits are free to period-double into chaos, resulting in 'bubbles' of chaotic behavior, as described in [29] and references therein. Close to the primary heteroclinic bifurcation these bubbles 'burst' via the formation of pairs of subsidiary homoclinic orbits. The red dashed and thin solid lines in fig. 19b show examples of this generic behavior in our problem; fig. 19c compares the homoclinic orbit at the green dashed asymptote with the corresponding period-doubled orbit on the red dashed branch at the same θ value. Further details are omitted. Thus, the primary symmetric periodic orbit is associated with a number of chaotic intervals located around subsidiary homo-
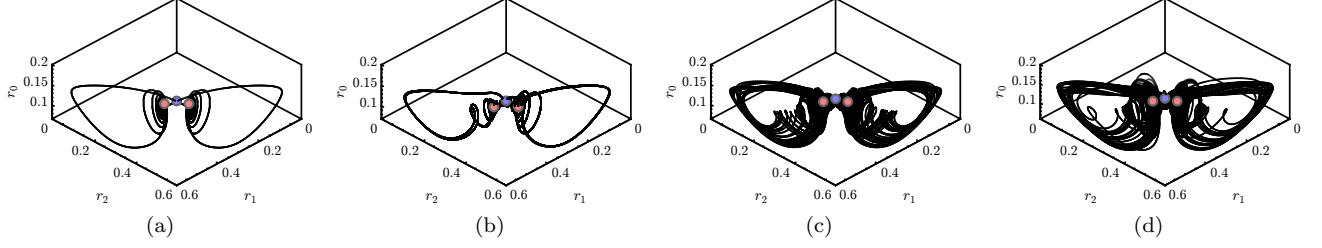
FIG. 18: Stable attractors in a (r_0, r_1, r_2) projection for (a) $\theta = 0.663$ (symmetric periodic orbit); (b) $\theta = 0.647$ (asymmetric orbit); (c) $\theta = 0.645$ (asymmetric orbit); (d) $\theta = 0.643$ (asymmetric orbit). The symmetry-related $\mathrm{PrW}_{G,2}$ fixed points corresponding to the saddle-node at $\theta \approx 0.663445$ are indicated by red points, with the PrW_A point (present in the degenerate case only) depicted as a blue point; these are shown for orientation only.

clinic orbits originating in global bifurcations of asymmetric orbits associated with it, cf. fig. 18. In particular, stable chaotic motion is also observed for θ *below* the primary heteroclinic bifurcation at $\theta_{het} \approx 0.6454$.

We mention that the periodic orbit originating from the Hopf point on the $\mathrm{PrW}_{G,1}$ branch ($\theta \approx 0.3841$, blue point in Fig 15) is stable from the Hopf point to $\theta \approx 0.4518$, where the first of several Neimark-Sacker bifurcations takes place. These are interspersed with additional global bifurcations and intervals of chaos as θ increases towards $\theta_{het} \approx 0.6454$. Some sample solutions are shown in fig. 21 to whet appetite. The details depend on the parameters used and are omitted.

VII. NORMAL FORM REDUCTION

The process of reducing the governing equations to normal form near a multiple bifurcation is based on center manifold reduction followed by a series of near-identity variable changes to simplify the dynamical equations on the center manifold. The resulting equations are then *unfolded* by introducing parameters that break apart the multiple bifurcation in a generic way. In infinite-dimensional problems, such as those arising in fluid mechanics, it is preferable to employ multiple scales techniques to compute both the normal form and the coefficients within it as part of the same calculation. We employ here this technique to determine all the coefficients in the third-order normal form (8).

First, let us introduce the following formal expression for the governing equations on a domain Ω:

$$\begin{aligned} \mathbf{B}\frac{\partial \mathbf{q}}{\partial t} &= \mathbf{F}(\mathbf{q}, \boldsymbol{\eta}) \equiv \mathbf{L}\mathbf{q} + \mathbf{N}(\mathbf{q}, \mathbf{q}) + \mathbf{G}(\mathbf{q}, \boldsymbol{\eta}), \ \mathbf{x} \in \Omega, \\ \mathbf{D}_{bc}\mathbf{q}(\mathbf{x}) &= \mathbf{q}_{\partial\Omega}, \ \mathbf{x} \in \partial\Omega. \end{aligned}$$
(62)

Here $\partial\Omega$ represents the domain boundary. This form of the governing equations takes into account a linear dependence on the state variable $\mathbf{q}$ through $\mathbf{L}$ and a quadratic dependence on state variable and the parameters $\boldsymbol{\eta}$ through the operators $\mathbf{G}(\cdot,\cdot)$ and $\mathbf{N}(\cdot,\cdot)$. Equation (62) formally includes the incompressible Navier–Stokes equations written in cylindrical coordinates for the TFC and WFA problems, whereas for WFA-MC one must consider the Boussinesq approximation of the incompressible Navier–Stokes equations written in cylindrical coordinates as well. The set of parameters $\boldsymbol{\eta} \in \mathbb{R}^{N_p}$, where N_p is the number of parameters, is composed of the two dimensionless angular velocities of the cylindrical annulus for TFC, the Reynolds number for WFA and the Reynolds, Richardson and Prandtl numbers for WFA-MC. In the following, we will consider the most general case, that is, the WFA-MC case where the vector of parameters takes the form $\boldsymbol{\eta} \equiv [\eta_0, \eta_1, \eta_2]^T$. Finally, without loss of generality, we suppose that the dependence of the solution on the trace (solution restricted to the boundary of the domain) is linear, i.e. we take $\mathbf{D}_{bc}$ to be a linear boundary condition operator. One can also consider the dependence of the boundary conditions on parameters, that is either $\mathbf{D}_{bc}(\boldsymbol{\eta})$ or $\mathbf{q}_{\partial\Omega}(\boldsymbol{\eta})$, which may be used, for instance, for modeling of a moving wall. For the sake of simplicity and without loss of generality, this case is not considered.

A. Multiple scales Ansatz

The multiple scales expansion of the solution $\mathbf{q}$ of eq. (62) consists of an expansion of eq. (1) in powers of a small parameter $\varepsilon \ll 1$:

$$\mathbf{q}(t, \tau) = \mathbf{Q}_0 + \varepsilon \mathbf{q}_{(\varepsilon)}(t, \tau) + \varepsilon^2 \mathbf{q}_{(\varepsilon^2)}(t, \tau) + O(\varepsilon^3) \quad (63)$$

Parameters $\boldsymbol{\eta}$ are assumed to be of second order, i.e. $\eta_i = O(\varepsilon^2)$ for $i = 0, 1, 2$. The expansion (63) encompasses a two-scale expansion of the original time, $t \mapsto t + \varepsilon^2\tau$, that incorporates the fast time scale t of the self-sustained instability and the slow time scale τ of the evolution of the amplitudes $a_i(\tau)$ in eq. (1), for $i = 0, 1, 2$. The resulting expansion of the left side of eq. (62) up to third order is as follows:

$$\varepsilon \mathbf{B}\frac{\partial \mathbf{q}_{(\varepsilon)}}{\partial t} + \varepsilon^2 \mathbf{B}\frac{\partial \mathbf{q}_{(\varepsilon^2)}}{\partial t} + \varepsilon^3 \left[\mathbf{B}\frac{\partial \mathbf{q}_{(\varepsilon^3)}}{\partial t} + \mathbf{B}\frac{\partial \mathbf{q}_{(\varepsilon)}}{\partial \tau}\right] \quad (64)$$

(a)

(b)

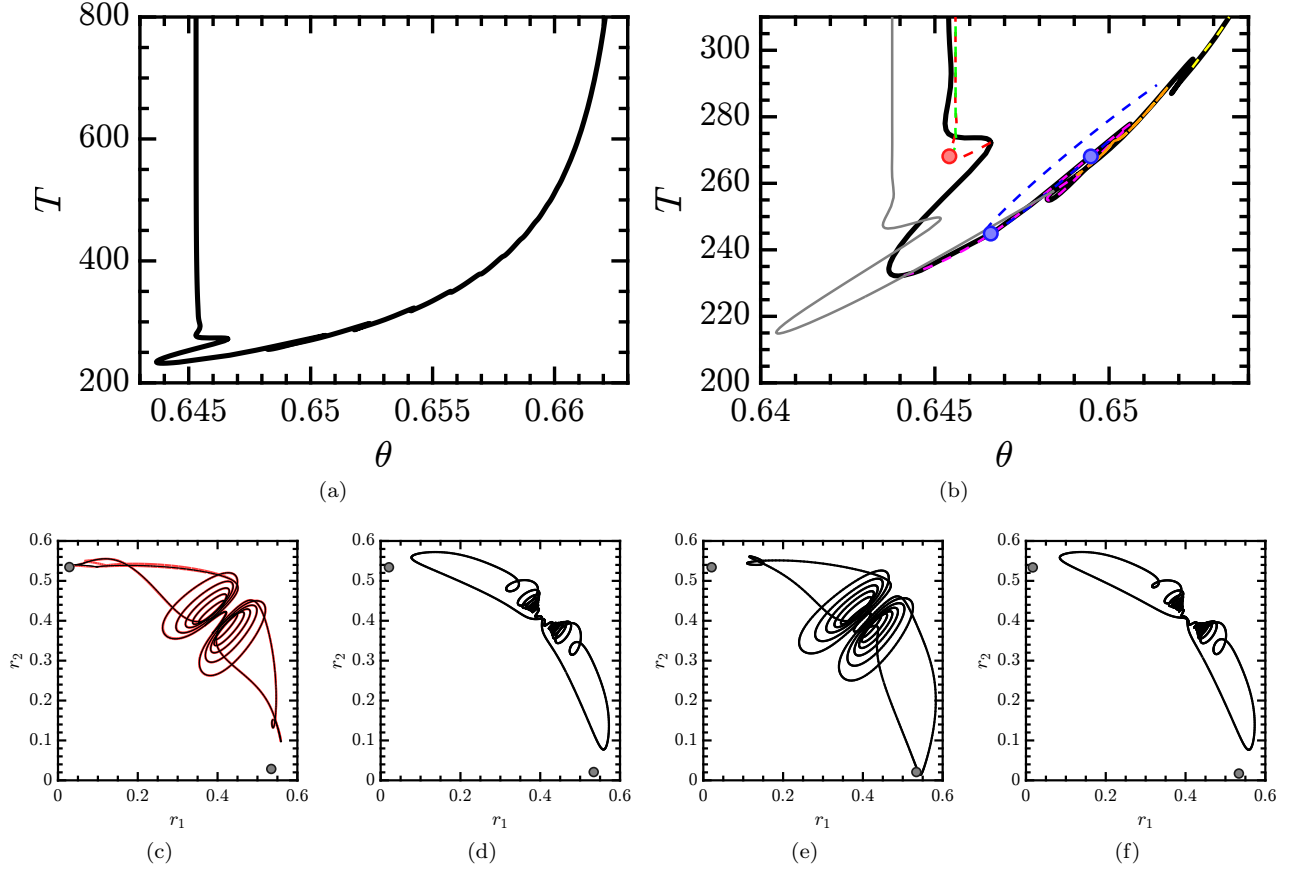(c)   (d)   (e)   (f)

FIG. 19: (a) Evolution of the period T of a symmetric periodic orbit born in the SNIPER bifurcation $\theta \approx 0.663445$ and terminating in a heteroclinic bifurcation at $\theta \approx 0.6454$ (thick solid line). Secondary branches of asymmetric states are displayed in thin lines: solid line for the branch whose period diverges at $\theta \approx 0.64377$ and dashed lines for the other branches, see panel (b) for more detail. The secondary branches are accompanied by back-to-back period-doubling cascades (three period-doubling points are indicated with solid circles of the same color as the branch) which open up via the formation of subsidiary homoclinic orbits as in panel (c), black line; the superposed red curve shows an accompanying period-doubled solution. Portraits (d-f) display the (r_1, r_2) projection at $\theta = 0.65$ for the dashed magenta, blue, and orange branches showing a symmetric and two asymmetric periodic orbits, respectively. The location of $\mathrm{PrW}_{G,1}$ is indicated with small circle in (c-f). Only (c) is close to homoclinic; the proximity of orbit (e) to the lower fixed point is a projection effect.
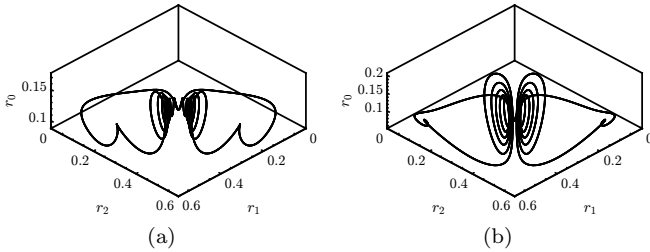

(a)   (b)

FIG. 20: The periodic orbit at the seventh and eighth folds from the right, with a period-doubling bubble in between (not shown). (a) $\theta = 0.6437$. (b) $\theta = 0.6466$.

while the right side is

$$\mathbf{F}(\mathbf{q}, \boldsymbol{\eta}) = \mathbf{F}_{(0)} + \varepsilon \mathbf{F}_{(\varepsilon)} + \varepsilon^2 \mathbf{F}_{(\varepsilon^2)} + \varepsilon^3 \mathbf{F}_{(\varepsilon^3)} . \qquad (65)$$

The expansion eq. (65) will be detailed at each order.

1. Order ε^0

The leading order solution $\mathbf{Q}_0$ of the multiple scales expansion eq. (63) is the steady state of the governing equations evaluated at the threshold of instability, i.e. $\boldsymbol{\eta} = \mathbf{0}$,

$$\begin{aligned} \mathbf{0} &= \mathbf{F}(\mathbf{Q}_0, \mathbf{0}) , \quad \mathbf{x} \in \Omega , \\ \mathbf{D}_{bc} \mathbf{Q}_0(\mathbf{x}) &= \mathbf{Q}_{0,\partial\Omega} , \quad \mathbf{x} \in \partial\Omega . \end{aligned} \qquad (66)$$
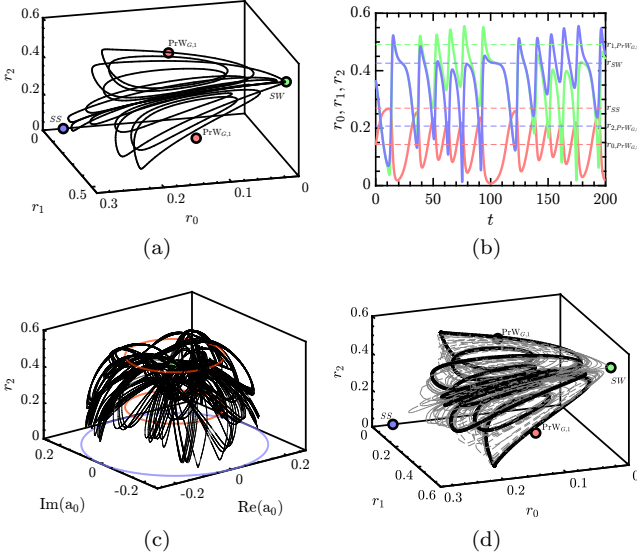
FIG. 21: (a) Phase portrait of a near-homoclinic orbit to the SW state in the (r_0, r_1, r_2) space at $\theta = 0.452$, and (b) the corresponding time series showing $r_0(t)$ (red), $r_1(t)$ (green) and $r_2(t)$ (blue). Near the homoclinic connection r_1 approaches r_2 and r_0 falls to zero. (c) A trajectory at $\theta = 0.457$ in the $(\mathrm{Re}(a_0), \mathrm{Im}(a_0), r_2)$ space showing that the trajectory intermittently visits SW states with different phases ϕ, each visit resulting in a switch between an oscillation about one $\mathrm{PrW}_{G,1}$ state to an oscillation about the other; red circles represent the group orbit of the two $\mathrm{PrW}_{G,1}$ states while the blue circle represents the group orbit of the SS states [30]. (d) Chaotic attractor at $\theta = 0.49$ (thin dashed grey line) together with an (unstable) κ-symmetric periodic orbit computed at $\theta \approx 0.4896$.

2. Order ε^1

The first order correction $\mathbf{q}_{(\varepsilon)}(t, \tau)$ in the multiple scales expansion of eq. (63) is composed of the eigenmodes of the linearized system

$$\mathbf{q}_{(\varepsilon)}(t, \tau) \equiv \mathrm{Re}\left(a_0(\tau)e^{-im_0\theta}\hat{\mathbf{q}}_0\right)$$
$$+ \mathrm{Re}\left(a_1(\tau)e^{-i\omega t}e^{-im_1\theta}\hat{\mathbf{q}}_1\right) \quad (67)$$
$$+ \mathrm{Re}\left(a_2(\tau)e^{-i\omega t}e^{i-m_2\theta}\hat{\mathbf{q}}_2\right),$$

where the reflection symmetry in $O(2)$ imposes the requirement $m_2 = -m_1$.

Each term $\hat{\mathbf{q}}_\ell$ in the first order expansion (67) solves the corresponding linear problem:

$$\mathbf{J}_{(\omega_\ell, m_\ell)}\hat{\mathbf{q}}_\ell = \left(i\omega_\ell\mathbf{B} - \frac{\partial\mathbf{F}}{\partial\mathbf{q}}|_{\mathbf{q}=\mathbf{Q}_0, \boldsymbol{\eta}=0}\right)\hat{\mathbf{q}}_\ell, \quad \mathbf{x} \in \Omega,$$
$$\mathbf{D}_{bc}\hat{\mathbf{q}}_\ell(\mathbf{x}) = 0, \quad \mathbf{x} \in \partial\Omega,$$
$$(68)$$

where $\frac{\partial\mathbf{F}}{\partial\mathbf{q}}|_{\mathbf{q}=\mathbf{Q}_0, \boldsymbol{\eta}=0}\hat{\mathbf{q}}_\ell = \mathbf{L}_{m_\ell}\hat{\mathbf{q}}_\ell + \mathbf{N}_{m_\ell}(\mathbf{Q}_0, \hat{\mathbf{q}}_\ell) + \mathbf{N}_{m_\ell}(\hat{\mathbf{q}}_\ell, \mathbf{Q}_0)$. The subscript m_ℓ indicates the azimuthal wavenumber used for the evaluation of the operator.

3. Order ε^2

The second order expansion term $\mathbf{q}_{(\varepsilon^2)}(t, \tau)$ is determined from the resolution of a set of forced linear systems, where the forcing terms are evaluated from first and zeroth order terms. The expansion in terms of amplitudes $a_i(\tau)$ of $\mathbf{q}_{(\varepsilon^2)}(t, \tau)$ is assessed from term-by-term identification of the forcing terms at the second order. The nonlinear second order terms are

$$\mathbf{F}_{(\varepsilon^2)} \equiv \sum_{j,k=0}^{2}\left(a_j a_k\mathbf{N}(\hat{\mathbf{q}}_j, \hat{\mathbf{q}}_k)e^{-i(m_j+m_k)\theta}e^{-i(\omega_j+\omega_k)t} + \mathrm{c.c.}\right)$$
$$+ \sum_{j,k=0}^{2}\left(a_j\overline{a}_k\mathbf{N}(\hat{\mathbf{q}}_j, \overline{\hat{\mathbf{q}}}_k)e^{-i(m_j-m_k)\theta}e^{-i(\omega_j-\omega_k)t} + \mathrm{c.c.}\right)$$
$$+ \sum_{\ell=0}^{2}\eta_\ell\mathbf{G}(\mathbf{Q}_0, \mathbf{e}_\ell),$$
$$(69)$$

where $\mathbf{e}_\ell$ is an element of the orthonormal basis of $\mathbb{R}^{N_p}$, a vector composed of zeros except at the position ℓ where it is equal to unity.

Since no quadratic combination of elements in eq. (67) results in resonant terms, the second order term can be expanded as

$$\mathbf{q}_{(\varepsilon^2)} \equiv \sum_{\substack{j,k=0 \\ k \leq j}}^{2}\left(a_j a_k\hat{\mathbf{q}}_{j,k} + a_j\overline{a}_k\hat{\mathbf{q}}_{j,-k} + \mathrm{c.c.}\right) + \sum_{\ell=0}^{2}\eta_\ell\mathbf{Q}_0^{(\eta_\ell)},$$
$$(70)$$

with the rules $\hat{\mathbf{q}}_{j,k} = \hat{\mathbf{q}}_{k,j}$ and $\hat{\mathbf{q}}_{-j,-k} = \overline{\hat{\mathbf{q}}}_{j,k}$. Note the slight abuse of notation with $\hat{\mathbf{q}}_{-0} = \overline{\hat{\mathbf{q}}}_0$. Terms $\hat{\mathbf{q}}_{j,j}$ are harmonics of the flow, $\hat{\mathbf{q}}_{j,k}$ with $j \neq k$ are coupling terms, $\hat{\mathbf{q}}_{j,-j}$ are harmonic base flow modification terms and $\mathbf{Q}_0^{(\eta_\ell)}$ are base flow corrections due to the assumed departure of the parameter η_ℓ from the critical point measured by ε.

Finally, the second-order terms are computed by solving the following nonresonant system of equations,

$$\mathbf{J}_{(\omega_j+\omega_k, m_j+m_k)}\hat{\mathbf{q}}_{j,k} = \hat{\mathbf{F}}_{(\varepsilon^2)}^{(j,k)}, \quad (71)$$

where $\hat{\mathbf{F}}_{(\varepsilon^2)}^{(j,k)} \equiv \mathbf{N}(\hat{\mathbf{q}}_j, \hat{\mathbf{q}}_k) + \mathbf{N}(\hat{\mathbf{q}}_k, \hat{\mathbf{q}}_j)$ and

$$\mathbf{J}_{(0,0)}\mathbf{Q}_0^{(\eta_\ell)} = \mathbf{G}(\mathbf{Q}_0, \mathbf{e}_\ell). \quad (72)$$

4. Order ε^3

At third order resonant terms are generated and these lead to secular (nonperiodic) terms in the expansion. We eliminate these terms by imposing a solvability condition on the system via the Fredholm alternative. This condition determines the required normal form at third order in ε. Specifically, the linear terms λ_s and λ_h are

determined as follows

$$\lambda_s = \frac{\langle \hat{\mathbf{q}}_0^\dagger, \hat{\mathbf{F}}_{(\epsilon^3)}^{(a_0)} \rangle}{\langle \hat{\mathbf{q}}_0^\dagger, \mathbf{B}\hat{\mathbf{q}}_0 \rangle}, \quad \lambda_h = \frac{\langle \hat{\mathbf{q}}_1^\dagger, \hat{\mathbf{F}}_{(\epsilon^3)}^{(a_1)} \rangle}{\langle \hat{\mathbf{q}}_1^\dagger, \mathbf{B}\hat{\mathbf{q}}_1 \rangle} = \frac{\langle \hat{\mathbf{q}}_2^\dagger, \hat{\mathbf{F}}_{(\epsilon^3)}^{(a_2)} \rangle}{\langle \hat{\mathbf{q}}_2^\dagger, \mathbf{B}\hat{\mathbf{q}}_2 \rangle}, \quad (73)$$

while the (real) cubic coefficients l_i for $i = 0, 1, 2, 3$ are given by

$$l_0 = \frac{\langle \hat{\mathbf{q}}_0^\dagger, \hat{\mathbf{F}}_{(\epsilon^3)}^{(a_0|a_0|^2)} \rangle}{\langle \hat{\mathbf{q}}_0^\dagger, \mathbf{B}\hat{\mathbf{q}}_0 \rangle}, \qquad l_3 = \frac{\langle \hat{\mathbf{q}}_0^\dagger, \hat{\mathbf{F}}_{(\epsilon^3)}^{(\bar{a}_0 a_1 \bar{a}_2)} \rangle}{\langle \hat{\mathbf{q}}_0^\dagger, \mathbf{B}\hat{\mathbf{q}}_0 \rangle}$$
$$l_1 - il_2 = \frac{\langle \hat{\mathbf{q}}_0^\dagger, \hat{\mathbf{F}}_{(\epsilon^3)}^{(a_0|a_1|^2)} \rangle}{\langle \hat{\mathbf{q}}_0^\dagger, \mathbf{B}\hat{\mathbf{q}}_0 \rangle}, \quad l_1 + il_2 = \frac{\langle \hat{\mathbf{q}}_0^\dagger, \hat{\mathbf{F}}_{(\epsilon^3)}^{(a_0|a_2|^2)} \rangle}{\langle \hat{\mathbf{q}}_0^\dagger, \mathbf{B}\hat{\mathbf{q}}_0 \rangle}.$$
$$(74)$$

Finally, the complex coefficients A, B, C and D are given by

$$B = \frac{\langle \mathbf{q}_1^\dagger, \hat{\mathbf{F}}_{(\epsilon^3)}^{(a_1|a_1|^2)} \rangle}{\langle \hat{\mathbf{q}}_1^\dagger, \mathbf{B}\hat{\mathbf{q}}_1 \rangle}, \quad A + B = \frac{\langle \mathbf{q}_1^\dagger, \hat{\mathbf{F}}_{(\epsilon^3)}^{(a_1|a_2|^2)} \rangle}{\langle \hat{\mathbf{q}}_1^\dagger, \mathbf{B}\hat{\mathbf{q}}_1 \rangle},$$
$$C = \frac{\langle \mathbf{q}_1^\dagger, \hat{\mathbf{F}}_{(\epsilon^3)}^{(a_1|a_0|^2)} \rangle}{\langle \hat{\mathbf{q}}_1^\dagger, \mathbf{B}\hat{\mathbf{q}}_1 \rangle}, \quad D = \frac{\langle \mathbf{q}_1^\dagger, \hat{\mathbf{F}}_{(\epsilon^3)}^{(a_0^2 a_2)} \rangle}{\langle \hat{\mathbf{q}}_1^\dagger, \mathbf{B}\hat{\mathbf{q}}_1 \rangle}.$$
$$(75)$$

The forcing terms associated with solvability conditions eqs. (73) to (75) are detailed in appendix A 1.

VIII. CONSTRUCTION OF BIFURCATION DIAGRAMS

We now explain how the results derived in the previous section can be used to construct consistent bifurcation diagrams. The method is similar to that used in Hirschberg & Knobloch [3] and is explained in fig. 22. As illustrated in this figure, the conditions for the occurrence of the various bifurcations can be interpreted as lines in the (λ_s, λ_h) plane. For example, the primary steady-state bifurcation occurs along the line $\lambda_s = 0$, which is the horizontal axis in this representation. Similarly, the primary Hopf bifurcation occurs along the line $\lambda_h = 0$, which is the vertical axis. The conditions relevant to the birth of mixed modes also correspond to straight lines, as displayed in the figure. For both the wake problem (WFA or WFA-MC) and the TCF problem, variation of the base-flow parameters defines a path in the (λ_s, λ_h) plane. The bifurcation diagram can then be constructed by considering the successive crossings of this path with the lines defining the bifurcations.

Let us consider first the bifurcation scenario of the WFA-MC case as a function of Reynolds numbers η_{Re} and η_{Ri}, at a constant distance in terms of the second parameter from the organizing centre. We denote by $\eta_{Re}|_{Ri=Ri_c}$ the path followed at a constant Richardson number equal to that at which the unsteady and steady modes become simultaneously unstable, i.e., at the same critical Reynolds number. Similarly, we denote by $\eta_{Re}|_{Ri=0}$ the straight line path from quadrant III (defined by $\lambda_s < 0$, $\lambda_h < 0$), traversing quadrant IV ($\lambda_s > 0$,

$\lambda_h < 0$), and then crossing into quadrant I ($\lambda_s > 0$, $\lambda_h > 0$). This path is relevant to the wake problem (WFA) for increasing the Reynolds number if we assume a linear dependence of the form eq. (13). When following this path, the first bifurcation is the primary bifurcation leading to the SS mode. There are two possible secondary bifurcations on this branch, leading to MM_0 and MM_π and these occur along the lines $-l_0\lambda_h + (C_r \pm D_r)\lambda_s = 0$ with positive sign for MM_0 and negative sign for MM_π. The sign of D_r indicates which of these bifurcations occurs first along the given path. For example, if $D_r < 0$, as displayed on the figure, the bifurcation to MM_π occurs first. Moreover, if $\Delta_- > 0$ (as assumed in the figure), this bifurcation is supercritical and gives rise to a stable branch. The bifurcation from SS to MM_π may occur subsequently, as found in the figure, but the branch born at this bifurcation is necessarily unstable, according to the considerations in section IV C.

Similarly, the lines $-(2B_r + A_r)\lambda_s + (l_1 \pm l_3)\lambda_h = 0$ indicate secondary bifurcations from SW to MM_0 (positive sign) and MM_π (negative sign). Starting from the pure SW mode and following the prescribed path backward, the sign of l_3 lets us distinguish which of these lines will be crossed first. For example, if $l_3 < 0$, as displayed on the figure, the bifurcation to MM_π occurs first, leading to a stable branch if $\Delta > 0$.

Figure 22b exhibits the case corresponding to $l_3 < 0$, $D_r < 0$, $\Delta_+ > 0$, $\Delta_- > 0$, the situation relevant to wake flow past a fixed disk. The figure displays the bifurcation diagram for a disk of aspect ratio $\chi = 10$. For more details, see section VIII B.

In the following we analyze the predicted transition behavior of the for flow past a fixed sphere and a fixed disk.

A. Mixed convection in the flow past a sphere

Let us revisit the problem of pattern formation behind a sphere falling through a stratified fluid. In our formulation the sphere is held fixed, with flow past it (the WFA-MC problem). This problem has many practical applications in engineering such as cooling, heating [31], sedimentation [32], melting [33], combustion [34], vaporization [35]. A heated sphere represents a heat source embedded within the physical domain, where the solid body is subjected to forces of hydrodynamic and thermal origin. There are two main cases of interest, the case of a hot falling sphere where the fluid within the wake is accelerated with respect to the spherical body. Such a configuration is called *assisting flow*. The opposite case, where the wake of a hot ascending spherical particle is decelerated by buoyancy effects, is referred to as *opposing flow*. Kotouc et al. [31] studied numerically both configurations for two Prandtl numbers, $Pr = 0.72$ and $Pr = 7$. The assisting flow case displays an organising center of Hopf-Hopf type with azimuthal wavenumbers $m = 1$ and $m = 2$. The opposing flow configuration ex-
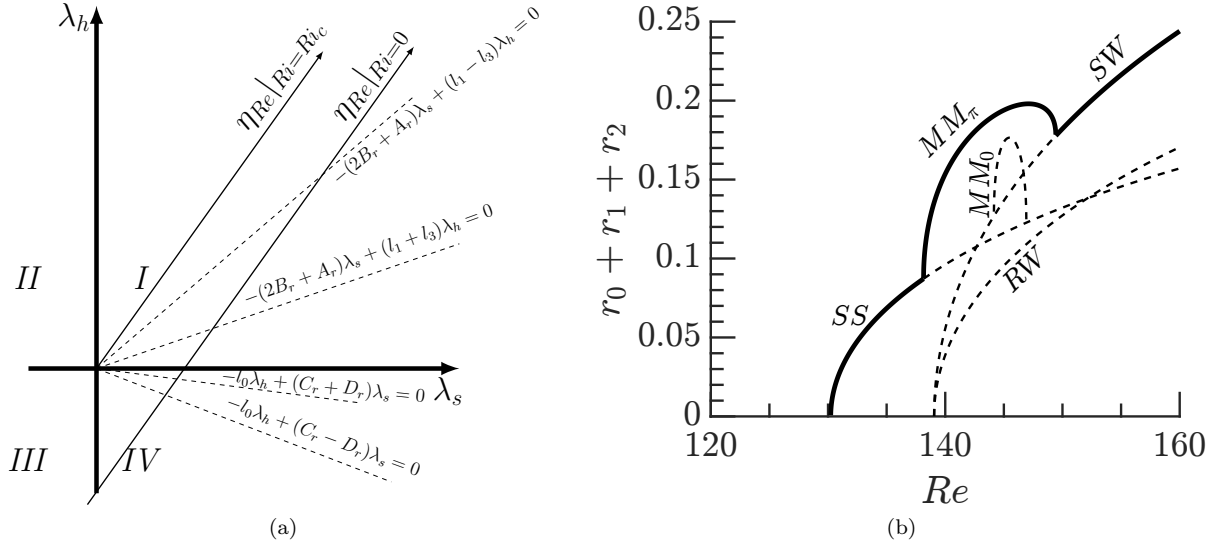
FIG. 22: Illustration of the construction of the stability diagram for the WFA problem with a fixed disk of aspect ratio $\chi = 10$. (a) The unfolding plane (λ_s, λ_h). Dashed lines indicate the loci of bifurcations from SS and SW to $MM_{0,\pi}$. The paths labeled $\eta_{Re}|_{Ri=Ri_c}$ and $\eta_{Re}|_{Ri=0}$ are the paths followed in this plane for $Ri = Ri_c$ and $Ri = 0$, respectively. (b) Bifurcation diagram corresponding to the $\eta_{Re}|_{Ri=0}$ path. See section VIII B for details.

TABLE XII: Location of the codimension-two point and the corresponding Strouhal number at unsteady onset, together with the linear coefficients in the normal form for the WFA-MC flow past a sphere or a disk.

Case	Re_c	Ri_c	St_c	λ_s	λ_h
Sphere	172	-0.13	$8.5 \cdot 10^{-2}$	$86.7 \cdot \eta_{Re} + 0.82 \cdot \eta_{Ri}$	$\left(84.7 - 67.9i\right) \cdot \eta_{Re} + \left(2.19 - 3.31i\right) \cdot \eta_{Ri}$
Disk $\chi = 10$	129.4	-0.069	$1.07 \cdot 10^{-1}$	$76.8 \cdot \eta_{Re} + 0.057 \cdot \eta_{Ri}$	$\left(66.0 - 25.2i\right) \cdot \eta_{Re} + \left(0.52 - 1.10i\right) \cdot \eta_{Ri}$
Disk $\chi = 3$	152.9	-0.079	$9.5 \cdot 10^{-2}$	$95.3 \cdot \eta_{Re} + 0.37 \cdot \eta_{Ri}$	$\left(92.5 - 40.0i\right) \cdot \eta_{Re} + \left(1.10 - 1.48i\right) \cdot \eta_{Ri}$

hibits instead a point in the (Re, Ri) parameter space where a steady-state mode and a pair of unsteady modes with azimuthal wavenumber $m = \pm 1$ are simultaneously unstable.

The opposing flow case at $Pr = 0.72$ displays a large variety of patterns. The codimension-two point at (Re_c, Ri_c) point, see tables XII and XIII, splits the parameter space in the following sense: for $Ri_c < Ri < 0$ the primary bifurcation breaks the axisymmetry of the steady-state solution, i.e., it corresponds to a steady-state mode (state I in Kotouc et al. [31]); for $Ri < Ri_c$ the primary branch is a standing wave (state XIV in Kotouc et al. [31]), i.e., a solution with mean-zero lift force preserving the symmetry plane. For Richardson numbers $Ri < Ri_c$ the observed transition to more complex spatio-temporal patterns is explained by the interaction between the unsteady pair of modes. In this regime the cubic truncation is degenerate, as already explained, and in order to lift the degeneracy between the modulated wave states MW and $\widetilde{\text{IMM}}$ (these states are labelled XX in Kotouc et al. and not distinguished) one must either include higher order terms in the normal form or introduce terms that break the $O(2)$ symmetry, see section IV C 2. These modulated wave states then bifurcate further, generating general Precessing Waves. In the study of Kotouc et al. [31], the authors did not observe PrW_G, and instead identified aperiodic states, i.e., states that did not display any particular spatiotemporal symmetry. This finding could be explained by a subsequent bifurcation towards a 3FW, although this is not taken into account in the normal form.

When $Ri > Ri_c$ a large variety of states exist. The axisymmetric steady state loses stability with respect to a nonaxisymmetric steady-state mode, thereby losing axisymmetry. The resulting SS state then transitions into a mixed mode MM_0 that preserves reflection symmetry and is associated with a nonzero mean lift. The MM_0 state further transitions into a general Precessing

TABLE XIII: Cubic and quintic coefficients of the normal form for the WFA-MC flow past a sphere.

l_0	l_1	l_2	l_3	F_r
-10.57	-4.57	-0.078	0.27	-201.1

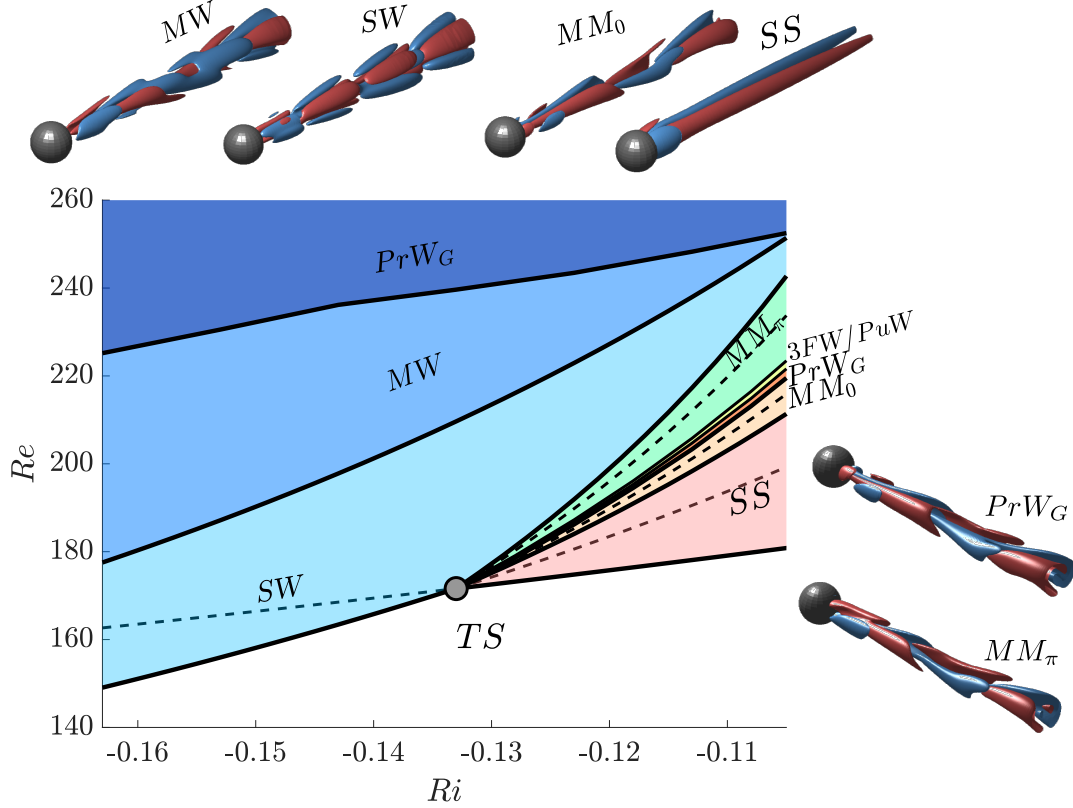| A	B	C	D	E_r
$1.07 + 0.75i$	$-2.8 + 3.54i$	$-3.78 + 3.02i$	$0.79 - 1.0i$	-18.10

FIG. 23: The predicted patterns in the flow past a sphere under mixed convection (opposing flow) conditions in parameter space. Snapshots of the reconstructed states are included.

Wave (PrW_G), i.e., a state without a symmetry plane and slowly rotating mean lift, which in turn bifurcates into a 3FW and finally to a Pulsating Wave state. These three states are located within small regions of the parameter space. However, they have been numerically determined: PrW_G was numerically observed by Kotouc et al. [31] for $Ri > -0.1$ (state XIII) and the 3FW or PuW state were identified for $Ri \approx -0.1$ (state XIX), which is a state that displays a temporary symmetry plane and at least two frequency components. The Pulsating Wave state eventually transitions into MM_π, i.e., a mixed mode without a symmetry plane (also state XIII in [31]). This series of bifurcations is followed either by a standing wave, or modulated wave modes or a Precessing Wave, which is in qualitative accordance with the study of Kotouc et al.

The WFA problem for $Ri = 0$ and $1/\chi \approx 0$ has already been studied by Fabre et al. [36] using numerical simulations and normal from coefficients fitted from the simulations. The case $\chi = 3$ was studied in detail by Auguste et al. [37]. A more rigorous study via multiple-scale analysis was performed by Meliga et al. [38]. Later, Chrust et al. [39] explored the flow dependence on the parameters (Re, χ) using numerical simulations and proposed a classification of the patterns observed. These studies demonstrated the importance of the disk thickness on the transition scenario. Chrust et al. observed that, when the thickness $1/\chi$ is large, for instance $\chi = 1$, the symmetry plane is preserved for large values of the Reynolds number, i.e., only SS and MM_0 (possibly with modulated mixed modes or precessing waves) are observed be-

B. Mixed convection in the flow past a disk

Let us now examine the transition scenario for axisymmetric wake flow past a disk, focusing on the *opposing flow* case under mixed convection conditions. This problem depends on three control parameters, the Reynolds number Re, the Richardson number Ri, and the aspect ratio of the disk χ, where $1/\chi$ is the dimensionless thickness.

TABLE XIV: Cubic and quintic coefficients of the normal form for the WFA-MC flow past a disk with $\chi = 10$.

l_0	l_1	l_2	l_3	F_r
-4.45	-5.94	0.92	-2.28	-50

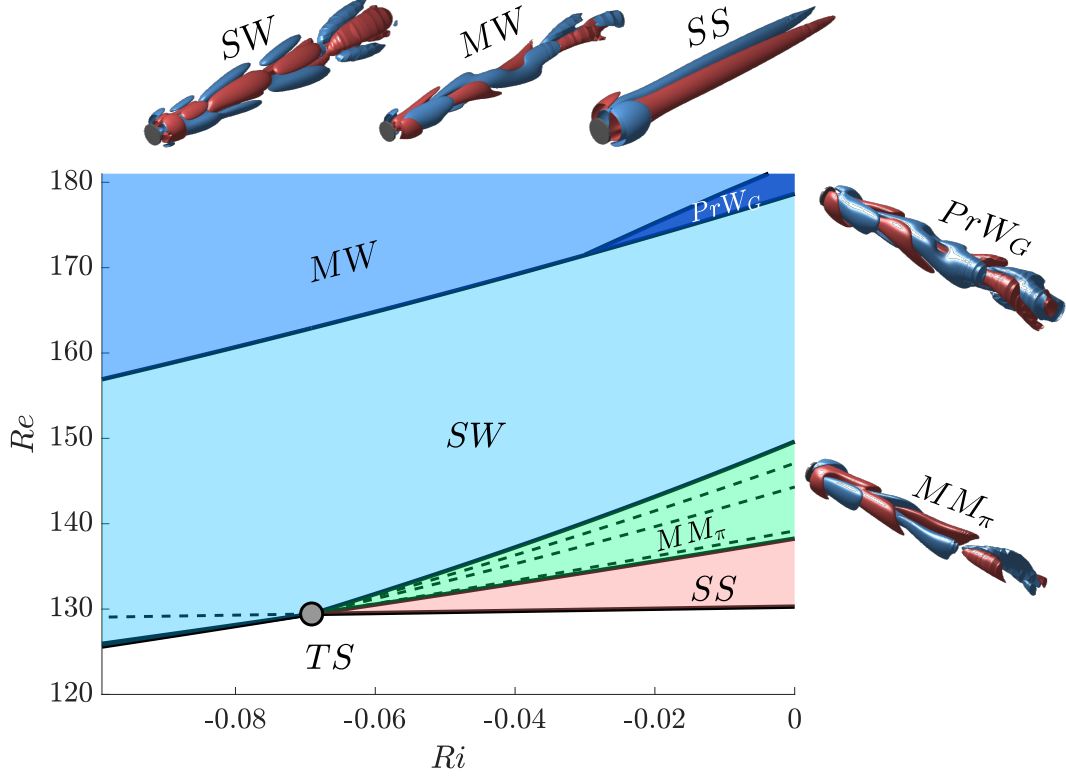| A	B	C	D	E_r
$0.1 - 1.29i$	$-2.14 + 1.69i$	$-0.64 - 2.35i$	$-1.05 + 1.10i$	-1

FIG. 24: The predicted patterns in the flow past a disk with $\chi = 10$ under mixed convection (opposing flow) conditions in parameter space. Snapshots of the reconstructed states are included.

fore spatio-temporal chaos appears. In the limit of zero thickness, when $1/\chi \approx 0$, we will see that the transition scenario starts with the formation of a SS pattern followed by the breaking of the symmetry plane, leading to a MM_π mode and eventually to standing waves SW. At intermediate values of the thickness, a large variety of spatio-temporal patterns may be observed, as highlighted by the study of Auguste et al. In the present study, we shall look for the connections between the *opposing flow* case in mixed convection and the situation at $Ri = 0$, in terms of the spatio-temporal patterns observed in the flow.

Figure 25 displays the location of the codimension-two point corresponding to the Hopf-Steady State bifurcation obtained by varying $1/\chi \in [0, 1]$. The top panels show the corresponding temperature distribution in space and the growing extent of the recirculation bubble in the steady states associated with two distinct values of the aspect ratio χ of the disk. In the range of aspect ratios considered here, the critical Reynolds number grows linearly with the thickness $1/\chi$ of the disk, as previously observed by Fernandes et al. [40]. In addition, the critical Richardson number displays a maximum around $1/\chi \approx 0.1$ followed by a linear decrease in the critical Richardson number. In the following we shall discuss in detail the two cases $\chi = 10$ and $\chi = 3$. The case $\chi = 10$ corresponds to a

case with a relatively simple transition scenario, similar to that explained by Meliga et al. [38]. On the other hand, the case $\chi = 3$ displays a larger number of spatio-temporal structures, and is qualitatively similar to the case of the sphere discussed in section VIII A.

The parameter space summarizing the normal form predictions for $\chi = 10$ is displayed in fig. 24. In this case, to the left of the codimension-two point (grey point in the diagram), the trivial steady state transitions to standing waves and the subsequent bifurcations are uniquely explained by the unsteady modes. To the right of the codimension-two point the primary bifurcation breaks the axisymmetry of the steady state, i.e., it generates the SS state, followed by a periodic state with no reflection symmetry and non-zero mean lift, i.e., the MM_π state. The mixed mode MM_π state eventually bifurcates into a standing wave solution, which finally bifurcates to MW via the effect of higher order terms.

The dynamics near the organizing center for the flow past a disk with thickness $1/\chi = 1/3$ is richer. As in the previous cases, to the left of the organizing center the transition scenario is based on the initial formation of standing waves, followed by modulated waves and an eventual tertiary bifurcation, not taken into account in the normal form, leading to temporal chaos. To the right of the organizing center the transition scenario is
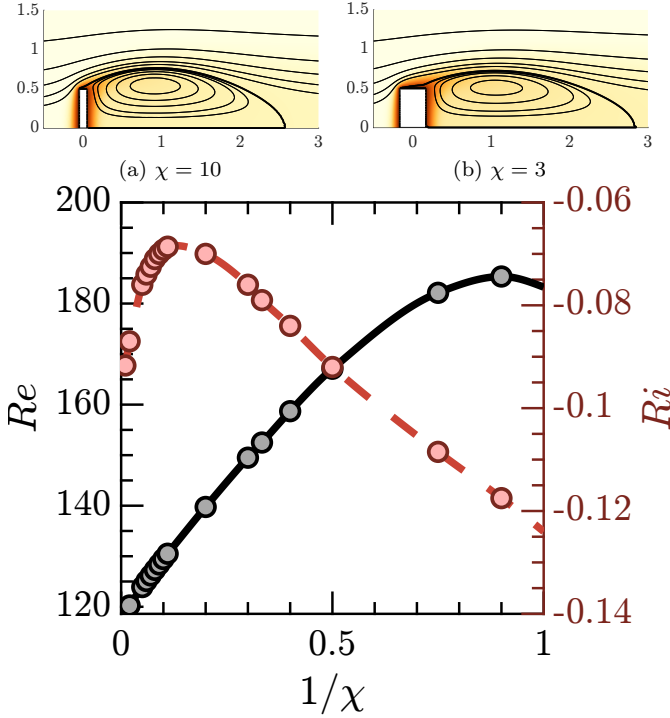
(a) $\chi = 10$ (b) $\chi = 3$

FIG. 25: The location of the codimension-two Hopf-Steady State bifurcation in the (Re, Ri) plane as a function of the aspect ratio χ of the disk (Re: black line; Ri: red line). The color-coded symbols refer to the points obtained in numerical computations. Top: temperature distribution of the trivial steady-state at (a) $1/\chi = 0.1$ ($Re \approx 130$, $Ri \approx -0.068$), (b) $1/\chi \approx 0.33$ ($Re \approx 150$, $Ri \approx -0.078$).

qualitatively similar to that of the sphere (compare section VIII A and fig. 26), although in the present case the codimension-two point is sufficiently close for the theory to provide quantitative predictions of the transition scenario. In other words, the transition scenario in the simple WFA problem of the disk with aspect ratio $\chi = 3$ is constrained by the dynamical structures emanating from the organizing center at $Ri \neq 0$, something that is not the case for the sphere, see Kotouc et al. [31, Fig 4.]. Figure 27 displays the reconstruction of the lift coefficient from the normal form at $Ri = 0$, in comparison to the results obtained numerically by Auguste et al. in [37]. It

TABLE XV: Cubic and quintic coefficients of the normal form for the WFA-MC flow past a disk with $\chi = 3$.

l_0	l_1	l_2	l_3	F_r
-6.19	-4.86	0.47	-2.76	-50

A	B	C	D	E_r
$0.56 - 0.38i$	$-2.3 + 2.3i$	$-1.7 + 0.32i$	$0.79 + 0.52i$	-6

distinguishes five regions, with the *Knit-Knot* (KK) region among them. The transition begins at $Re \approx 159.4$ ($Re \approx 159.8$ [37]) via the formation of a steady-state pattern (SS), which eventually bifurcates into a mixed mode (MM$_0$) at around $Re \approx 182.5$ ($Re \approx 179.9$ in [37]). The MM$_0$ state loses stability at around $Re \approx 184.5$. Quantitatively, up to this point, the sequence of bifurcations is reasonably well predicted with regard to the data reported by [37]. The Knit-Knot region in our analysis covers a large variety of states with similar characteristics in terms of the frequency components (at least two), and the lift coefficient C_L. Auguste et al. [37] identified this motion as temporally quasiperiodic motion resulting from spontaneously broken reflection symmetry. The temporal dynamics of the KK state may be described as the composition of a state with frequency ω_h and a low frequency state, whose frequency experiences large variation within its region of existence (from $T_p \approx 96 \frac{2\pi}{\omega_h}$ at $Re = 185$ to $T_p \approx 48 \frac{2\pi}{\omega_h}$ at $Re = 187$ and then to $T_p \approx 54 \frac{2\pi}{\omega_h}$ at $Re = 190$, cf. fig. 29). This bifurcation sequence is followed by the appearance of the MM$_\pi$ state, estimated to be around $Re \approx 198.5$ ($Re \approx 190.4$ in [37]) which connects to the standing wave branch at around $Re \approx 214$ ($Re \approx 215.2$ in [37]). According to theory, this sequence of bifurcations should be followed by the formation of a modulated wave branch and precessing waves. However, we do not discuss these patterns here due to the lack of simulation data to compare with and because these patterns can only be described using the fifth order normal form whose coefficients we have not computed. For more information, see fig. 26.

Let us return to the discussion of the Knit-Knot region. In our more detailed analysis, this state is actually composed of several simpler states, see fig. 28. The MM$_0$ bifurcates into a precessing wave PrW$_G$ at $Re \approx 184.5$. This precessing wave is stable up to $Re \approx 186.3$, where a saddle-node bifurcation takes place leading to a $3FW$, denoted as 3FW$_A$ in fig. 28. The three-frequency wave is observable only in a small interval, however, and eventually reconnects to a Pulsating Wave via a global homoclinic bifurcation at around $Re \approx 186.9$. This Pulsating Wave is stable up to around $Re \approx 191.9$. At this stage, we can observe two other bifurcations leading to three-frequency waves with 3FW$_B$ (unstable) and 3FW$_C$ (stable); both of these branches reconnect to the main branch (PuW) following a saddle node bifurcation of limit cycles. The pulsating wave state finally reconnects with the symmetry-breaking mixed mode (MM$_\pi$) branch.

IX. DISCUSSION & CONCLUSION

In this article, we have analyzed the properties of the normal form and the bifurcation scenario relevant to the bifurcations observed in axisymmetric wakes described by the Navier–Stokes equation. We have shown that near the onset of instability, it is possible to reduce the dynamics via center manifold reduction, to a normal form, i.e.,
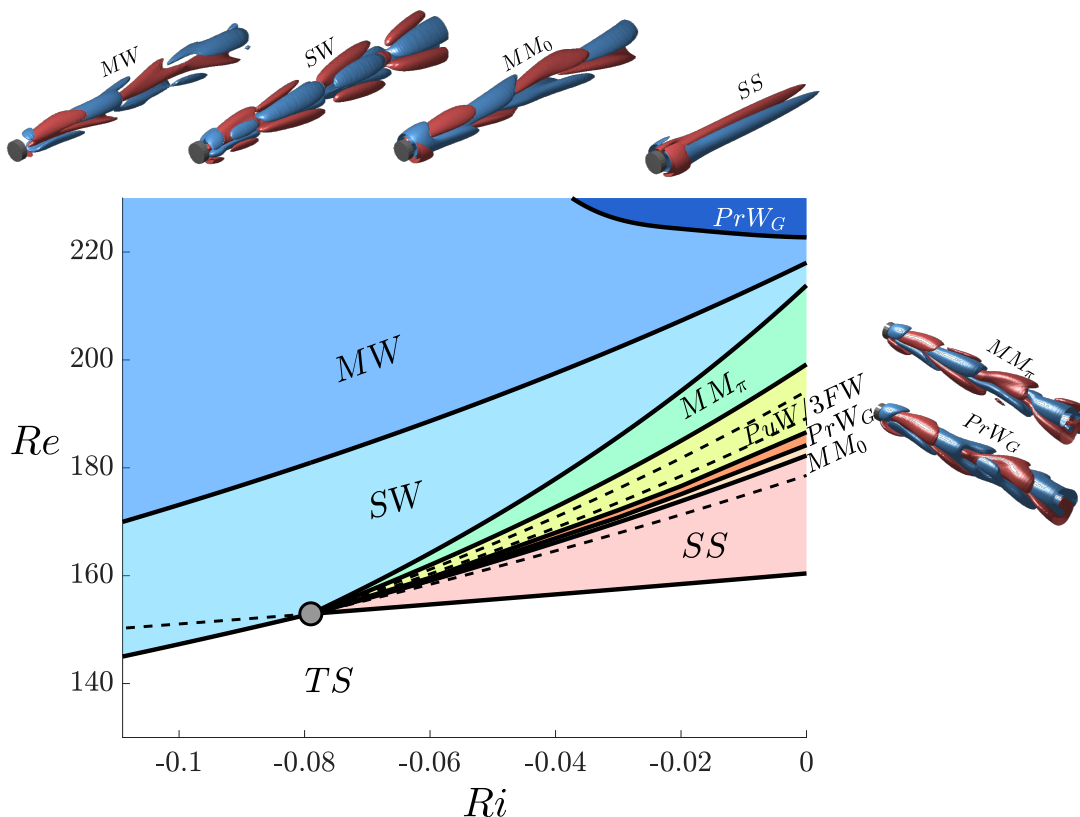
FIG. 26: The predicted patterns in the flow past a disk with $\chi = 3$ under mixed convection (opposing flow) conditions in parameter space. Snapshots of the reconstructed states are included.

an ordinary differential equation, whose unfolding fully captures the local behavior of the Navier-Stokes equation. Such a normal form inherits the discrete and continuous symmetries of the system, in the present case $O(2)$ symmetry. We have shown that this approach, carried out in the vicinity of a steady state-Hopf interaction, suffices to predict much of the observed behavior.

Our analysis of the generic steady state-Hopf case relied on a reduction to polar coordinates. The fixed point solutions of the normal form, e.g. pure modes, mixed modes, have been observed in a variety of fluid flows, including Taylor-Couette and wake flows. Here, we have attempted to provide a complete description of the fixed point solutions of the normal form, as well as possible bifurcations to periodic solutions of the polar normal form, e.g. such a two- and three-frequency waves.

Particularly noteworthy is our discovery of robust, potentially stable, heteroclinic cycles in this mode interaction. In previous studies [41, 42], self-sustained processes have been related to a three-step process involving rolls advecting streamwise velocity, leading to streaks which once unstable lead to wavy perturbations whose nonlinear interaction with itself feeds the rolls. In terms of the mode interaction, the self-sustained cycle described by Dessup *et al.* [41] corresponds to a Het_{SS-SW} cycle or to an orbit that shadows it. In this sense, one could ex-

pect that other, more complex dynamics, for instance a Het_{PrW_A} cycle, may also be observed in the bifurcation scenario of real fluid systems. We mention that the indefinite increase in period associated with the approach to an attracting robust heteroclinic cycle cannot in general be seen in numerical integration of the normal form, on account of rounding error. Instead, the solution trajectory settles into a statistical limit cycle with a finite mean period [43]. This is even more so for partial differential equations [44] and in experiments where the presence of noise prevents approach to such a cycle [45]. This fact points to the importance of fluctuations in applications of the theory to fluid dynamics problems, as also emphasized in [25] in connection with the SNIPER bifurcation.

We have applied here the general theory to several distinct fluid flows and used it to explore the bifurcation scenario of wake flows behind a sphere or disk falling through a constant density fluid and a vertically stratified fluid (problems WFA and WFA-MC, respectively). In particular, in section VII, we determined the normal form coefficients for these problems on the assumption that each object is held fixed, and used these results in section VIII to construct consistent stability diagrams for these flows, comparing the predicted bifurcation scenarios for mixed-convection flow past a fixed axisymmetric object, a disk, and a sphere, with the results of direct nu-
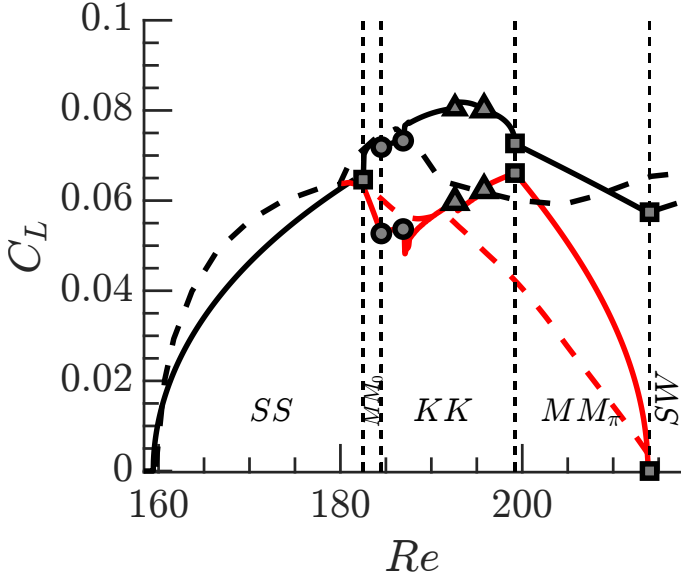
FIG. 27: Bifurcation diagram in terms of the lift coefficient C_L for the WFA problem ($Ri = 0$) with $\chi = 3$. Solid lines were computed from the normal form, dashed lines were extracted from [37]. Black lines denote $C_{L,max}$ and red lines denote the average of C_L. See legend in fig. 28 for a description of the markers.
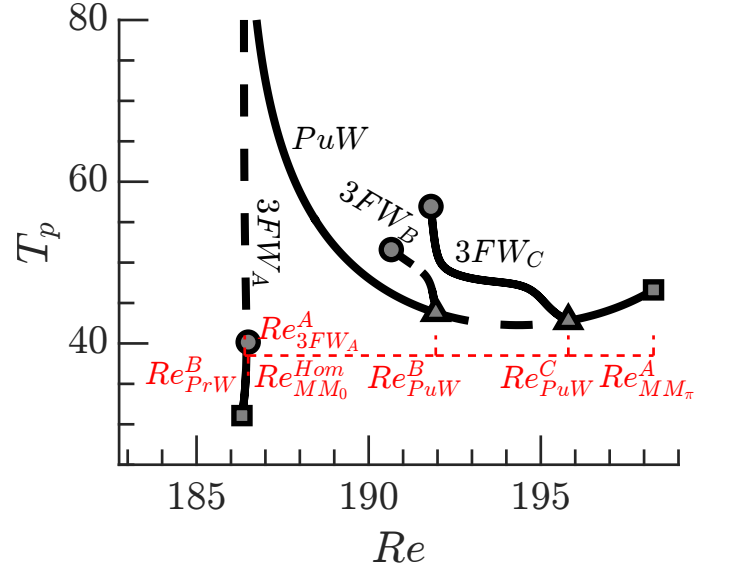

FIG. 28: Bifurcation diagram in the *Knit-Knot* region of fig. 27 in terms of the period T_P of the low frequency modulation. Square markers: Hopf bifurcation. Circles: saddle-node bifurcation. Triangles: Neimark-Sacker bifurcation.

merical simulations of these flows. These results enabled us to rationalize the results of previous numerical studies including those in the complicated Knit-Knot region of Auguste *et al.* [37] for the WFA problem for a disk with thickness $\chi = 3$ and the WFA-MC problem for a sphere of Kotouč *et al.* [31], states XIII or XIX, thereby demonstrating the utility of our bifurcation-theoretic approach. Unfortunately, neither of these cases predicts the presence of structurally stable heteroclinic cycles, although such states may arise for other parameter values.

Appendix A: Normal form reduction

1. Third order forcing terms

The third order forcing terms are obtained from the substitution of the Ansatz 63 into $\mathbf{F}(\mathbf{q}, \boldsymbol{\eta})$. The general expression of the third order forcing term $\mathbf{F}_{(\varepsilon^3)}$ is as fol-

lows:

$$
\begin{aligned}
\mathbf{F}_{(\varepsilon^3)} &\equiv \sum_{\substack{j=-2 \\ k,\ell=-2}}^{2} a_j a_k a_\ell \big[\mathbf{N}(\hat{\mathbf{q}}_j, \hat{\mathbf{q}}_{k,\ell}) + \mathbf{N}(\hat{\mathbf{q}}_{k,\ell}, \hat{\mathbf{q}}_j)\big] e^{-im_n\theta} e^{-i\omega_n t} \\
&+ \sum_{j=-2,\ell=0}^{2} a_j \eta_\ell \big[\mathbf{N}(\hat{\mathbf{q}}_j, \mathbf{Q}_0^{(\eta_\ell)}) + \mathbf{N}(\mathbf{Q}_0^{(\eta_\ell)}, \hat{\mathbf{q}}_j)\big] e^{-im_j\theta} e^{-i\omega_j t} \\
&+ \sum_{j=-2,\ell=0}^{2} a_j \eta_\ell \mathbf{G}(\hat{\mathbf{q}}_j, \mathbf{e}_\ell) e^{-im_j\theta} e^{-i\omega_j t},
\end{aligned}
$$

(A1)

with a slight abuse of notation such that $\hat{\mathbf{q}}_j = \bar{\hat{\mathbf{q}}}_{-j}$, $\hat{\mathbf{q}}_{k,j} = \bar{\hat{\mathbf{q}}}_{-k,-j}$ and $a_j = \bar{a}_{-j}$. Therefore, the azimuthal wavenumber and the frequency associated with a negative index are both considered to be of the opposite sign, i.e., $\omega_{-j} = -\omega_j$ and $m_{-j} = -m_j$. Finally, ω_n and m_n are defined by the relations $\omega_n = \omega_j + \omega_k + \omega_\ell$, $m_n = m_j + m_k + m_\ell$, where $n = j + k + \ell$.

Resonant terms are those for which (ω_n, m_n) is equal to either $(0, m_0)$, (ω_1, m_1) or $(\omega_1, -m_1)$ (plus the complex conjugate pairs). The remaining terms only play a role in higher-order truncations.

Hierarchically, the first class of third-order forcing terms are those which are linear with respect to the amplitude a_j for $j = 0, 1, 2$,

$$
\hat{\mathbf{F}}_{(\varepsilon^3)}^{(a_j)} \equiv \sum_{\ell=0}^{2} \eta_\ell \Big(\big[\mathbf{N}(\hat{\mathbf{q}}_j, \mathbf{Q}_0^{(\eta_\ell)}) + \mathbf{N}(\mathbf{Q}_0^{(\eta_\ell)}, \hat{\mathbf{q}}_j)\big] + \mathbf{G}(\hat{\mathbf{q}}_j, \mathbf{e}_\ell) \Big).
$$

(A2)

The second type of resonant forcing terms are those used to compute the real coefficients l_j for $j = 0, 1, 2, 3$.

by

$$\hat{\mathbf{F}}_{(\varepsilon^3)}^{(a_0|a_0|^2)} \equiv \left[\mathbf{N}(\hat{\mathbf{q}}_0, \hat{\mathbf{q}}_{0,-0}) + \mathbf{N}(\hat{\mathbf{q}}_{0,-0}, \hat{\mathbf{q}}_0)\right] \\ + \left[\mathbf{N}(\hat{\mathbf{q}}_{-0}, \hat{\mathbf{q}}_{0,0}) + \mathbf{N}(\hat{\mathbf{q}}_{0,0}, \hat{\mathbf{q}}_{-0})\right], \quad \text{(A3)}$$

with the notation $\hat{\mathbf{q}}_{-0} = \bar{\hat{\mathbf{q}}}_0$.

Similarly, the terms $\hat{\mathbf{F}}_{(\varepsilon^3)}^{(a_0|a_j|^2)}$ for $j = 1, 2$ are as follows:

$$\hat{\mathbf{F}}_{(\varepsilon^3)}^{(a_0|a_j|^2)} \equiv \left[\mathbf{N}(\hat{\mathbf{q}}_0, \hat{\mathbf{q}}_{j,-j}) + \mathbf{N}(\hat{\mathbf{q}}_{j,-j}, \hat{\mathbf{q}}_0)\right] \\ + \left[\mathbf{N}(\hat{\mathbf{q}}_{-j}, \hat{\mathbf{q}}_{0,j}) + \mathbf{N}(\hat{\mathbf{q}}_{0,j}, \hat{\mathbf{q}}_{-j})\right] \\ + \left[\mathbf{N}(\hat{\mathbf{q}}_j, \hat{\mathbf{q}}_{0,-j}) + \mathbf{N}(\hat{\mathbf{q}}_{0,-j}, \hat{\mathbf{q}}_j)\right]. \quad \text{(A4)}$$

Finally, $\hat{\mathbf{F}}_{(\varepsilon^3)}^{(\bar{a}_0 a_1 \bar{a}_2)}$ is expressed as

$$\hat{\mathbf{F}}_{(\epsilon^3)}^{(\bar{a}_0 a_1 \bar{a}_2)} \equiv \left[\mathbf{N}(\hat{\mathbf{q}}_{-0}, \hat{\mathbf{q}}_{1,-2}) + \mathbf{N}(\hat{\mathbf{q}}_{1,-2}, \hat{\mathbf{q}}_{-0})\right] \\ + \left[\mathbf{N}(\hat{\mathbf{q}}_1, \hat{\mathbf{q}}_{-0,-2}) + \mathbf{N}(\hat{\mathbf{q}}_{-0,-2}, \hat{\mathbf{q}}_1)\right] \\ + \left[\mathbf{N}(\hat{\mathbf{q}}_{-2}, \hat{\mathbf{q}}_{-0,1}) + \mathbf{N}(\hat{\mathbf{q}}_{-0,1}, \hat{\mathbf{q}}_{-2})\right]. \quad \text{(A5)}$$

The third class of forcing terms are those used for the computation of the complex coefficients A, B, C and D. These are $\hat{\mathbf{F}}_{(\varepsilon^3)}^{(a_j|a_j|^2)}$ for $j = 1, 2$:

$$\hat{\mathbf{F}}_{(\varepsilon^3)}^{(a_j|a_j|^2)} \equiv \left[\mathbf{N}(\hat{\mathbf{q}}_j, \hat{\mathbf{q}}_{j,-j}) + \mathbf{N}(\hat{\mathbf{q}}_{j,-j}, \hat{\mathbf{q}}_j)\right] \\ + \left[\mathbf{N}(\hat{\mathbf{q}}_{-j}, \hat{\mathbf{q}}_{j,j}) + \mathbf{N}(\hat{\mathbf{q}}_{j,j}, \hat{\mathbf{q}}_{-j})\right], \quad \text{(A6)}$$

$\hat{\mathbf{F}}_{(\epsilon^3)}^{(a_j|a_k|^2)}$ for $j = 1, 2$ and $k = 0, 1, 2$ with $j \neq k$,

$$\hat{\mathbf{F}}_{(\varepsilon^3)}^{(a_j|a_k|^2)} \equiv \left[\mathbf{N}(\hat{\mathbf{q}}_j, \hat{\mathbf{q}}_{k,-k}) + \mathbf{N}(\hat{\mathbf{q}}_{k,-k}, \hat{\mathbf{q}}_j)\right] \\ + \left[\mathbf{N}(\hat{\mathbf{q}}_{-k}, \hat{\mathbf{q}}_{j,k}) + \mathbf{N}(\hat{\mathbf{q}}_{j,k}, \hat{\mathbf{q}}_{-k})\right] \\ + \left[\mathbf{N}(\hat{\mathbf{q}}_k, \hat{\mathbf{q}}_{j,-k}) + \mathbf{N}(\hat{\mathbf{q}}_{j,-k}, \hat{\mathbf{q}}_k)\right]. \quad \text{(A7)}$$

Finally, the term $\hat{\mathbf{F}}_{(\epsilon^3)}^{(a_0 a^2)}$ is expressed as

$$\hat{\mathbf{F}}_{(\varepsilon^3)}^{(a_0 a^2)} \equiv \left[\mathbf{N}(\hat{\mathbf{q}}_0, \hat{\mathbf{q}}_{0,2}) + \mathbf{N}(\hat{\mathbf{q}}_{0,2}, \hat{\mathbf{q}}_0)\right] \\ + \left[\mathbf{N}(\hat{\mathbf{q}}_2, \hat{\mathbf{q}}_{0,0}) + \mathbf{N}(\hat{\mathbf{q}}_{0,0}, \hat{\mathbf{q}}_2)\right]. \quad \text{(A8)}$$
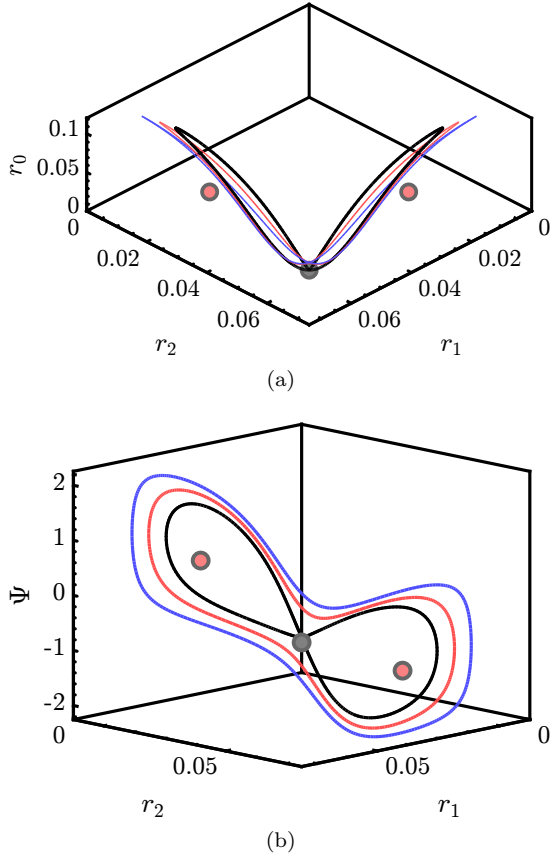

FIG. 29: The ambiclinic orbit $Re_{MM_0}^{\mathrm{Hom}}$ (gray line) at Re = 186.4 of fig. 28. The gray dot is the location of MM_0 while the red markers indicate the location of the PrW_G states. The red and blue trajectories represent limit cycles for higher values of Re; the period T_P of these states diverges logarithmically as Re $\to$ 186.4 from above (not shown).

They are proportional to the cubic terms in the first equation of the complex normal form eq. (8), and are given

[1] M. Golubitsky, I. Stewart, and D. G. Schaeffer, *Singularities and Groups in Bifurcation Theory: Volume II*, Vol. 69 (Springer Science & Business Media, 2012).

[2] M. Golubitsky and W. Langford, Pattern formation and bistability in flow between counterrotating cylinders, Physica D: Nonlinear Phenomena **32**, 362 (1988).

[3] P. Hirschberg and E. Knobloch, Zigzag and varicose instabilities of a localized stripe, Chaos: An Interdisciplinary Journal of Nonlinear Science **3**, 713 (1993).

[4] P. Hirschberg and E. Knobloch, A robust heteroclinic cycle in an steady-state mode interaction, Nonlinearity **11**, 89 (1998).

[5] J. D. Crawford and E. Knobloch, Symmetry and symmetry-breaking bifurcations in fluid mechanics, Annual Review of Fluid Mechanics **23**, 341 (1991).

[6] P. Chossat and G. Iooss, *The Couette-Taylor Problem*, Vol. 102 (Springer Science & Business Media, 2012).

[7] G. Mougin and J. Magnaudet, Path instability of a rising bubble, Physical Review Letters **88**, 014502 (2001).

[8] E. Knobloch, On the degenerate hopf bifurcation with o(2) symmetry, Contemporary Mathematics **56**, 193 (1986).

[9] S. A. van Gils and J. Mallet-Paret, Hopf bifurcation and symmetry: travelling and standing waves on the circle, Proceedings of the Royal Society of Edinburgh, Section A: Mathematics **104**, 279 (1986).

[10] M. Golubitsky and M. Roberts, A classification of degenerate hopf bifurcations with o(2) symmetry, Journal

of Differential Equations **69**, 216 (1987).

[11] A. S. Landsberg and E. Knobloch, Direction-reversing traveling waves, Physics Letters A **159**, 17 (1991).

[12] A. Hill and I. Stewart, Hopf-steady-state mode interactions with o(2) symmetry, Dynamics and Stability of Systems **6**, 149 (1991).

[13] J. D. Crawford, M. Golubitsky, and W. F. Langford, Modulated rotating waves in o(2) mode interactions, Dynamics and Stability of Systems **3**, 159 (1988).

[14] M. Field, Equivariant dynamical systems, Transactions of the American Mathematical Society **259**, 185 (1980).

[15] J. Guckenheimer and P. Holmes, Structurally stable heteroclinic cycles, Mathematical Proceedings of the Cambridge Philosophical Society **103**, 189 (1988).

[16] M. Krupa and I. Melbourne, Asymptotic stability of heteroclinic cycles in systems with symmetry, Ergodic Theory and Dynamical Systems **15**, 121 (1995).

[17] M. Krupa and I. Melbourne, Asymptotic stability of heteroclinic cycles in systems with symmetry. ii, Proceedings of the Royal Society of Edinburgh, Section A: Mathematics **134**, 1177 (2004).

[18] I. Melbourne, P. Chossat, and M. Golubitsky, Heteroclinic cycles involving periodic solutions in mode interactions with o(2) symmetry, Proceedings of the Royal Society of Edinburgh, Section A: Mathematics **113**, 315 (1989).

[19] E. Knobloch and M. Silber, Oscillatory convection in a rotating layer, Physica D: Nonlinear Phenomena **63**, 213 (1993).

[20] D. A. Weinberg, Canonical forms for symmetric tensors, Linear algebra and its applications **57**, 271 (1984).

[21] J. Porter and E. Knobloch, New type of complex dynamics in the 1:2 spatial resonance, Physica D: Nonlinear Phenomena **159**, 125 (2001).

[22] J. Porter and E. Knobloch, Complex dynamics in the 1:3 spatial resonance, Physica D: Nonlinear Phenomena **143**, 138 (2000).

[23] W. Govaerts, Y. A. Kuznetsov, H. Meijer, B. Al-Hdaibat, V. De Witte, A. Dhooge, W. Mestrom, N. Neirynck, A. Riet, and B. Sautois, *MATCONT: Continuation toolbox for ODEs in Matlab* (2019).

[24] M. K. S. Yeung and S. H. Strogatz, Nonlinear dynamics of a solid-state laser with injection, Physical Review E **58**, 4421 (1998).

[25] F. Pétrélis, S. Fauve, E. Dormy, and J.-P. Valet, Simple mechanism for reversals of Earth's magnetic field, Physical Review Letters **102**, 144503 (2009).

[26] L. P. Shil'nikov, A case of the existence of a countable number of periodic motions, Soviet Math. Doklady **6**, 163 (1965).

[27] P. Glendinnning and C. Sparrow, Local and global behaviour near homoclinic orbits, Journal of Statistical Physics **35**, 645 (1984).

[28] L. P. Shilnikov and A. Shilnikov, Shilnikov bifurcation, Scholarpedia **2**, 1891 (2007), revision #194931.

[29] E. Knobloch, D. R. Moore, J. Toomre, and N. O. Weiss, Transitions to chaos in double-diffusive convection, Journal of Fluid Mechanics **166**, 409 (1986).

[30] E. Knobloch and D. R. Moore, Minimal model of binary fluid convection, Physical Review A **42**, 4693 (1990).

[31] M. Kotouč, G. Bouchet, and J. Dušek, Transition to turbulence in the wake of a fixed sphere in mixed convection, Journal of Fluid Mechanics **625**, 205 (2009).

[32] H. Gan, J. Chang, J. J. Feng, and H. H. Hu, Direct numerical simulation of the sedimentation of solid particles with thermal convection, Journal of Fluid Mechanics **481**, 385 (2003).

[33] P. Mcleod, D. S. Riley, and R. S. J. Sparks, Melting of a sphere in hot fluid, Journal of Fluid Mechanics **327**, 393 (1996).

[34] S. S. Sadhal, P. S. Ayyaswamy, and J. N. Chung, *Transport phenomena with drops and bubbles* (Springer Science & Business Media, 2012).

[35] C. H. Chiang and W. A. Sirignano, Interacting, convecting, vaporizing fuel droplets with variable properties, International Journal of Heat and Mass Transfer **36**, 875 (1993).

[36] D. Fabre, F. Auguste, and J. Magnaudet, Bifurcations and symmetry breaking in the wake of axisymmetric bodies, Physics of Fluids **20**, 051702 (2008).

[37] F. Auguste, D. Fabre, and J. Magnaudet, Bifurcations in the wake of a thick circular disk, Theoretical and Computational Fluid Dynamics **24**, 305 (2010).

[38] P. Meliga, J.-M. Chomaz, and D. Sipp, Global mode interaction and pattern selection in the wake of a disk: a weakly nonlinear expansion, Journal of Fluid Mechanics **633**, 159 (2009).

[39] M. Chrust, G. Bouchet, and J. Dušek, Parametric study of the transition in the wake of oblate spheroids and flat cylinders, Journal of Fluid Mechanics **665**, 199 (2010).

[40] P. C. Fernandes, F. Risso, P. Ern, and J. Magnaudet, Oscillatory motion and wake instability of freely rising axisymmetric bodies, Journal of Fluid Mechanics **573**, 479 (2007).

[41] T. Dessup, L. S. Tuckerman, J. E. Wesfreid, D. Barkley, and A. P. Willis, Self-sustaining process in taylor-couette flow, Physical Review Fluids **3**, 123902 (2018).

[42] Y. Bengana and L. S. Tuckerman, Spirals and ribbons in counter-rotating taylor-couette flow: Frequencies from mean flows and heteroclinic orbits, Physical Review Fluids **4**, 044402 (2019).

[43] F. H. Busse, Transition to turbulence in Rayleigh-Bénard convection, in *Hydrodynamic Instabilities and the Transition to Turbulence* (Springer-Verlag, Berlin, New York, 1981) pp. 97–137.

[44] I. Mercader, J. Prat, and E. Knobloch, Robust heteroclinic cycles in two-dimensional Rayleigh-Bénard convection without Boussinesq symmetry, International Journal of Bifurcation and Chaos **12**, 2501 (2002).

[45] E. Stone and P. Holmes, Random perturbations of heteroclinic attractors, SIAM Journal on Applied Mathematics **50**, 726 (1990).

[46] E. Weisshaar, F. H. Busse, and M. Nagata, Twist vortices and their instabilities in the taylor–couette system, Journal of fluid mechanics **226**, 549 (1991).

[47] M. Krupa, Robust heteroclinic cycles, Journal of Nonlinear Science **7**, 129 (1997).

[48] W. Nagata, A perturbed hopf bifurcation with reflection symmetry, Proceedings of the Royal Society of Edinburgh, Section A: Mathematics **117**, 1 (1991).